Theses and Dissertations | 1. Thesis and Dissertation Collection, all items

1990

Interaction of a vortex pair with a free surface : measurements and computations

Suthon, Peter B. R.

Monterey, California: Naval Postgraduate School

http://hdl.handle.net/10945/34834

②

NAVAL POSTGRADUATE SCHOOL
Monterey, California

DTIC
ELECTE
S MAR 1 8 1991
D

D THESIS

INTERACTION OF A VORTEX PAIR
WITH A FREE SURFACE:
MEASUREMENTS AND COMPUTATIONS

by

Peter B. R. Suthon

June 1990

Thesis Advisor: T. Sarpkaya

Approved for public release; distribution is unlimited.

91 3 14 027

REPORT DOCUMENTATION PAGE		Form Approved OMB No. 0704-0188

1a. REPORT SECURITY CLASSIFICATION Unclassified	1b. RESTRICTIVE MARKINGS

2a. SECURITY CLASSIFICATION AUTHORITY	3. DISTRIBUTION AVAILABILITY OF REPORT
2b. DECLASSIFICATION/DOWNGRADING SCHEDULE	Approved for public release; distribution unlimited.

4. PERFORMING ORGANIZATION REPORT NUMBER(S)	5. MONITORING ORGANIZATION REPORT NUMBER(S)

6a. NAME OF PERFORMING ORGANIZATION Naval Postgraduate School	6B OFFICE SYMBOL (If applicable) ME	7a. NAME OF MONITORING ORGANIZATION Naval Postgraduate School
6c. Address (City, State, and ZIP Code) Monterey, CA 93943-5000		7b. ADDRESS (City, State, and ZIP Code) Monterey, CA 93943-5000

8a. NAME OF FUNDING/SPONSORING ORGANIZATION	8b OFFICE SYMBOL (If applicable)	9. PROCUREMENT INSTRUMENT IDENTIFICATION NUMBER

8c. ADDRESS (City, State, and ZIP Code)	10. SOURCE OF FUNDING NUMBERS			
	PROGRAM ELEMENT No.	PROJECT No.	TASK No.	WORK UNIT ACCESSION No.

11. TITLE *(Include Security Classification)* INTERACTION OF A VORTEX PAIR WITH A FREE SURFACE: MEASUREMENTS AND COMPUTATIONS

12. PERSONAL AUTHOR(S) PETER B. R. SUTHON

13a. TYPE OF REPORT Master of Science and Engineer's Thesis	13b. TIME COVERED From: To:	14. DATE OF REPORT *(Year, Month, Day)* June 1990	15. PAGE COUNT 136

16. SUPPLEMENTARY NOTATION The views expressed in this thesis are those of the author and do not reflect the official policy or position of the Department of Defense or the U. S. Government.

17. COSATI CODES			18. SUBJECT TERMS *(Continue on reverse if necessary and identify by block number)*
FIELD	GROUP	SUB-GROUP	Surface Disturbances, Scars, Striations, Trailing Vortices, Vortex Dynamics

19. ABSTRACT *(Continue on reverse if necessary and identify by block number)*

An investigation of the interaction of two counter-rotating vortices with a free surface has been undertaken. Experiments were carried out in two water basins and in a long towing tank through the use of measurements, flow visualization, and an infra-red camera. The results have shown that all types of vortex pairs over a wide range of Froude Numbers give rise to three-dimensional surface disturbances, known as scars and striations. The striations are a consequence of the short wavelength instability inherent to the vortex pair itself. The scars are transported outward by the vortex pair and are comprised of a constellation of coherent vortical structures (whirls). The experiments have provided sufficient understanding of the physics of the phenomenon and led to the development of a numerical model based on vortex dynamics. This model proved to be capable of explaining the physical processes involved in the evolution of the three-dimensional footprints of the vortex pair.

20. DISTRIBUTION/AVAILABILITY OF ABSTRACT [X] UNCLASSIFIED/UNLIMITED ☐ SAME AS RPT. ☐ DTIC USERS	21. ABSTRACT SECURITY CLASSIFICATION Unclassified	
22a. NAME OF RESPONSIBLE INDIVIDUAL Professor T. Sarpkaya	22b TELEPHONE *(Include Area code)* (408) 646-3425	22c. OFFICE SYMBOL ME-SL

DD Form 1473, JUN 86   Previous editions are obsolete.   SECURITY CLASSIFICATION OF THIS PAGE

Unclassified

i

**Interaction of a Vortex Pair
With a Free Surface:
Measurements and Computations**

by

Peter B. R. Suthon
Lieutenant, United States Navy
B.S.E., Tulane University, 1983

Submitted in partial fulfillment of the
requirements for the degrees of

MASTER OF SCIENCE IN MECHANICAL ENGINEERING

and

MECHANICAL ENGINEER

from the

NAVAL POSTGRADUATE SCHOOL

June 1990

Author: _____
Peter B. R. Suthon

Approved by: _____
T. Sarpkaya, Thesis Advisor

_____
Anthony J. Healey, Chairman,
Department of Mechanical Engineering

_____
Dean of Faculty and Graduate Studies

ABSTRACT

An investigation of the interaction of two counter-rotating vortices with a free surface has been undertaken. Experiments were carried out in two water basins and in a long towing tank through the use of measurements, flow visualization, and an infra-red camera. The results have shown that all types of vortex pairs over a wide range of Froude Numbers give rise to three-dimensional surface disturbances, known as scars and striations. The striations are a consequence of the short wavelength instability inherent to the vortex pair itself. The scars are transported outward by the vortex pair and are comprised of a constellation of coherent vortical structures (whirls). The experiments have provided sufficient understanding of the physics of the phenomenon and led to the development of a numerical model based on vortex dynamics. This model proved to be capable of explaining the physical processes involved in the evolution of the three-dimensional footprints of the vortex pair.

TABLE OF CONTENTS

LIST OF FIGURES

LIST OF SYMBOLS

b	Instantaneous spacing between the vortex centers
b_0	Initial distance between the two vortices
c	The average whirl spacing in the x-direction
d_0	The depth at which the vortex pair is generated
E	Energy density averaged over the total whirl population
L	The length of the scar band
N_w	The number of whirls in each scar band
r_c	The core size of the whirl
Rnd	A random number
s	The inboard edge of the scar front
t	time
Δt	The time step
u	Velocity in the x-direction
v	Velocity in the y-direction
V_b	The velocity imposed on a scar by the vortex pair
V_0	The initial mutual-induction velocity of the vortex pair
V_t	The tangential velocity at the edge of the whirl core
w	The width of the scar front
z	The position of the whirl center (in the Complex plane)
β	The wave number
Γ_m	The initial mean circulation of the whirls
Γ_0	The initial circulation of the vortex pair

Γ_w The circulation of a whirl

γ_{min} The minimum survival strength of a whirl

δ The cut-off distance in velocity calculations

ε The critical amalgamation distance

ACKNOWLEDGEMENTS

I. INTRODUCTION

Trailing vortices created by the motion of a lifting body and the vortex wakes produced from their interaction with a free surface have become major research topics in hydrodynamics. An ascending vortex pair produces a three-dimensional complex signature, comprised of a narrow dark band bordered by two bright lines in synthetic-aperture-radar (SAR) images. The surface signature has two distinct modes: **striations** and **scars**. These surface disturbances were first reported by Sarpkaya and Henderson (1984, 1985), and Sarpkaya (1985, 1986). The striations appear first as ridges normal to the path of the lifting surface as seen in Figure 1. They come into existence when the trailing vortices are about one initial vortex spacing (b_0) from the free surface. The striations or humps rise slightly above the free surface and then retreat back as they dissipate through splitting and pairing. As the humps begin to recede, the depressions formed at their edges lead to the creation of scars (Figure 2). Consequently, the scars appear toward the end of the striation phase and when the vortices are at a distance of about $0.6b_0$ from the free surface (Figure 3). The scars are slaved to the trailing vortices and move outward almost directly above them. The trailing vortices diffuse rapidly due to the counter-sign vorticity generated in the overlapping regions of the vortex pair in the recirculation cell and at the free surface, depending on surface contamination (Figure 4).

As noted above, the striated region appears as a dark narrow band and the scars as two narrower bright bands in synthetic aperture radar (SAR)

1

images of a ship's wake (Figure 5). The interpretation and use of this multi-spectral data requires a clear understanding of the physics of the phenomenon to explain the life-history of the surface signatures. The basis of the current intense interest in the interaction of internal waves, wakes, and vortices with the free surface is that the reasons for the existence of the SAR images have not yet been explained and that the surface signatures of sub-surface phenomena can give trace of the generating bodies.

Traditionally, the most significant ship wake has been the Kelvin wave having the classical 38.9 degree wake angle (Figure 6). However, with the advent of technological advances in the area of remote sensing and satellite communication, this perception is no longer true. The narrow surface signature, with a wake angle of about 3 degrees, exists for several hours behind the ship with no indication or existence of the Kelvin wake (Figure 7). It is known that the narrow dark band in SAR images does not reflect incident electromagnetic waves back to the source/receiver and has been observed to bifurcate. They appear to be due to a reduction, and not due to an increase, in radar backscatter along the edges of the wake.

Various mechanisms have been proposed to provide a feasible explanation of this dark band: (i) interaction of the wake of a vortex pair with the free surface (Sarpkaya and Henderson 1984, Lyden et al. 1985); (ii) suppression of surface waves near the ship track and an enhancement of the waves near the edges of the suppressed area by the vortices produced by the ship's hull; (iii) turbulence and surface mean flow resulting from ship motion, although it is not clear that turbulence alone is responsible for their appearance (Witting and Vaglio-Laurin 1985); (iv) a redistribution of

surface impurities by large scale vortical motions, as in Reynolds ridges (see, e.g., Scott 1982) or Langmuir circulations (Langmuir 1938, Garrett 1976); and (v) air subsequently entrained in the wake, bubble scavenging of surface and subsurface surfactant materials, the interaction of Kelvin waves, ambient waves, and momentum waves and the generation of vorticity-retaining inverse bubbles and drops by a Kelvin-Helmholtz instability (Baird 1959, Garrett and Smith 1984, Furey 1989 & 1990). Each one of these models, and others not mentioned, tries to provide a meaningful explanation of the SAR images of ships' wakes.

Although the impetus for the present research comes from the understanding of the narrow dark bands, bounded by two bright lines, found in SAR images, this thesis will deal primarily with the investigation of the physics of two counter-rotating vortices rising towards and interacting with a free surface.

Sarpkaya and Henderson's (1984) and Sarpkaya's (1986) theoretical analyses of the scars created by the trailing vortices were based on the classical solution of Lamb (1930), assuming the vortices to be two-dimensional and the free surface to be a rigid plane. For small Froude numbers Fr (Fr $= V_0/\sqrt{gb_0}$, where V_0 is the initial mutual induction velocity of the vortices), each scar front was shown to coincide with the stagnation point on the Kelvin oval, formed by one of the pair of the trailing vortices and its image. For Froude numbers larger than about 0.15, not only the deformation of the free surface but also the nonlinear interaction between the said deformation and the motion of the vortices are significant. Thus, the free surface may no longer be assumed rigid.

3

Even though it was fully realized at the outset that the problem ultimately to be solved is the understanding of the three-dimension nature of the phenomenon, the relative ease of the two dimensional counterpart has attracted the immediate attention of experimentalists and numerical analysists alike (e.g., Sarpkaya et al. 1988, Dahm et al. 1988, Rau 1989, Willmarth et al. 1989, Marcus and Berger 1989, Ohring and Lugt 1989, just to name a few).

Sarpkaya, Elnitsky, and Leeker's (1988) two-dimensional experiments were conducted in a twelve foot long, three foot wide, and four foot deep water basin. The nearly two-dimensional vortex pair was generated through the use of two counter-rotating plates. Rau (1989) described improvements on the method of generating vortices using a piston-nozzle assembly. Neutrally buoyant fluorescent dye was used to visualize the flow. The group at the Naval Postgraduate School also carried out a numerical analysis of the scar cross section through the use of vortex dynamics. Their results have shown that the two-dimensional evolution of the free surface can be calculated (up to certain normalized times) through the use of line vortices or dipoles. The analysis becomes more robust as the Froude number is increased. At larger times, the results become unrealistic because the laminar and turbulent diffusion of vorticity are ignored. No wave train was observed on either side of the scars for any of the Froude numbers encountered in the analysis or experiments, as anticipated by Kochin et al. (1964).

Using Sarpkaya et al.'s (1988) idea of counter-rotating plates to generate vortices, Dahm et al. (1988), and Willmarth et al. (1989) at the

University of Michigan, carried out similar experiments on vortex-pair free-surface interaction. They too have used vortex methods to calculate the path of the vortices and the deformation of the free surface. However, no detailed comparisons were made between the observed and calculated scar cross sections.

Telste (1988) used vortex dynamics to investigate the same phenomenon (inviscid two-dimensional interaction between a two-dimensional vortex pair and the free surface). At medium and lower Froude numbers, his calculations required extensive numerical filtering to avoid or to delay numerical instability. The calculations were generally terminated when the free surface formed a sharp corner or when difficulties were encountered in obtaining rapid convergence. There does not seem to be any direct relation between the breakdown of the numerical model, breakdown of the waves, and the attainment of maximum scar conditions. Telste offered no comparisons with experiments.

Marcus (1988) and Marcus and Berger (1989), at UC Berkeley, used the finite-difference method to investigate the inviscid, two-dimensional interaction between a pair of counter-rotating line vortices and a free surface. They have not conducted any experiments and encountered considerable numerical-stability problems at lower Froude numbers. At higher Froude numbers, their predictions were somewhat larger than those measured and calculated by Sarpkaya, et al. (1988). However, more recently, Marcus (1990) made very stable predictions of the scar cross section through the use of projection methods (Figure 8, reproduced here with his permission).

Ohring and Lugt (1989) performed numerical computations of the said interaction in a viscous, incompressible fluid, assuming laminar two-dimensional flow and obtained results similar to those cited earlier. No comparisons were made with experiments.

Even though some insight has been gained through the use of two-dimensional models, the three-dimensional nature of the phenomenon and its significance in the interpretation of long dark narrow bands cannot be ignored. It is because of this reason that the present investigation deals once again with the three-dimensional nature of the surface signatures by constructing a physical and numerical model of the phenomenon. The analysis of the problem is extremely difficult, particularly for inclined vortex pairs as in trailing vortices. In view of this fact, it was decided first to carry out experiments and numerical analysis of three dimensional surface structures resulting from a vortex pair initially parallel to the free surface. Subsequently, the experiments and the numerical analysis were extended to the case of trailing vortices.

Experiments were conducted in two water basins using a piston-nozzle assembly to create a vortex pair (initially parallel to the free surface) and in a towing tank using a suitable lifting surface to create inclined trailing vortices. Effective methods have been developed for structural and eddy center identification based on digital image analysis, shadowgraph technique, and infra-red spectrography. The striational instability and the mutual interaction of the vortical structures, or whirls, are studied in detail. The size and angular velocities of the whirls are determined in order to explore the statistics of the surface structures and to calculate the

distribution of vorticity in the field of whirls. The interaction and the decay rates of the surface eddies are obtained from the evolution of the whirl size and strength spectrum. The instantaneous free-surface signature is compared with the predictions of a numerical model based on the vortex element method (see Sarpkaya 1989).

II. EXPERIMENTAL APPARATUS AND PROCEDURES

Experiments were conducted in three different water basins. The first was a long towing tank for the towing submerged lifting bodies. It was used previously for the exploration of the characteristics of scars and striations generated by lifting bodies (see, e.g., Henderson 1984, Gray 1985). The second, a multipurpose basin, was used for the study of the scar cross section in a two-dimensional mode (Elnitsky 1987, Leeker 1988, Sarpkaya, Elnitsky, and Leeker 1988, and Rau 1989). The third water basin was constructed partway through the current investigation when it was realized that the existing basins were insufficient for the type and scope of experiments desired. Each experiment was repeated at least twice to assure that the results could be reproduced.

Experimental data were collected using the same equipment regardless of which basin the experiments were conducted in. Two video-recorder systems were used, one with a black-and-white video camera and the other with a color video camera. The output signal of the camera was sent to a date/timer prior to the video-cassette recorder and monitor. The black-and-white camera was used primarily with the shadowgraph technique (for optimum contrast and clarity of the shadows of the surface disturbances), and the color camera was used primarily with the visualization of the striations. In addition, two still cameras (a 35-mm and a 120-mm) were used with films of different speed, either black-and-white or color. Thermal-imaging was conducted using an infra-red camera

which sent a video signal to a date/timer and then to a video-cassette recorder.

A. THE TOWING TANK

The towing basin has been used extensively at this facility for the past twelve years, and its detailed descriptions have been given by (Turkmen 1982, Johnson 1982, Sarpkaya and Johnson 1982, Sarpkaya 1983, Henderson 1984, and Gray 1985, among others). The salient features and important characteristics are reproduced here, together with recent modifications, for the sake of completeness.

1. Equipment Description

The towing tank is 36 feet long, 3 feet wide and 5 feet deep, fabricated from 1/2-inch thick aluminum plates (Figure 9). The front wall is fitted with square windows of 1-inch thick Plexiglass and the rear wall is reinforced to prevent bulging under hydrostatic pressure. The aluminum interior of the tank is painted with marine epoxy to prevent corrosion.

The components of the operating system include plumbing for filling and draining, a turbulence management system, top and bottom carriages, velocity measuring system, lighting system and the models. The filling pipes lie on the bottom of the tank. They are 2-inch diameter PVC pipes with 1/16-inch perforations along their entire length. The drain lines penetrate the bottom at each end of the tank.

Two parallel rails are mounted along the bottom and top of the tank. The submerged lifting body was mounted on a carriage which rides smoothly on the lower set of rails (Figure 10). The carriage is pulled at a constant velocity with an endless cable and a DC motor; the velocity was

measured and continuously monitored using a magnetic linear displacement transducer. The transducer yielded a signal proportional to the velocity of the model with less than 1 percent error. The turbulence management system (consisting of a 1-inch thick polyurethane foam sandwiched between two perforated aluminum plates) is located about 9 inches above the tank bottom to eliminate the propagation of the disturbances generated by the motion of the carriage into the test section.

A mirror, inclined about 45 degrees from horizontal, is attached to the top of the tank near the mid-section to view from above the trailing vortex pair and the surface disturbances. As the shadows of the surface disturbances rather than the disturbances themselves were photographed and video-taped, a single light was positioned along the axis. Ideally, one needs fairly strong parallel rays of light at the test section. Nearly the same results are achieved by a strong light source, far enough to reduce glare and parallax, yet near enough to produce sharp images (shadows) of the surface disturbances. Flat black sheets were placed on the side walls to eliminate undesirable reflections.

Two major modifications were made to the towing basin for the current investigation. A movable platform was constructed on the upper set of rails for mounting different cameras and for suspending high-intensity lamps. A 2-inch hole was drilled partway up and near the end wall of the tank for drainage and recirculation to minimize or to remove, prior to each experiment, airborne contaminants and other flow-visualization particles (e.g., aluminum powder) which may have otherwise affected the physical characteristics of the free surface.

A streamlined flat plate, with a cross section of a NACA 0012 foil, was used in the experiments. The model was mounted on its base by means of a thin streamlined bar with a cross section of a NACA 0006 foil and set at a 12-degree angle of attack. This lifting body and configuration was chosen partly because it best illustrates the surface disturbances produced by a trailing vortex pair and partly because additional data (Gray 1985) about the mutual induction of the vortices generated by it were already available (see Appendix B).

2. Test Procedure

The model was mounted on the carriage and set at a negative angle of attack of 12 degrees. Then the basin was filled up to the desired level and allowed to sit for sufficiently long time to eliminate any internal currents in the basin. In all cases, a transparent ruler, placed on the water surface, and its shadow at the bottom of the basin, were photographed or recorded on video tape in order to establish the proper scale ratio between the actual disturbances, their shadow, and the ruler. Then the appropriate method of recording the experimental run was chosen and the model was set in motion at the desired speed.

For thermal-imaging, the infrared camera was mounted on the platform, energized and its electronics were tested while the basin was filling. Prior to running the model, the water surface was heated uniformly with heat lamps for 3 to 5 minutes. The camera's sensitivity and base level temperatures were adjusted such that the water surface was at the high end of the temperature band. The trailing vortices brought up colder water as they rose to the surface. This gave rise to widely spaced

bands of lower temperature normal to the direction of the model's movement (a manifestation due to the birth of the striations). The bands elongated and thickened as newer bands emerged in the spaces between the existing ones. This process of multiplying and spreading of the striations continued until there was a well defined region of V-shaped colder water, bordered by the scar fronts. Thermal-imaging showed the creation, evolution and demise of the striations but was unable to show the finer structure of the scar front.

When taking time-lapsed photography of the disturbances, the water was dyed a dark blue color. This provided excellent contrast between the water surface and the aluminum particles which were sprinkled sparingly on the water surface just prior to the model run. Initially, photographs with several configurations of lighting and shutter speed were taken to determine the best configuration. The best shutter speed was between 1/15-th and 1/8-th of a second: A slower shutter speed produced cluttered and overlapping pathlines, a faster shutter speed produced pathlines which were too short. With the optimal configuration, the runs were repeated to photograph all stages of the life-history of the surface disturbances (Figure 11).

The video cameras were also mounted on the platform to record the surface disturbances for real-time motion analysis. With a light sprinkling of aluminum powder on the surface, it was possible to delineate some of the general features of the scars and striations. As the vortices rose, the powder was pushed into bands, separated by clean spaces (striations). Eventually, the region between the scars had very little or no

powder, indicating that the striations had vortex-induced lateral currents (in opposite directions in the two halves). Flow visualization by aluminium markers also helped to show the mean pathlines in the scar front.

The shadowgraph technique was also used to observe the surface disturbance characteristics. The shape, position and motion of the surface signatures were projected onto the bottom of the tank which was covered with a line-engraved Plexiglass sheet coated with a highly reflective substance. The surface signatures were recorded on tape, through the use of the inclined mirror, until they had completely disappeared. Previous studies (Henderson 1984 and Gray 1985) used high-speed Polaroid film, and have accurately described the creation and growth of the striations, their progression into scars, and diffusion of the scars into the surrounding media. This is a rather remarkable feat considering that they were using only still photography. However, still photography is not able to show the mutual interaction of the small scale structures within the wake.

B. THE MULTI-PURPOSE BASIN

1. Equipment Description

This basin, made of aluminum and Plexiglass, measured twelve feet long, three feet wide, and four feet deep (Figure 12). An internal Plexiglass wall, painted black, was installed six inches behind the transparent front wall. The internal wall was six feet long and rested on a false bottom of the tank, about 8.5 inches above the actual bottom. The false bottom hid the gears and rods comprising the vortex generating mechanism. Additional equipment associated with the tank is the

plumbing used to fill and drain the basin as well as the collimated light source used to illuminate the test area.

A rising vortex pair was generated through the use of a streamlined nozzle, mounted on top of a piston chamber. The piston was actuated by a solenoid which released a group of weights attached to a wire line; a set of gears and a system of pulleys connected to a rod then forced the piston smoothly upwards, generating two oppositely-signed vortices. The Froude number of the rising vortex pair was varied by controlling the weight on the wire line and the stroke of the piston. The vortices generated using this nozzle had superior quality to those generated by other methods.

For flow visualization, a fluorescein dye was introduced at the inner walls of the nozzle from a flow control valve, just outside the water basin and near the dye exit.

2. Test Procedure

The tank was first filled to the desired level and allowed to sit until the fluid had come to rest. Water level was varied throughout the experimentation to assess its effect on the stability of flow within the Kelvin oval. While waiting for the fluid to come to rest, the piston was placed at the bottom of its stroke and the weights reset. With the fluid at rest, the dye was slowly introduced into the system. When the dye had risen just above the tips of the streamlined nozzle, the video recording system was set to run. The weights were then actuated creating the vortex pair. The vortices rose by their mutual induction velocity and formed a Kelvin oval (Figure 2). As it will be discussed in greater detail later, the oval did not remain two-dimensional and developed three-dimensional short-wavelength

instabilities. These instabilities, resembling corrugations, eventually became the initial striations when the vortices reached the surface. As the vortices continued to rise, the free surface started to deform, leading to the formation of scars. The scars then propagated outward, slightly ahead of the vortices.

C. THE VORTEX GENERATING TANK

The vortex generating tank was constructed after the observance of regular striations in an otherwise two-dimensional vortex flow field. It was desired to generate vortex pairs with a larger aspect ratio, i.e., 18-inch instead of 6-inch long line vortices. This was necessary in order to ascertain the wall-affects on the stability of the Kelvin oval and of the observed striations. Also a new facility was needed to investigate the stability of the rotational flow resulting from the motion of two adjacent counter-rotating cylinders (of identical diameter and angular velocity), at a prescribed depth below the free surface. Prior to the construction of a new tank some experiments were conducted with rotating cylinders in the multipurpose tank to determine to feasibility and practicality of the idea.

1. Equipment Description

The tank, 6 feet long, 18 inches wide, and 18 inches deep, was constructed from 1-inch Plexiglass sheets (Figure 13). It was mounted on a wooden structure for ease of observation and photography. The support structure could be canted up to 7 degrees from the horizontal using jacking screws. The auxiliary systems associated with the tank included plumbing, an air compressor with reducer, and an electrical power source.

An 18-inch long streamlined nozzle, similar to that used previously, was fitted to the bottom of this tank. A pneumatically-actuated cylinder was fabricated to generate the vortices. The actuating cylinder was divided into two chambers by a piston, the lower chamber was connected to an air line and the upper chamber was filled with water and connected to the vortex generating chamber. When triggered, air from a solenoid-actuated valve forced the piston upwards. Water was pushed through the streamlined nozzle, creating the vortex pair without the bottom effects. The air was then vented from the lower chamber and the actuating piston was reset by hydrostatic pressure. The Froude number of the rising vortex pair was controlled by varying the stroke of the piston and the pressure of the compressed air.

To visualize the flow patterns created by the rising vortices, slightly buoyant fluorescein dye was introduced at several points along the inner walls of the nozzle from the dye control valves, located just outside the water basin. To improve contrast in photographs, the fluid in the tank was dyed a different color. Additionally, thin sheets of white and/or black Plexiglass were used to achieve mixed contrast in order to outline the undulations in the striations (Figure 14).

The tank was also constructed to house the rotating cylinders. Operation with the rotating cylinders and the streamlined nozzle was mutually exclusive due to interference with each other. With the streamlined nozzle installed, the rotating cylinders were removed, and vice versa. The two cylinders were mounted in their bearings on removable plates cut out of the side of the tank. The removable plates allowed several

sets of cylinders to be used with variable spacing between them. On one side of the tank a shaft coupled to each cylinder penetrated the tank through a water tight fitting. The shafts were connected to a set of gears through a belt and pulley system (Figure 15). The gears were driven with a variable speed, reversible motor. The cylinders were painted with a reflective white paint to enhance the contrast when using the shadowgraph method.

2. Test Procedure

The procedure for using the streamlined nozzle was identical to that described above except for the method of generating the vortex pair. Using the jacking screws, the streamlined nozzle was tilted from the horizontal to generate an inclined vortex pair. The scar pattern produced on the free surface was therefore slightly divergent. No analysis was conducted to determine the relationship between the angle of divergence of the scars and the angle of inclination of the nozzle. However, it was noted that an approximate 1-to-1 correspondence exists, i. e., a 3-degree inclination from horizontal produced about a 3-degree angle of divergence.

With the streamlined nozzle removed, the cylinders were installed. After filling the tank and connecting the pulleys with belts, the drive motor was started. Water level and rotation speed were varied to determine their effect on the generation of striations and scars. The rotating cylinders simulated the instantaneous circulation produced by two vortices. By controlling the water level, various stages of striation and scar development could be observed.

Both shadowgraph and surface markers were used in the flow visualization. The experiments were video-taped from different angles with

17

different background lighting. Experiments with the streamlined nozzle were brief and the entire event occurred in about a second. The rotating cylinders produced an interesting quasi-steady flow and allowed the indefinite observation of various instabilities as well as the mutual interaction of surface whirls.

D. THE COMPUTING FACILITY

Following extensive observations and measurements, the vortex dynamics or the vortex-element method was used to simulate the phenomenon. In doing so, the most important features to be reproduced by this or any other model was formulated and a numerical code, with very little or no sensitivity to the perturbations in the input parameters, was developed.

The simulation was conducted on a VAX-2000 workstation connected to a MicroVax II server via DECnet[1]. The numerical analysis was coded in FORTRAN-77 (Vax extension), using the resources of the STAT/Library[2]. The plots and graphs were made using routines from the DISSPLA Library[3].

---

[1]VAX-2000, MicroVax II, and DECnet are products of the Digital Equipment Corporation.

[2]STAT/Library is a Registered Trademark and contains proprietary software copyrighted by IMSL, Inc.

[3]DISSPLA is a Registered Trademark and the library contains proprietary software copyrighted by Computer Associates, Inc.

III. NUMERICAL SIMULATION

A. INTRODUCTION

In this investigation, b_0, V_0, and Γ_0 have been chosen as the fundamental reference length, velocity, and vortex strength, respectively, and all lengths have been normalized by b_0, all vortex strengths by Γ_0, all velocities by V_0, and all times by b_0/V_0 (Figure 16). The distance b_0 and the circulation Γ_0, characterizing the initial state of the vortex pair, are related by

$$V_0 = \frac{\Gamma_0}{2\pi b_0}.$$ (1)

The numerical model embodies the mutual interactions of the whirls on the free surface, beginning with their creation, through the use of a two-dimensional discrete vortex method (see e.g., Sarpkaya 1989). The results of the previous investigations (Henderson 1984, Gray 1985, Sarpkaya et al. 1988), and the experimental results obtained in this investigation helped to define the parameters necessary for the construction of the numerical model. As shown in Figure 17, the position of the inboard edge of the scar band is denoted by s, the width of the scar band by w, the average spacing of whirls in the longitudinal direction (a measure of whirl population density per unit length) by c, and the velocity imposed on the free surface due to the main vortex pair by V_b. Note that V_b is normal to the scar band. A right-handed coordinate system has been defined in the complex plane where the real x-axis is parallel to the scar bands and the imaginary y-axis is

19

perpendicular to the scar bands. Ideally, the length of the scar band should extend from $-\infty$ to $+\infty$. However, this is not numerically possible. Instead, a finite scar length L, defined by

$$L = c\,N_w\,,\qquad\qquad(2)$$

and extending from $(-\frac{L}{2},y)$ to $(\frac{L}{2},y)$, is used. N_w is the number of whirls in each scar band.

B.   METHOD OF CALCULATION

In many of the calculations used for modelling vortex dynamics, a parameter representing the core radius (r_c) appears. For the present investigation r_c is taken to be proportional to the square root of the whirl strength. For each time step, the whirl core is given a solid-body rotation of angular velocity ω. The whirl strength can then be written as

$$\Gamma_w = 2\pi\,r_c V_t = 2\pi\omega\,r_c^2\,,\qquad\qquad(3)$$

where the tangential velocity at the core boundary is $V_t = r_c\,\omega$. The angular velocity of the whirl core was determined from observations of the slow-motion video-tapes made from the laboratory experiments and was found to be in the range from about 0.6 ~ 1.2, after normalization. Thus, the core radius is given by

$$r_c = \sqrt{\frac{\Gamma_w}{2\pi}}\,,\qquad\qquad(4)$$

where now ω is taken to be the nearly average value of unity.

20

The numerical analysis began by randomly placing the whirls into two parallel scar bands,

$$z = \left[Rnd_1 L - \frac{L}{2} \right] + i Rnd_2 w, \tag{5}$$

where z is the position of the whirl center and Rnd_1 and Rnd_2 are independently seeded random numbers with a uniform distribution from 0.0 to 1.0, inclusive. Each whirl is also assigned a vortex strength in a random manner,

$$\Gamma_w = (Rnd_3 \Gamma_m)(-1)^{Rnd_4}, \tag{6}$$

where Γ_w is the strength of a whirl, Γ_m is the mean absolute value of all of the whirl strengths, Rnd_3 is a random number from a standard normal distribution (with a mean of Γ_m and a standard deviation one-quarter the expected range of the whirl strengths), and Rnd_4 is a random integer from 1 to 10, inclusive. (Figure 17)

When two or more whirl cores overlap, they are amalgamated into a single whirl, i. e., amalgamation occurs if the distance between whirl centers is less than a critical distance ε, where ε is the sum of the core radii. From equation (4), it follows that

$$\varepsilon = \frac{\sum \sqrt{\Gamma_k}}{\sqrt{2\pi}}. \tag{7}$$

The strength of the combined whirl is the sum of the strengths of the original whirls and its position is the center of vorticity, given by

21

$$z = \frac{\sum \Gamma_k z_k}{\sum \Gamma_k}.$$ (8)

Like-signed whirls merge into a larger whirl and oppositely-signed whirls partly annihilate each other and merge into a smaller whirl. If the resulting whirl strength is below a minimum threshold, the whirl is removed from the scar. The amalgamation process does not conserve total vorticity nor is the linear or angular momentum conserved due to the merging of oppositely-signed whirls and the removal of weak whirls. Nevertheless, the conservation of these quantities is not considered important for a number of reasons. First, the purpose of the simulation is not an exact treatment of the viscous diffusion although the removal of very small whirls do in fact accomplish this purpose indirectly. Second, the random nature of the distribution has far greater effect on the mutual interaction of the whirls than the occasional amalgamation of the whirls. Third, the calculations with different ranges of the fundamental parameters, such as the whirl density, minimum survival strength (γ_{min}), amalgamation distance, etc., have shown that the fundamental nature of the randomly distributed vortices within a narrow band is to self-limit the amalgamation process and to reduce the effect of the large variations in the parameters on the resulting characteristics of the scars.

For an incremental time step Δt, the mutual induction velocity of each whirl is calculated using a cutoff scheme similar to that first proposed by Rosenhead (1930):

22

$$\frac{\Delta z}{\Delta t} = u - iv = \sum_{k} \frac{i\Gamma_{k}}{2\pi(z-z_{k})}\left(\frac{|z-z_{k}|^{2}}{|z-z_{k}|^{2}+\delta^{2}}\right).\qquad(9)$$

The cutoff parameter δ is proportional to the sum of the core sizes. Numerical experiments were conducted to determine the constant of proportionality for δ which most closely agreed with data as well as with that previously used by others,

$$\delta = \frac{0.5}{\sqrt{2\pi}}\left(\sqrt{\Gamma_{w}} + \sqrt{\Gamma_{k}}\right).\qquad(10)$$

The selected constant of proportionality, $0.5/\sqrt{2\pi}$, nearly corresponds to that used by Krasny (1987). Each whirl is moved to a new position, after the calculation of the induction velocity, using

$$z(t+\Delta t) = z(t) + \left\{u + i[v + V_{b}]\right\}\Delta t,\qquad(11)$$

and then the whirl-energy density or the specific energy in the system is estimated through the use of

$$E \propto \sum_{k}(V_{t})_{k}^{2} \propto \sum_{k}\Gamma_{k}\omega_{k}.\qquad(12)$$

The diffusion of vorticity due to viscosity is introduced artificially by reducing the strength of each whirl by the same percentage each time step, in a manner similar to that done previously by others (for details see, e.g., Sarpkaya 1989). Numerical experiments did not show a significant dependence on this circulation reduction. Thus, a factor specified by

$$\Gamma(t+\Delta t) = 0.995 \ \Gamma(t) \qquad\qquad (13)$$

was used in the calculations.

A few additional features of the model need to be explained. These concern the creation of the whirls at early times, sensitivity analysis, and the selection of the numerical parameters (c, s_0, w, Γ_m, δ, ϵ, N_w, Δt, γ_{min}). During the initial periods of the numerical experiments, whirls were created to simulate the physical observations which have shown that the whirl generation spans the period during which the striations recede. The sensitivity or lack of sensitivity of the predictions to the parameters involved in the simulation was examined with great care and full awareness of its consequences. Accordingly, every significant parameter involved in the calculations was varied within reasonable limits. For example, c was varied by 200 percent and w was varied from 0.0 to 0.4. The other parameters, such as Γ_m, δ, ϵ, N_w, Δt, γ_{min}, were varied by at least 100 percent.. The initial inboard position of the scar front s_0 was kept at the experimentally-observed value of 1.6 and was not varied further since it naturally increased as a function of time and since it influenced only indirectly the mutual interaction of the two scar strips. Several runs were made with identical sets of parameters, changing only the seeding of the random numbers involved, in order to ascertain that the insensitivity of the results and basic conclusions to the variation of the parameters selected was not a consequence of the use of a particular set of random numbers. In fact, the randomization was performed by the computer using the system clock time at the commencement of each run.

24

Several plots were created at regular intervals during the execution of the numerical simulation which were terminated at times corresponding to the disappearance of the surface structures in the experiments: The position-plot of whirls (Figure 18), the instantaneous streamlines of the flow field with (Figure 19) and without (Figure 20) the contribution of the transport velocity V_b of the vortex pair, and a plot of the vectored velocity field of the two scars (Figure 21). At the conclusion of the simulation, more plots were created for the purpose of comparison with the results of flow-visualizations: A plot of pathlines (Figure 22) and a similar plot of streaklines, a graph showing the energy density or the specific energy of the whirl constellation as a function of time (Figure 23), a three-dimensional plot describing the evolution and cascading of whirl strength (Figure 24), and the distribution of whirl strength as a function of time (Figure 25).

IV. DISCUSSION OF RESULTS

A. EXPERIMENTAL RESULTS

The experimental observations and measurements will be discussed in three separate but closely related items. The first will be the characteristics of the surface signatures generated by a trailing vortex pair; the second, the vortex pair resulting from a streamlined nozzle and its interaction with the free surface; and the third, the flow instabilities resulting from the motion of two counter-rotating cylinders. The first case will deal with the three-dimensional nature of the surface disturbances, the second with the demonstration of the fact that even two-dimensional vortex pairs lead to three-dimensional structures, and the third with the argument that even though the surface impurities certainly contribute to the development of surface shear stresses, and thereby to the generation of some new vorticity, the presence of surface contamination is neither necessary nor sufficient for the formation of scars and striations. Subsequently, there will be a discussion of the relationship between the generation of striations and whirls, the evolution of the short wavelength instability, and the residual vorticity carried to the free surface, which will result in the formulation of a physical model of the phenomenon.

The path of a vortex pair generated by trailing vortices has been discussed in detail by Sarpkaya et al. (1988). The surface disturbances created by the pair are characterized by three basic features. The first is the appearance of isolated hump-like striations normal to the axes of the vortex pair, then the inception of scars parallel to the vortex pair, and finally, two

fully-developed scar bands, comprised of numerous randomly distributed whirls, separated by a region of relatively small striations (Figures 1 and 3-4).

The detailed analysis and observations of scars, whirls, and striations were made through the use of image processing. The thermal-imaging showed the creation, evolution and demise of the striations but was unable to show the finer structure of the scar front. It is because of this reason that only the observations and measurements made through the use of the shadowgraph technique will be discussed herein.

The recordings have shown that a striation rises to a maximum height, as the two ends of the ridge plow through the medium in directions normal to the vortex pair. Then the ridge falls back, as the two ends exhibit whipping motions in a more or less random manner (similar to that of the tail of a fish near the free surface). These give rise either to symmetrical whirl pairs (see, e.g., the Kelvin oval, marked A in Figure 3) or to numerous asymmetrical whirls. It is not implied here that the whipping motion or the meandering of the scar front is entirely responsible for the generation of vorticity that goes into a whirl, but, it is emphasized that the whipping motion is responsible in organizing the existing vorticity into whirls.

Figure 1 shows that the inception of scars and whirls occur some time after the creation of striations. This experimental fact has already been used in the evolution of the numerical model as far as the creation of whirls is concerned. Additional observations of the above cited figures show that as one goes through the transition from the pure-striation phase to the fully

developed scar-phase, the number of striations increase rapidly as the amplitude of the striations decrease.

It is a well-known fact that in a homogeneous fluid, vorticity generation results from the tangential acceleration of a boundary, from tangential initiation of boundary motion and from tangential pressure gradients acting along the boundary. Thus, the major source of vorticity is the lifting surface in the case of trailing vortices and the streamlined nozzle in the case of the nearly-two dimensional vortex pair. As the vortices approach the free surface, some vorticity of opposite sign is produced at the surface due to the surface tension gradients. The amount of the oppositely-signed vorticity depends on the degree of surface contamination. However, the surface tension always exists at a free surface (due to intermolecular cohesive forces) regardless of whether or not the interface is contaminated by agents foreign to either fluid. The interaction of the vortex pair and the surface vorticity cause some mutual annihilation of vorticity and move the center of vorticity away from the free surface. This phenomenon is known as the rebounding of trailing vortices and is particularly pronounced in trailing vortices approaching a rigid wall, as in the case of aircraft trailing vortices approaching the ground. Thus, the vorticity resulting from the fluid motion near a contaminated surface has some bearing on the phenomena discussed herein. The fundamental question to be resolved is this: Is the contamination-generated vorticity (as in the case of Reynolds ridges) entirely responsible for the observed phenomena (scars and striations) or is it just an unwelcome and unavoidable phenomenon tending to obscure the basic facts?

Experiments reported herein were carried out with freshly-skimmed surfaces (nearly uncontaminated free surfaces). In general, the contaminated surface has a viscosity much higher than the bulk viscosity of water and behaves as a highly stratified layer between air and the fresh medium below the free surface. Thus, it can serve as a source of new vorticity, as noted above, and the whipping action of the ends of a striation ridge is exactly the type of fluid motion needed to convert that vorticity into whirls. What is missing from this description is the explanation of the source or the cause of striations and whether the mechanisms which give rise to striations are also responsible for the transportation of a fraction of vorticity of the main vortex pair to the free surface.

As seen in Figure 1, the striations do not generate whirls as they rise into existence even though they create large surface tension gradients. Thus, it would not be acceptable to say that it is the surface-tension gradients that lead to the generation of the secondary vortices (whirls). The motion of the striations is further complicated by the fact that they not only multiply in number by division but also occasionally pair to form a slightly 'stronger' ridge. Finally, the striations, after giving rise to whirls, reduce to very small disturbances, filling the region between the fully developed scars. This corresponds, more or less, to the end of the time period during which the vorticity is transferred from the main vortex pair to the scars and reconstituted there into a large number of whirls through the whipping action of the striations.

The striations and/or the scars are neither related to nor are a consequence of the capillary waves. The observations and the calculations based on them, through the use of the video tapes, and the comparison of

the scars with the capillary waves generated simultaneously, but occasionally, by an air bubble have shown conclusively that the two phenomena have nothing in common.

The surface disturbances resulting from the trailing vortices in a towing tank have provided extremely useful information regarding the origin of scars and striations but left a number of unanswered questions: Is the three-dimensionality of the vortex pair (inclination, temporal and convective evolution at a given axial location, velocity distribution in the vortex core (particularly the axial velocity), the method of generation of vortices, and other related phenomena such as the sinusoidal instability of the vortex pair) responsible for the generation of the striations and scars? Or is it possible to obtain similar surface disturbances through the use of an essentially two-dimensional vortex generator? These questions led to the experiments performed in the vortex generating tank.

Figures 26-30 show the evolution of the vortex pair and the free surface. A number of important results can be deduced from these figures and from a careful frame-by-frame perusal of the video recordings of literally hundreds of test runs. The inclination of the vortex pair or the generation of vortices by a lifting surface in a towing tank is not necessary to produce nearly identical or better surface signatures. The three-dimensional instability does not originate at the free surface but rather at the Kelvin oval, long before the latter 'sees' the free surface (Figure 26). The free surface subsequently interacts with and is modified by the instability transported to the free surface by the Kelvin oval. In other words, the short wavelength instability of the vortex pair manifests itself in the form of striations when it encounters a free surface. The striations obtained with

the streamlined nozzle are nearly uniform 'corrugations' normal to the axes of the vortices, at least during the initial stages of their formation. The characteristics of the scar front (Figures 29 and 30) are clearly identifiable and show the creation of whirls. The only contribution of the inclination of the trailing vortex pair is the divergence of the scar lines and the fact that the striations come into existence sequentially rather than simultaneously.

The wavelength λ of the striations has been deduced from numerous runs as a function of the initial spacing of the main vortex pair. The histograms of the striation wavelength have shown that λ/b_0 varies from about 0.75 to 1.25, depending primarily on the initial roll-up of the vortex sheets as dictated by the Froude number. As far as the sinusoidal instability of a vortex pair in an infinite homogeneous medium is concerned, the striational instability corresponds to the short wavelength instability. In the case of the trailing vortices, however, the striations are not always normal to the axes of the vortex pair. Helical disturbances coupled with the short wavelength instability give rise to spiral vortex flow. Such flows have also been observed between concentric counter-rotating cylinders, flow with rotating inner cylinder and a through-flux, just to mention few. In the context of the present study, the phenomenon is rendered far more complex by the interaction of gravitational, centrifugal, and surface tension effects. Thus, what begins as a short wavelength instability quickly degenerates into a far more complex three-dimensional free-surface instability. A single wavelength is no longer discernible. Furthermore, a series of ridges, rising above the free surface and subjected to extremely complex surface-tension distribution and vortex-induced velocities, is far from stable. The strongest *surface-tension concentration*
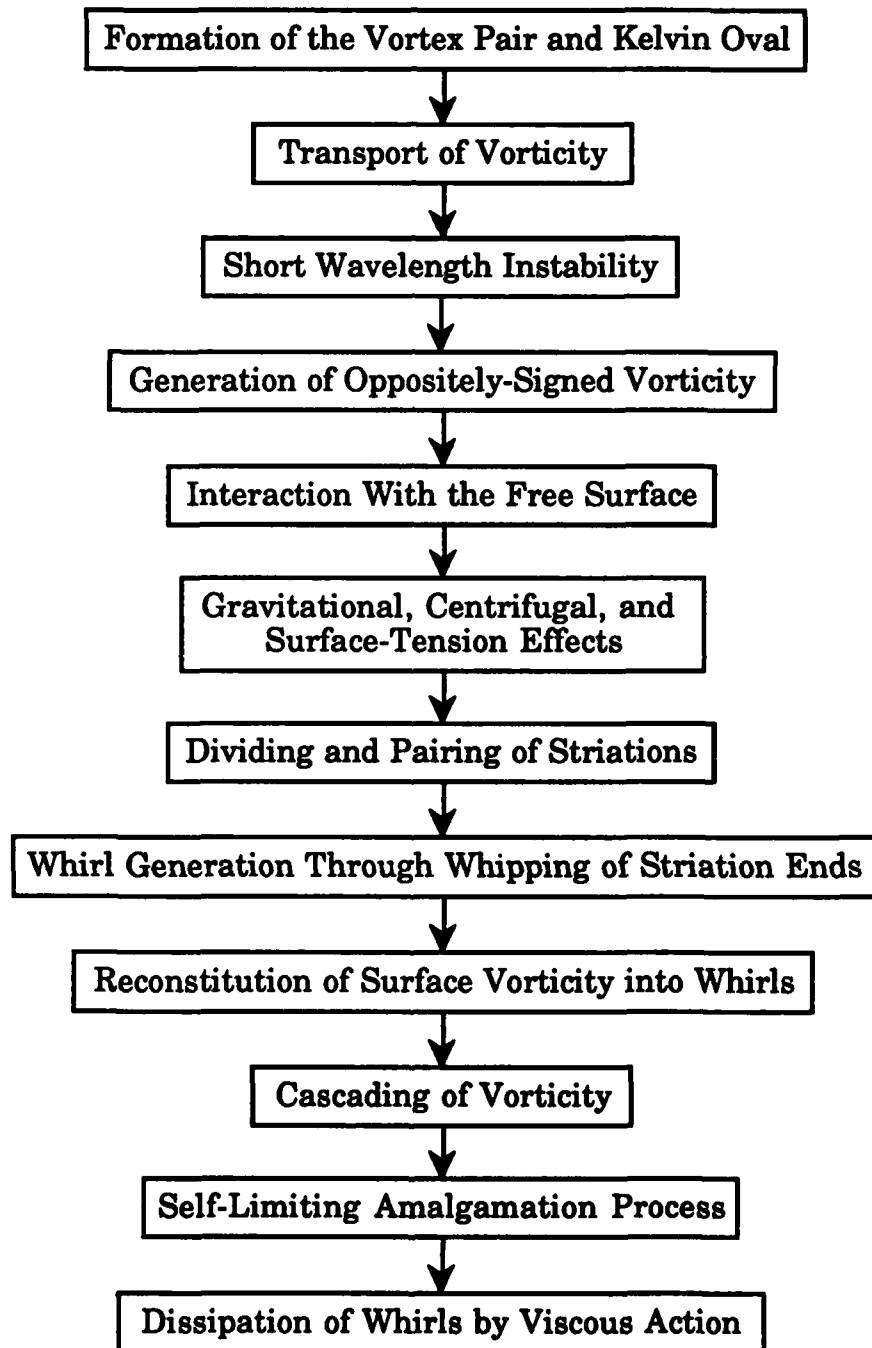
31

occurs near the tips of the striations since these are the obvious natural places for them to occur. Consequently, these are the regions where new whirls could be produced. In fact, the search for an equilibrium leads to the whipping action and its attendant consequences, described in detail previously. This type of structure or whirl formation has not been discussed previously and appears to be unique to the scar generation. The emerging picture for the explanation of the entire phenomenon now needs a brief discussion of the long- and short-wavelength instabilities.

Crow (1970) idealized a vortex pair as interacting line vortices and developed a theory which accounts for the instability during the early stages of its growth. He has shown that there are primarily two types of instabilities: The long wavelength instability and the short wavelength instability. Figure 31 shows the stability diagram for the vortex pair. The shaded areas show the stability regions. The solid curve shows the wavelengths of maximum amplification for each r_c/b_0. The upper curve shows the most unstable long wave, the lower curve the most unstable short wave. The preferred mode of instability at the longest wavelength is $8.6 b_0$. The wave number β for the short wavelength instability varies from about 4 to 17, corresponding to wavelengths of $\lambda = 0.37 b_0$ to $1.57 b_0$. As noted above, the short wavelength in the present investigation varied from about $0.75 b_0$ to $1.25 b_0$. One may hypothesize the possibility that what perhaps started out as an instability may end up as a new steady state, i. e., the short wavelength instability may lead into a stable steadily translating pair of filaments with waves at wave numbers near $\beta = 17$. This will not, of course, occur unless the long wave instability is prevented. To test this hypothesis, experiments were carried out in the towing tank with larger and larger

32

depths of water so as to induce long wavelength instability in the trailing vortices prior to their approach near the free surface. Figure 32 shows that the striations and scars develop in spite of the long wavelength instability.

Experiments with rotating cylinders have shown that even at fairly low angular velocities and at fairly large depths of immersion (as much as one diameter below the free surface), the rotation of the cylinders give rise to striations and whirls. Figures 33-35 show the whirl motion at three randomly selected times. It is clear that neither a trailing vortex pair nor a nearly two-dimensional Kelvin oval, neither a contaminated surface nor a Reynolds ridge is necessary to create scars and striations. The mere presence of two counter-rotating circulations near a free surface is sufficient to create all the phenomena observed in other scar experiments. There is much more to be explored with rotating cylinder experiments. The only purpose of reference to them at this time is to point out that conjectures regarding surface contamination and Reynolds ridge are not necessary. There are, however, fundamental differences between the rotating cylinder experiments and the actual vortex experiments. In the case of rotating cylinders, vorticity is continuously being supplied to the flow by the cylinders while the stationary circulation of water maintains a contaminant-free surface. In the case of trailing vortices, the vortices approach the free surface with the vorticity they are born with and no new vorticity (of the same sign) can be added to vortices. In fact, the oppositely signed vorticity generated at the free surface helps to reduce somewhat the strength of the vortices. This is in addition to the fact that the vorticity diffuses over a larger and larger area with time due to viscous and turbulent diffusion.

The picture emerging from the experimental results may best be described through the use of the event chart shown below.

```
┌─────────────────────────────────────────────┐
│ Formation of the Vortex Pair and Kelvin Oval │
└─────────────────────────────────────────────┘
                      │
                      ▼
        ┌──────────────────────────┐
        │   Transport of Vorticity  │
        └──────────────────────────┘
                      │
                      ▼
        ┌──────────────────────────┐
        │ Short Wavelength Instability │
        └──────────────────────────┘
                      │
                      ▼
     ┌─────────────────────────────────────┐
     │ Generation of Oppositely-Signed Vorticity │
     └─────────────────────────────────────┘
                      │
                      ▼
       ┌────────────────────────────────┐
       │ Interaction With the Free Surface │
       └────────────────────────────────┘
                      │
                      ▼
       ┌────────────────────────────────┐
       │ Gravitational, Centrifugal, and  │
       │      Surface-Tension Effects     │
       └────────────────────────────────┘
                      │
                      ▼
       ┌────────────────────────────────┐
       │ Dividing and Pairing of Striations │
       └────────────────────────────────┘
                      │
                      ▼
┌──────────────────────────────────────────────────┐
│ Whirl Generation Through Whipping of Striation Ends │
└──────────────────────────────────────────────────┘
                      │
                      ▼
   ┌──────────────────────────────────────────┐
   │ Reconstitution of Surface Vorticity into Whirls │
   └──────────────────────────────────────────┘
                      │
                      ▼
        ┌──────────────────────────┐
        │   Cascading of Vorticity  │
        └──────────────────────────┘
                      │
                      ▼
     ┌─────────────────────────────────────┐
     │ Self-Limiting Amalgamation Process   │
     └─────────────────────────────────────┘
                      │
                      ▼
    ┌──────────────────────────────────────┐
    │ Dissipation of Whirls by Viscous Action │
    └──────────────────────────────────────┘
```

The vortices are created with a finite core radius in both the trailing-vortex experiments and the nozzle experiments. These, in turn, form a fairly-well defined Kelvin oval. Contrary to theoretical predictions (because of obvious reasons), the Kelvin oval is not completely closed and there is some drainage of flow and vorticity out of the oval. In addition, the oval is always born near a boundary or nozzle. Thus, it is under the influence of the images of the vortices, even though this influence diminishes rapidly as the oval rises. The oval created by the nozzle sees only the tip region of the nozzle and not the bottom boundary. Thus, the said image-influence is minimized as much as possible.

As the Kelvin oval rises the spiralling vortex sheets in each vortex undergo Helmholtz and, subsequently, Rayleigh instability and, eventually, degenerate into turbulent motion. The distance travelled by the oval more or less determines the sequence of events. In the present experiments the said distance to the free surface has been kept below $6b_0$ in order to obtain a clearly defined oval near the free surface. The vorticity is initially confined to the Kelvin oval and the motion outside it is irrotational. With the passage of time, the vorticity diffuses over a wider area and some vorticity gets annihilated in the overlapping regions of oppositely-signed vorticity. In any case, vorticity is transported towards the free surface. The distance between the vortices during the initial period of rise of the Kelvin oval remains fairly constant but the core radius and, hence, r_c/b_0 increases due to diffusion. As the short wavelength instability begins to grow, the initial value of λ/b_0 in Figure 31 is in the order of unity. Had the cores touched, λ/b_0 would have been as large as 2.45 (point B in Figure 31). However, the vortex cores do not grow to such large sizes, not at least during the short

period of migration of the Kelvin oval toward the free surface. Once the striations appear at the free surface, the interaction of gravitational, centrifugal, and surface tension forces create an extremely complex texture of conditions under which the striations and scars begin to evolve. In the meantime, however, the vortices diverge, as in the case of parallel line vortices approaching a rigid plane, and thus the distance b between them increases. This decreases the mutual interaction of the vortices and the relative wavelength λ/b decreases. It is not, therefore, surprising to see that the striations multiply quickly and concentrate in the regions directly above the vortices and adjacent to the scars (Figures 3-4). The dividing and the pairing of the striations are accompanied by the whipping action described earlier. It is this action that is thought to be responsible for the reconstitution of vorticity, brought near the surface by the vortices, into numerous, randomly distributed whirls.

A number of whirls in close proximity to each other may give rise to a series of complex interactions: Amalgamation, annihilation (at least partially), or a short-time combination and separation. Thus, it is clear that the interaction of three-dimensional whirls, penetrating only a short distance into the fluid, is not a simple matter and needs further study through the inclusion of viscous effects. The amalgamation as well as annihilation is particularly strong during the formation period of the scars. The amalgamation amounts to cascading of circulation into larger vortices and hence to their longer life-span. It is this process that is thought to be responsible for the long length of the SAR images. Evidently, some sort of regeneration process is necessary without violating the principles of conservation of energy and circulation. One could interpret this whirl-

36

growth phenomenon as an indication of an inverted energy cascade. This does not imply an increase in energy with time. In fact, the total internal energy goes down rather than up in spite of the definite growth in whirl size. Thus, whirl-merging leads to an accumulation of energy in the larger structures (i. e., to an up-cascading process in size and energy in fewer whirls while the total energy decreases rapidly). In the final analysis, the energy of the system is dissipated by viscous action and the whirls as well as the scars must disappear. This completes the observed as well as perceived evolution of the surface signatures. It will be interesting to discover as to how the scar band, comprised of whirls, tend to increase the radar return in order to provide bright lines in the SAR images.

B. NUMERICAL RESULTS

Experiments have provided sufficient understanding of the physics of the phenomenon and led to the development of a numerical model which proceeded to the point where many of the physical processes involved in the evolution of the three-dimensional wake can be predicted.

Figures 36-41 show at t = 0.0 − 2.0, at Δt = 0.4 increments, the evolution of the scars and the whirls distributed randomly on them during the time interval t = 0.0 − 0.2. The size of the whirls is drawn proportional to the square root of the strength. A solid circle denotes clockwise circulation and a hollow circle indicates counter-clockwise circulation. Thus, it is seen that the whirls amalgamate as time increases. Additional facts emerging from these figures are as follows: The spacing between the scar bands increases naturally because of the transport velocity imposed on them by the main vortex pair. It is remarkable that the band essentially retains its overall identity even though its width increases slightly due to the mutual

interaction of the whirls. Only rarely that one or two whirls leave the scar band due to mutual induction. This leads to the conclusion that the net velocity induced at any whirl at any moment by the surrounding whirls is rather small due to their random distribution in space and strength. Obviously, the mutual influence of scar bands is small and diminishes rapidly as time increases. Finally, Figures 39-41 show the inception and growth of the long wavelength instability. This comes about because of the fact that the scar length is sufficiently long to allow for its development in a manner expected by the analysis (Figure 31).

Figures 42-47 show the instantaneous streamlines in a small portion of the scar band as they would be seen by an observer travelling with the scar. This type of a plot enables one to see the whirls and compare them with those observed experimentally. In fact a comparison of, for example, Figures 4 and 42 shows the remarkable similarity between the two scar bands. What is more remarkable is the fact that the later stages of the scar evolution in the numerical model compare equally well with those obtained experimentally.

Figures 48 through 53 show the instantaneous streamlines as they would be seen by an observer fixed to the coordinate system. The wide region between the scar bands is fairly calm whereas the scar bands are a constellation of depressions created by the whirls. Figures 54 and 55 show the plot of the vectored velocity field at time 0.0 and 2.0. These figures, as the previous ones, compare quite well with the overall character of those seen in the experiments.

The specific energy of the whirl distribution, the evolution of the vortex strength, and the distribution and cascading of the vortex strength have

been shown previously in Figures 23-25, respectively. The whirls represent a reservoir of rotational kinetic energy, which may be described by an energy density E which is averaged over the total whirl population. Figure 23 shows the specific energy distribution and its decay with time. Figures 24 and 25 show clearly that the total strength of the whirl system decreases with time. However, the amalgamation process does lead to a set of larger whirls. The increase of the number of large structures slows down or stops after a short time period. In other words, the whirl system reaches an equilibrium.

Clearly, the whirl-whirl interaction should contribute most significantly to the evolution of the initial distribution, and such events should occur only if the number of whirls is high enough. In the present calculations, the whirl population has been doubled several times to explore this very question. Furthermore, numerical experiments were carried out with different random-number seedings to ascertain that the results concerning the energy-density distribution and the cascading of the energy did not depend on either the number of the whirls or on their statistical distribution (Figure 56). It has been found that the population density and the number of random samplings are sufficiently large to arrive at statistically meaningful conclusions. The time variations of the distributions, therefore, allow one to estimate whether whirl-whirl interactions are important. The results presented above show that the shift in the size distribution toward larger structures and the concentration of energy in these structures are an important ingredient of the scar formation and scar life-span.

The numerically-simulated scars were intentionally started parallel, with no further intrusion into their evolution in succeeding steps. As described above, the scars evolved, remaining essentially parallel, with the superposition of a long wavelength sinusoidal instability as seen in Figures 40-41. At no time did the scar fronts exhibit a V-shaped divergence as observed in the SAR images. This was entirely expected because it is the sequential evolution of the trailing vortices that give rise to the V-shaped scar bands with an included angle of 2α [where α is $\arctan(V_0/U)$]. It was deemed necessary to apply the numerical model to the trailing vortex case with a few minor differences, partly to further substantiate the predictive power of the model and partly to observe the similarities or differences between the measurements and calculations. The said differences concerned the instantaneous rather than sequential creation of the initial state of the scar band. This is of no particular concern since the structural differences between two points along a sufficiently long stretch of a relatively old scar are quite small. Figures 57 through 60 show the evolution of the scars and the whirls distributed randomly on them, Figures 61 through 64 show the instantaneous streamlines as they would be seen by an observer moving with the scars, and the Figures 65 through 68 show the instantaneous streamlines as they would be seen by an observer fixed to the coordinate system. Finally, Figures 69 and 70 show a comparison of the experimental and numerical results. One half of these figures is a partial reproduction of Figure 4 and the other half is an appropriately-reduced size of Figure 59. A comparison of the two halves show the remarkable similarity between the observations and predictions.

Thus, it is seen that the experimental data, resulting from the analysis of the images, serve both as an input to the numerical analysis and also as a comparison for the predictions at a later time.

V. CONCLUSIONS

The numerical and experimental results presented herein warranted the following conclusions:

1. Three-dimensionality of the vortex pair (as in the case of trailing vortices) is not necessary to produce surface signatures or foot prints of vortex wakes in the form of scars and striations. An initially two-dimensional vortex pair yields similar structures.

2. A fully submerged vortex pair is subject to both long- and short-wavelength instabilities. The latter is particularly prevalent when the former is suppressed. The experiments have revealed their existence and the role played by them in the generation of striations.

3. The short-wavelength instability has a wavelength in the order of unity, compared with the initial spacing of the main vortex pair. The wavelength decreases as the vortex spacing increases.

4. The strongest surface-tension concentration occurs near the tips of the striations. Consequently, these are the regions where the new whirls are created through the use of the surface vorticity. This type of whirl formation appears to be unique to the scar generation.

5. The scar and striation generation may be affected by the degree of surface contamination. However, the changes in surface tension and surface elasticity brought about by contamination, beyond that due to intermolecular cohesive forces, are neither necessary nor sufficient for the creation of striations and scars. The most indispensable ingredients for the generation of whirls are the viscosity of fluid, generation of surface vorticity due to surface curvature, and the unstable motion of the ends of whirls.

Also, it is equally important to note that the so-called Reynolds ridge is akin to but not related to the scar formation. The Reynolds ridges do not give rise to whirls.

6. The numerical simulation of the phenomenon through the use of vortex dynamics or vortex element methods has shown that all of the fundamental characteristics of the scar evolution (e.g., the preservation of scar-band width, whirl distribution, whirl-whirl interaction, energy cascading, mutual annihilation of whirls, self-limiting amalgamation, etc.) are faithfully reproduced.

7. Among the numerous mechanisms proposed to explain the physics of the ship wakes in SAR images, the hypothesis of the interaction of a vortex pair with the free surface emerges as the most viable one in view of the observations and measurements made and the conclusions arrived at in this investigation. It is proposed that the vortex pair (generated by a nozzle or lifting body) gives rise to a Kelvin oval and to the rapid transport of vorticity; this leads to the occurrence of short wavelength instabilities on the Kelvin oval without the effect of a free surface; the interaction of these instabilities with the free surface brings in the effects of gravity, surface tension and centrifugal forces and leads to the formation of striations; the striations occasionally pair but mostly increase in number by division in the course of their rapid evolution; they change the surface physics and in particular the surface-tension concentration zones; this instability leads to the whipping motion and to the reorientation and reconstitution of the vorticity brought near the free surface by the main vortices, culminating in whirls and scars. Thus, it is concluded that the scars and striations in

SAR images are most likely due to vortex wakes interacting with the free surface rather than due to any other source or mechanism.

8.   The above conclusions are further vindicated by the experiments carried out with two rotating cylinders. The analogy between the two types of circulatory motions need to be further explored, partly because such experiments will provide an excellent opportunity to discover many new and interesting vortex patterns and partly because they will lead to the closer examination of the similarities between the striations, whirls, and scars generated by the two types of circulations.
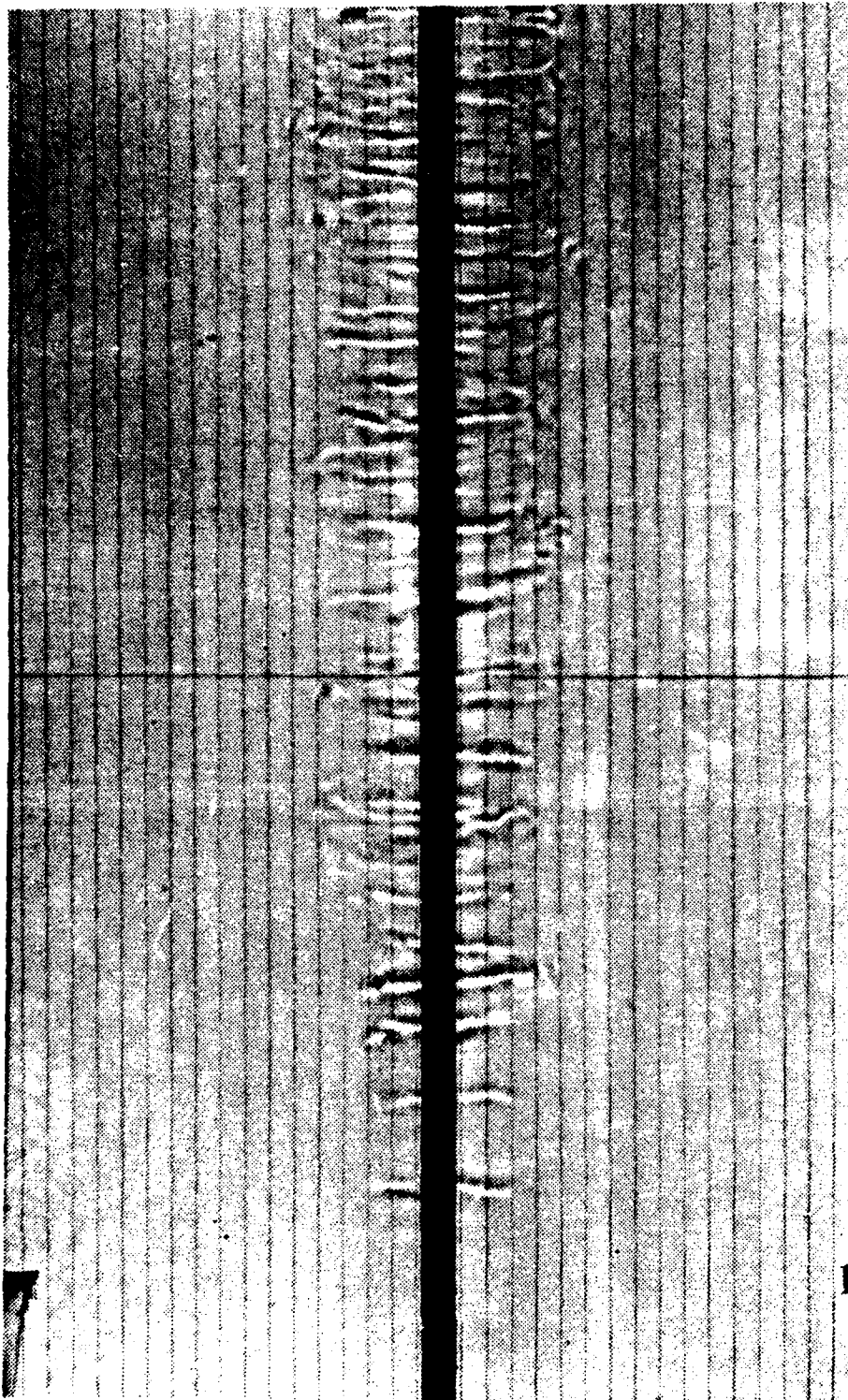
Figure 1   The Appearance of Striations

Figure 2   Cross Section of a Rising Vortex Pair

46
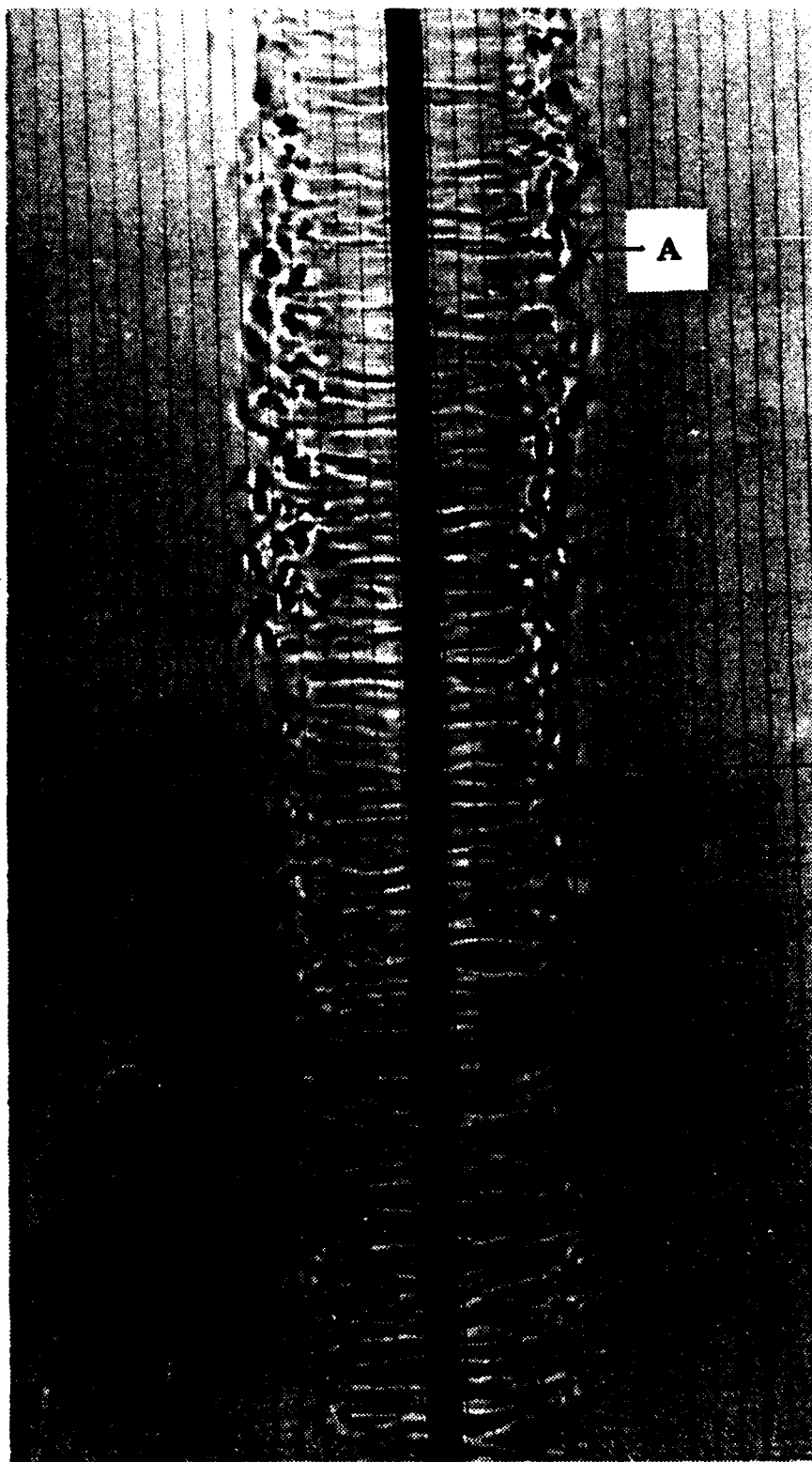
Figure 3   Scar Formation at the End of the Striation Phase

47

Figure 4   The Scar Dominated Phase

48
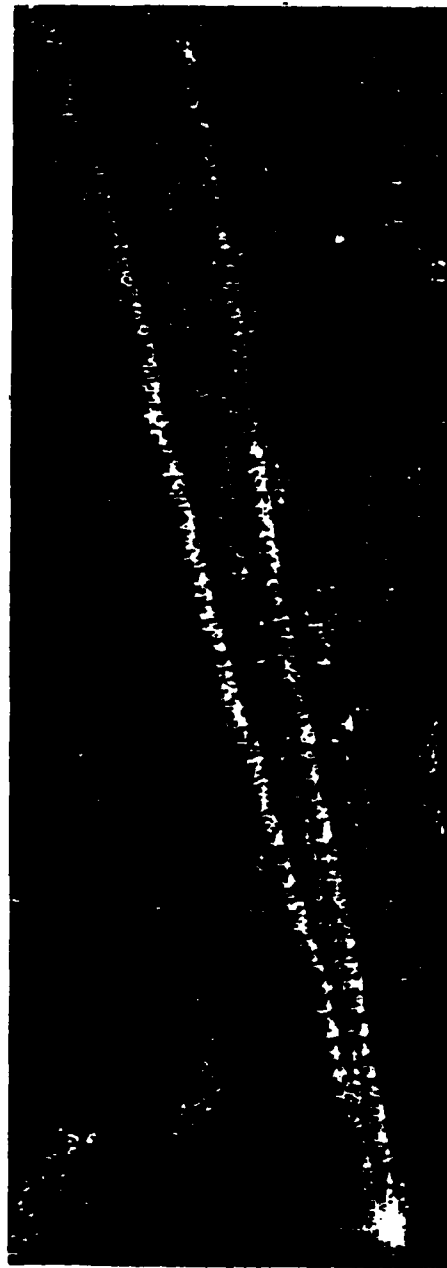
500 m

Figure 5   Striations and Scars in a Synthetic Aperture Radar Image
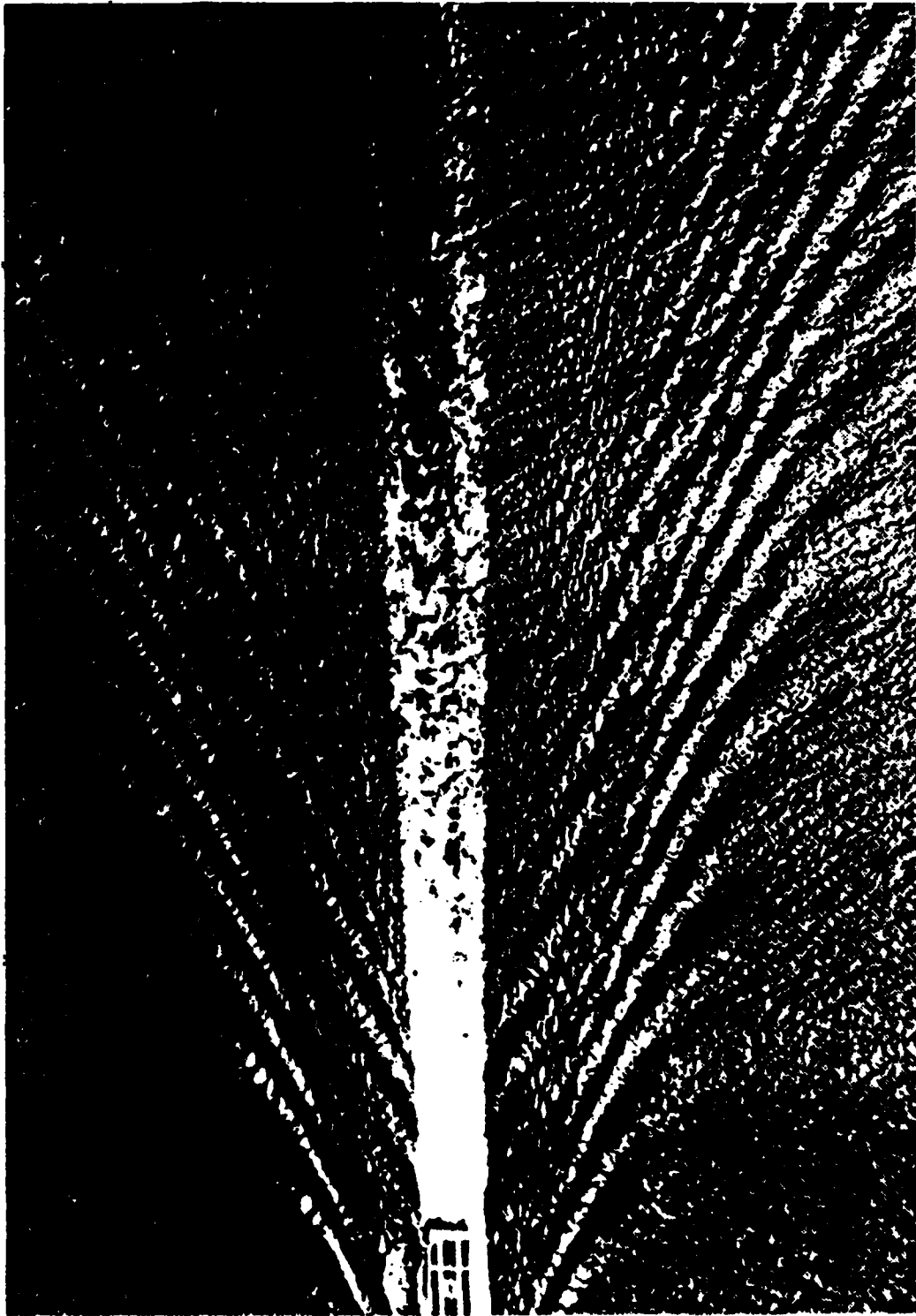
Figure 6   Kelvin Waves Behind a Ship
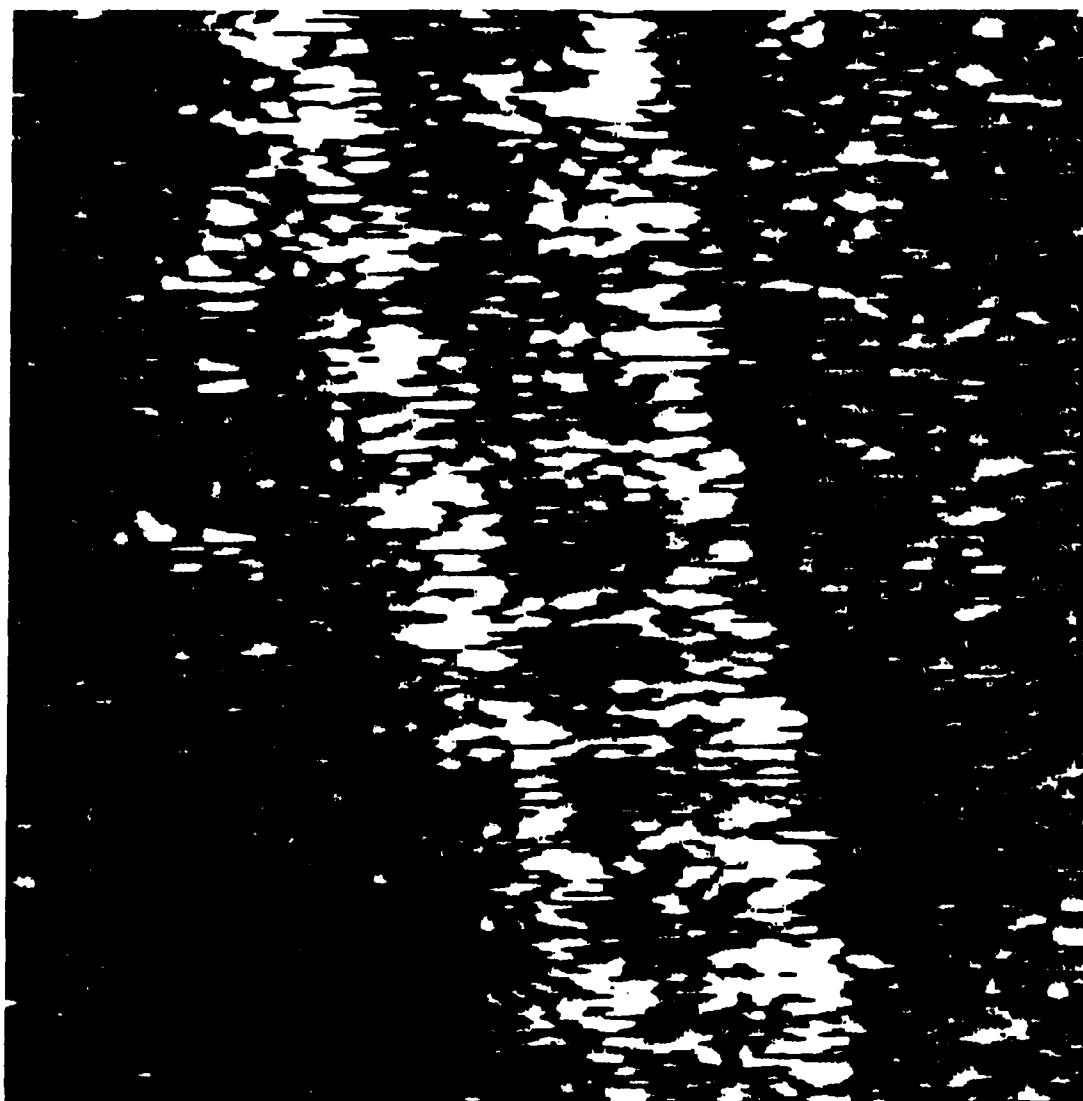
100 m

Figure 7   A Synthetic Aperture Radar Image of a Ship's Wake
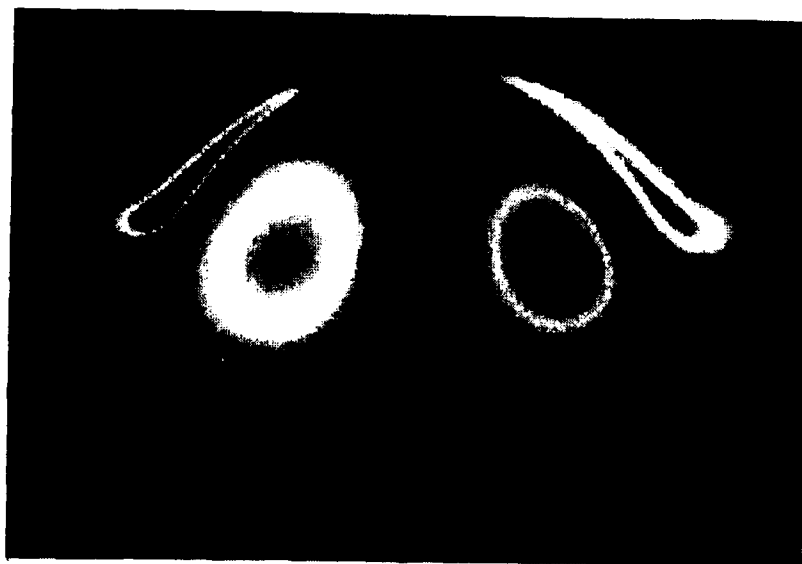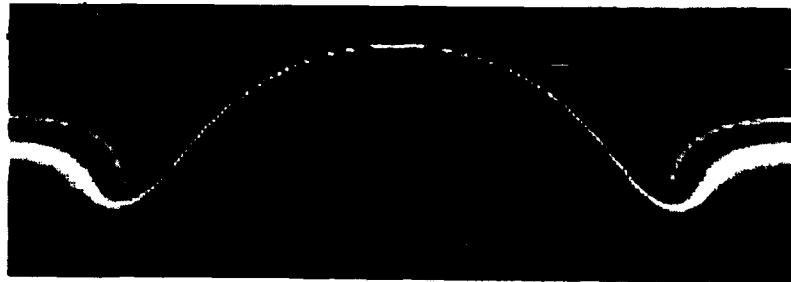
Figure 8   **A Scar Cross Section From Projection Methods**

Figure 9   The Towing Tank

53
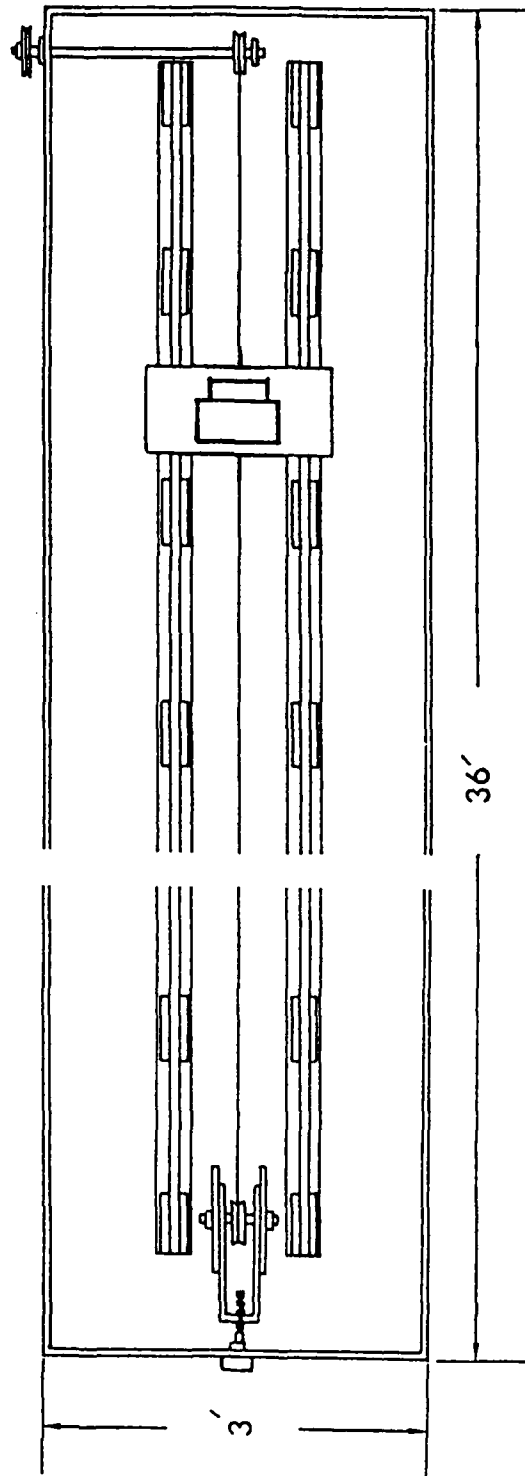
Figure 10   The Towing Carriage

36'

3'

Figure 11   Time-Lapsed Photograph of the Surface Disturbances
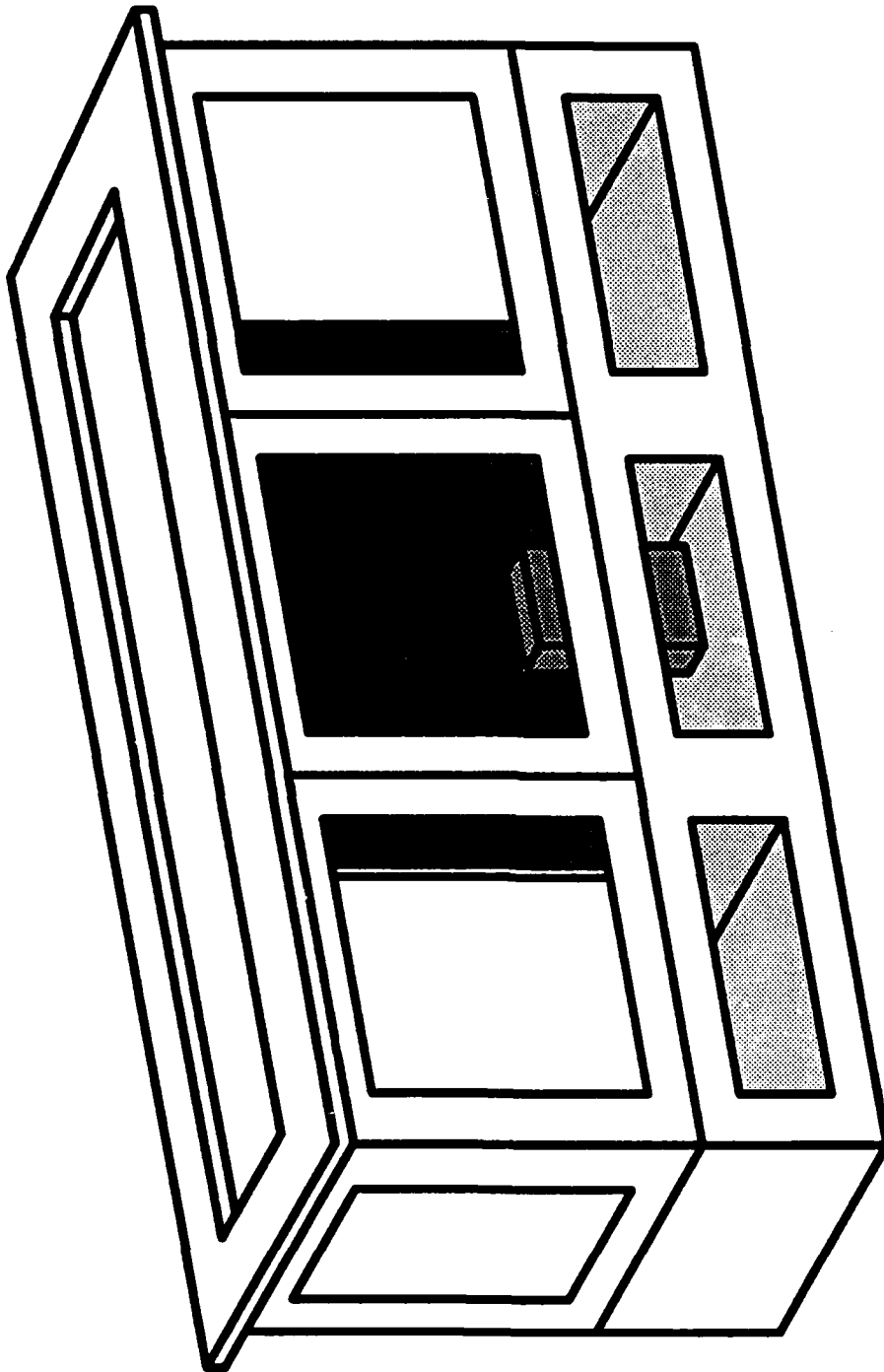
Figure 12   The Multipurpose Tank

Cut-out for the Plate
Rotating Cylinder

Vortex Generator
Vortex Chamber
Piston Chamber
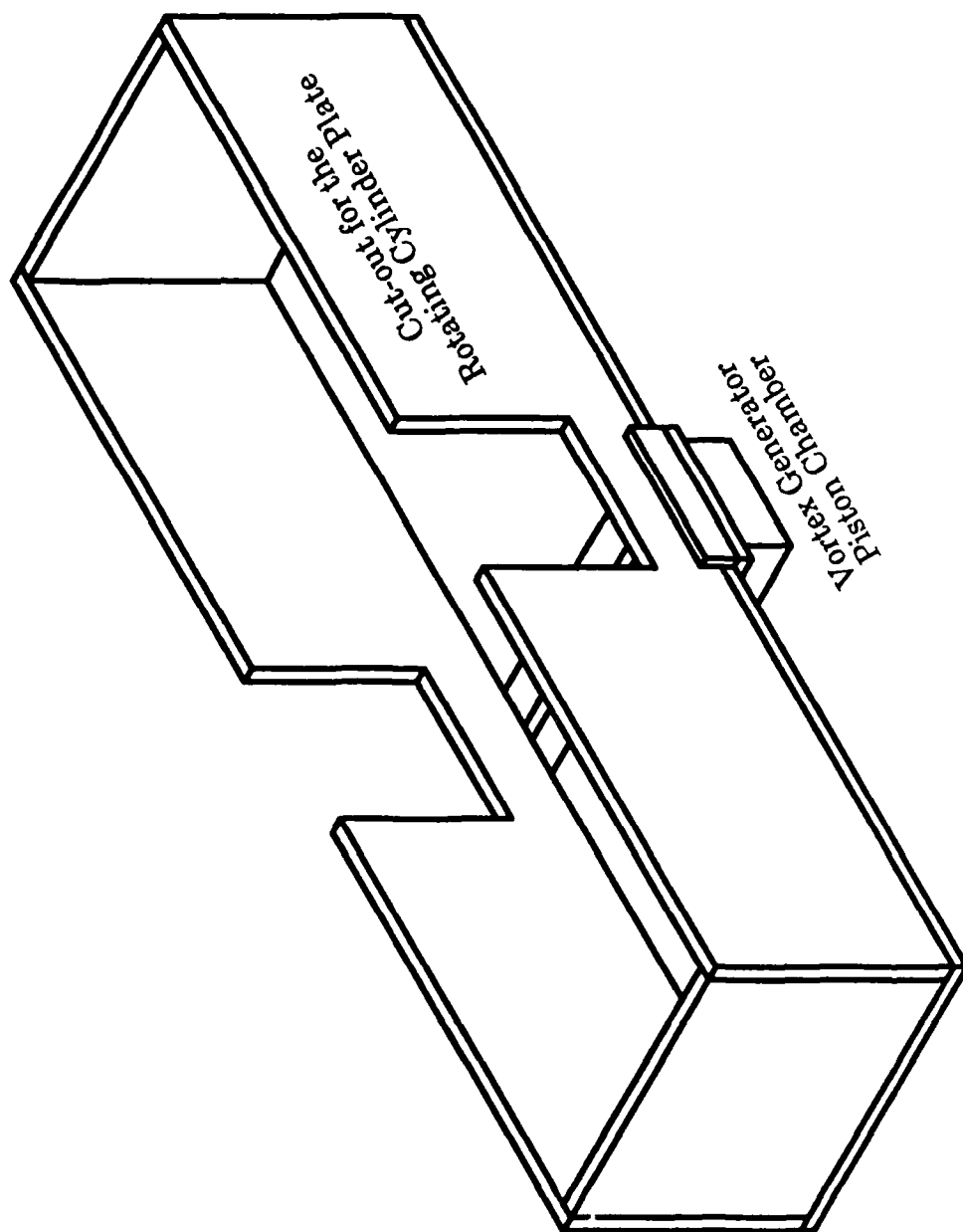
Figure 13   The Vortex Generating Tank

57
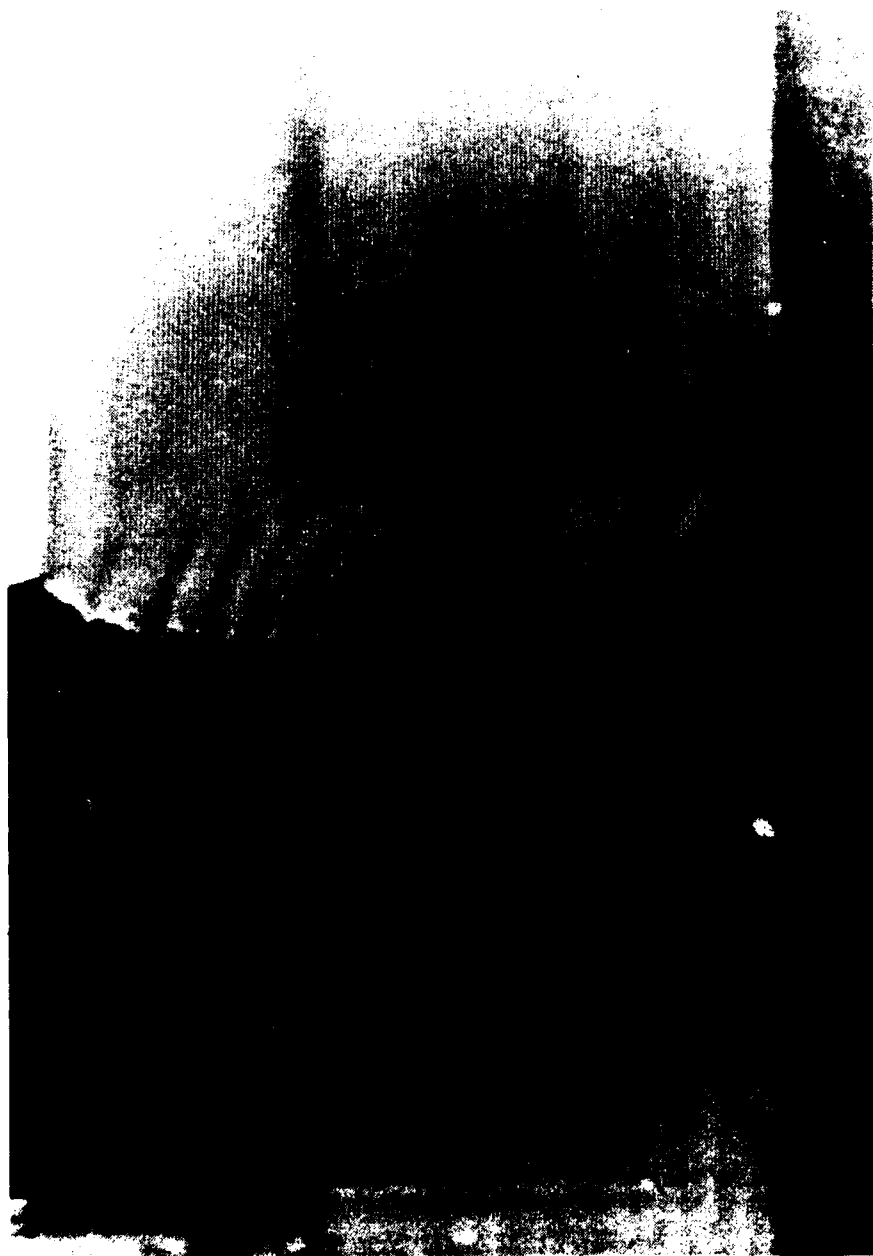
Figure 14   Contrast Control Using Black and White Plexiglass Sheets
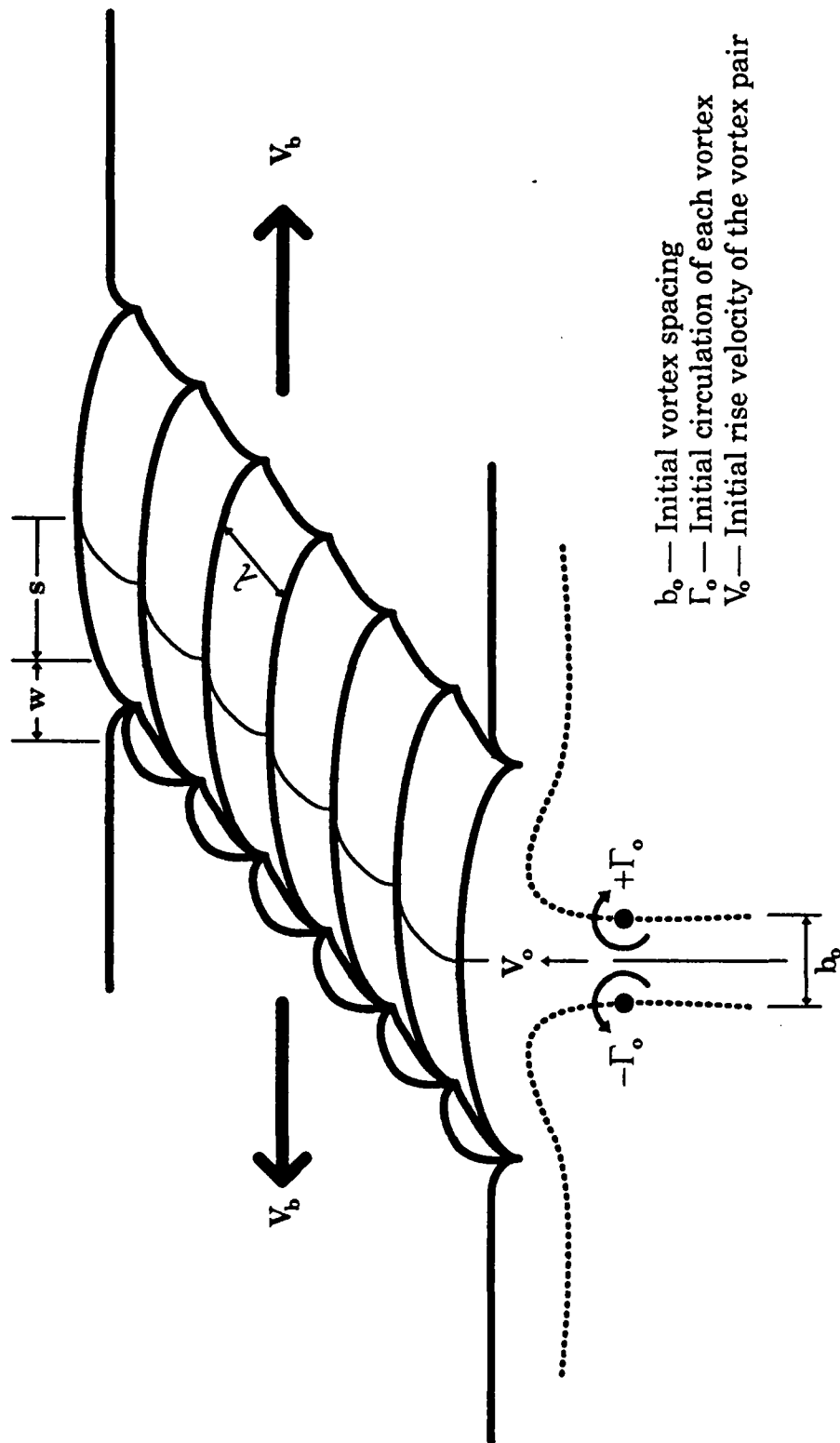
b_o — Initial vortex spacing
Γ_o — Initial circulation of each vortex
V_o — Initial rise velocity of the vortex pair

Figure 16   Fundamental Reference Parameters

59
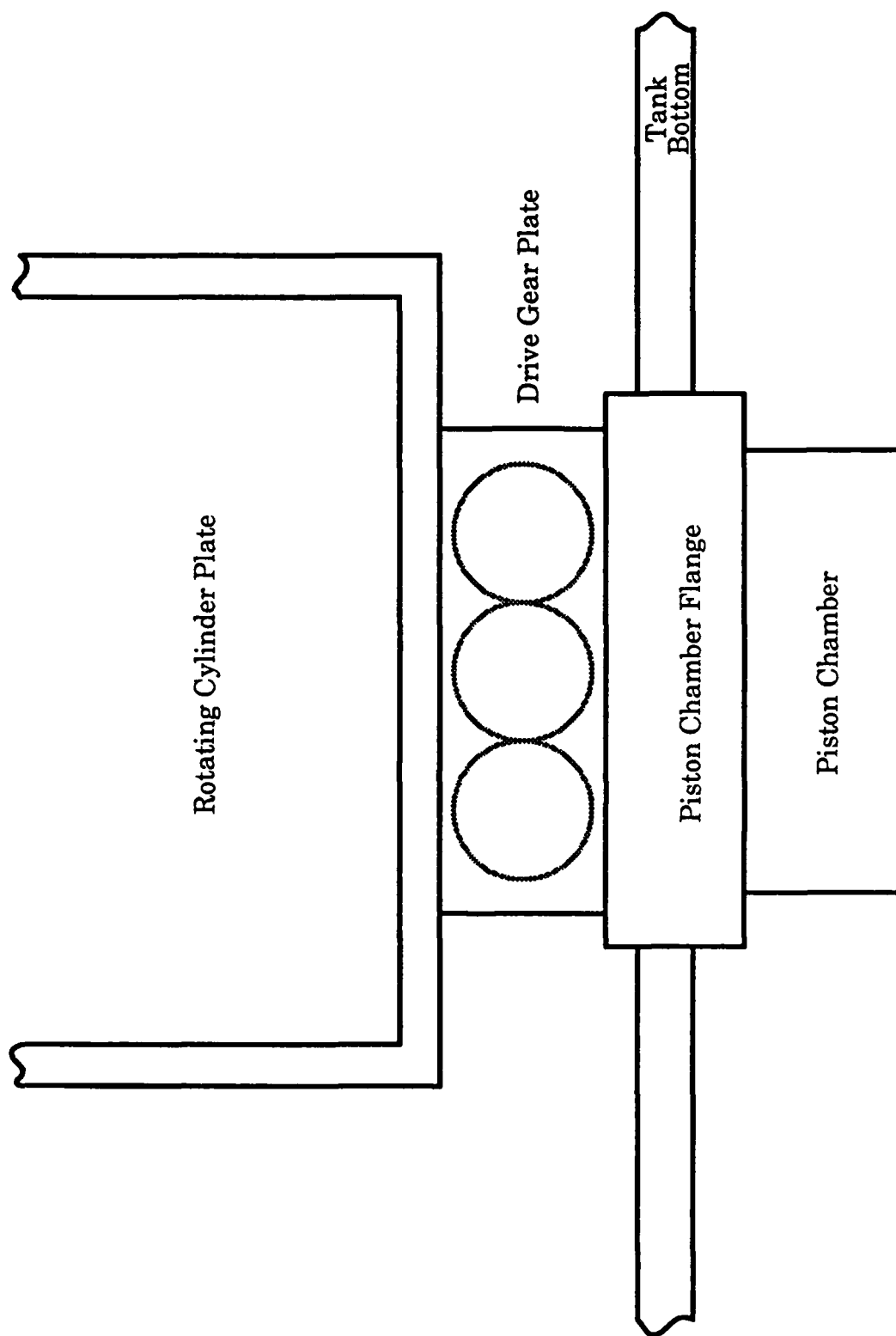
Figure 15   Side View of the Vortex Generating Tank

60
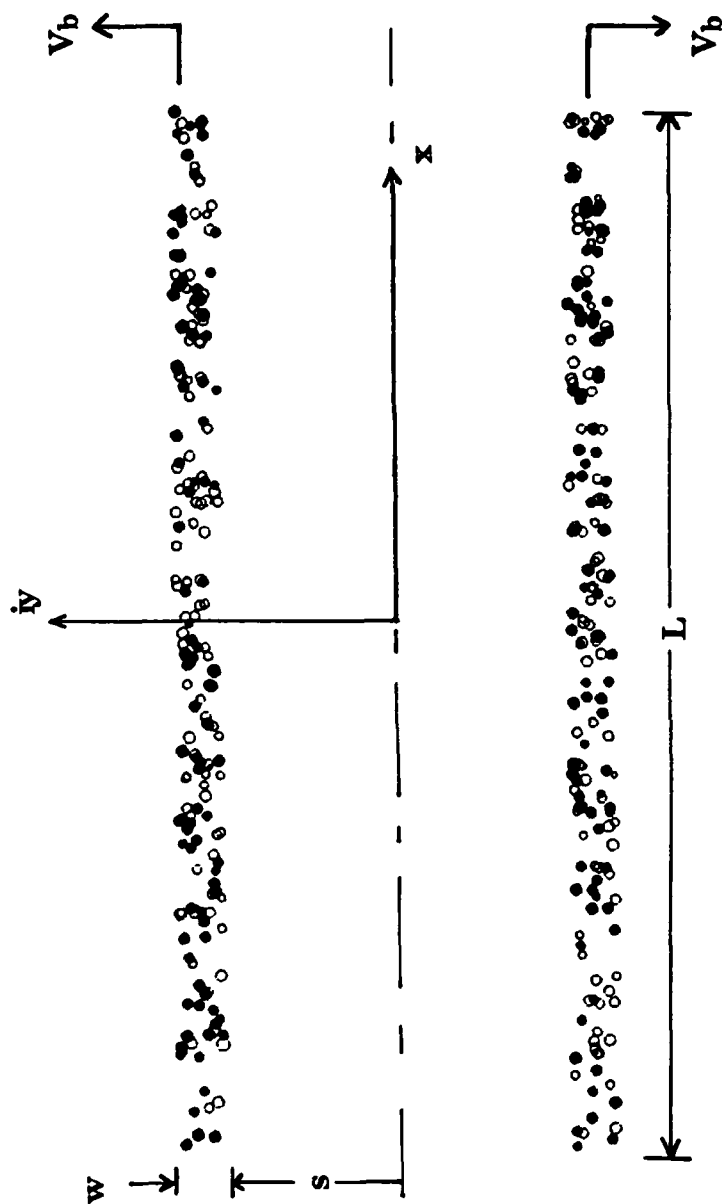
Figure 17   Parameters of the Numerical Model

61
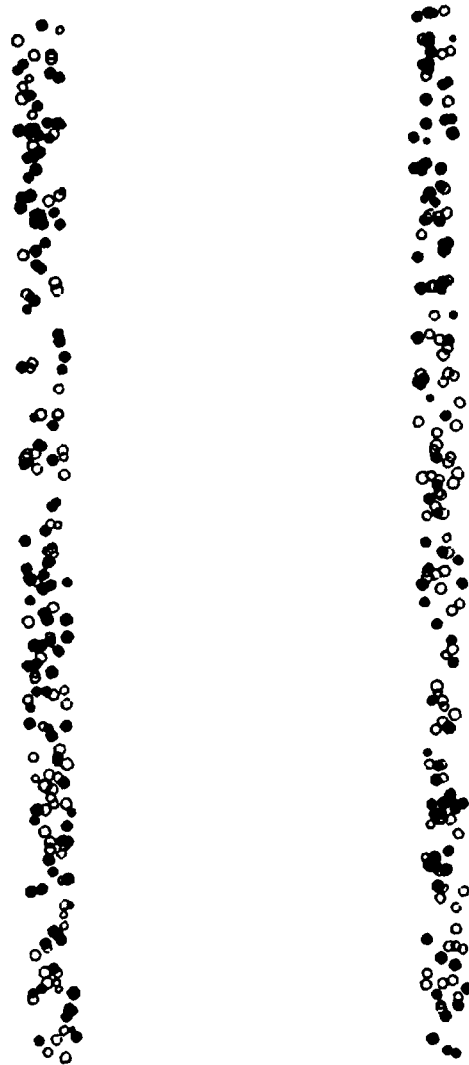
Figure 18   Typical Position-Plot of the Whirls

62
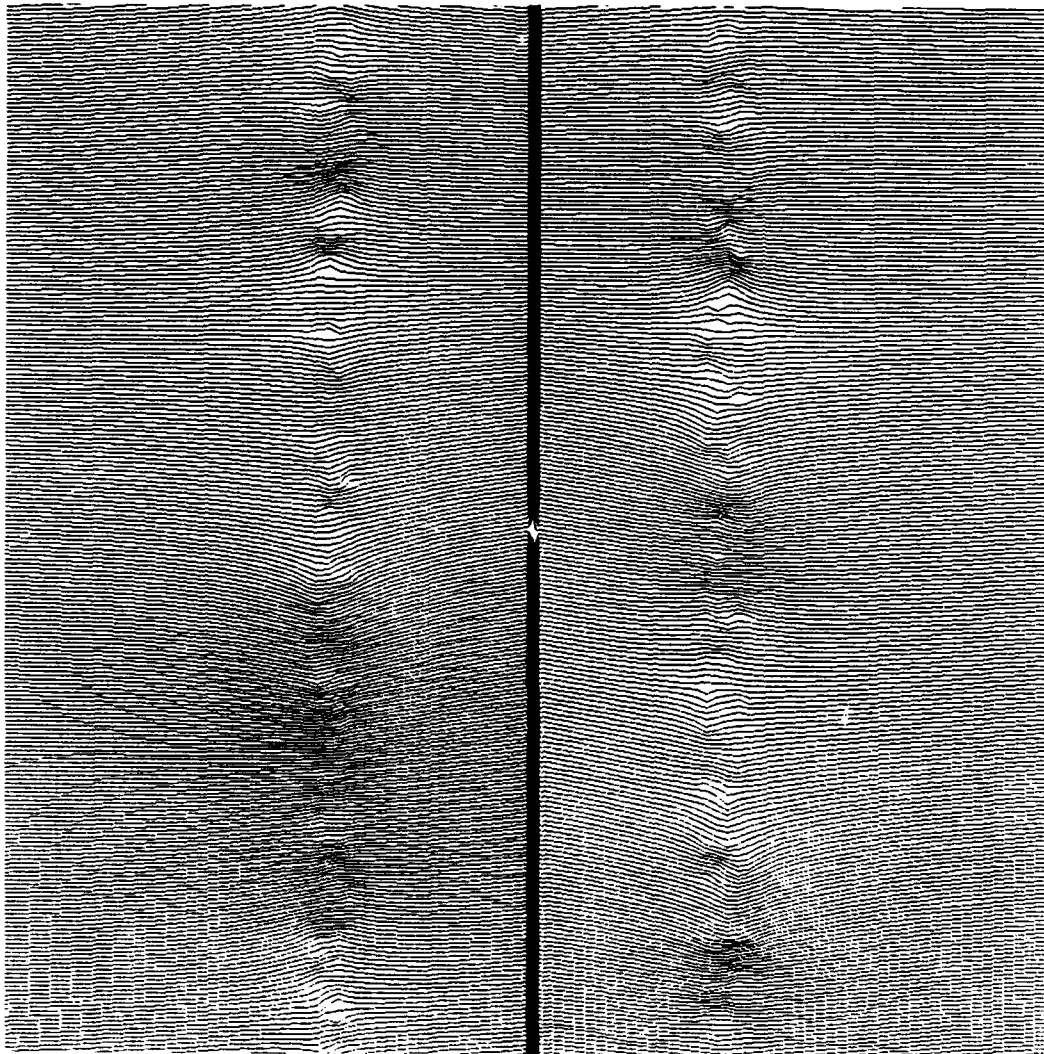
Figure 19   Typical Streamlines Including the Transport Velocity
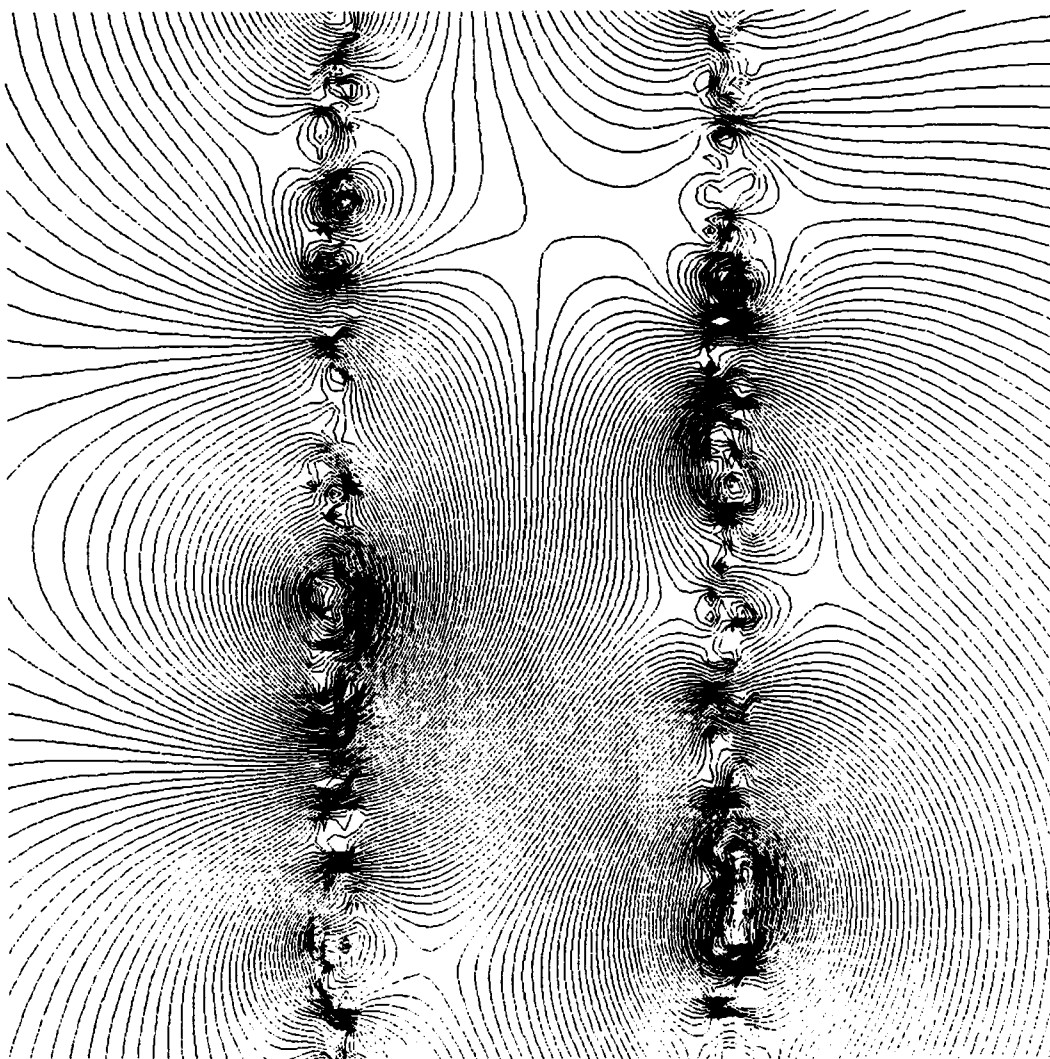
Figure 20   Typical Streamlines Excluding the Transport Velocity

64

Figure 21   Typical Velocity Vector Field of the Scars
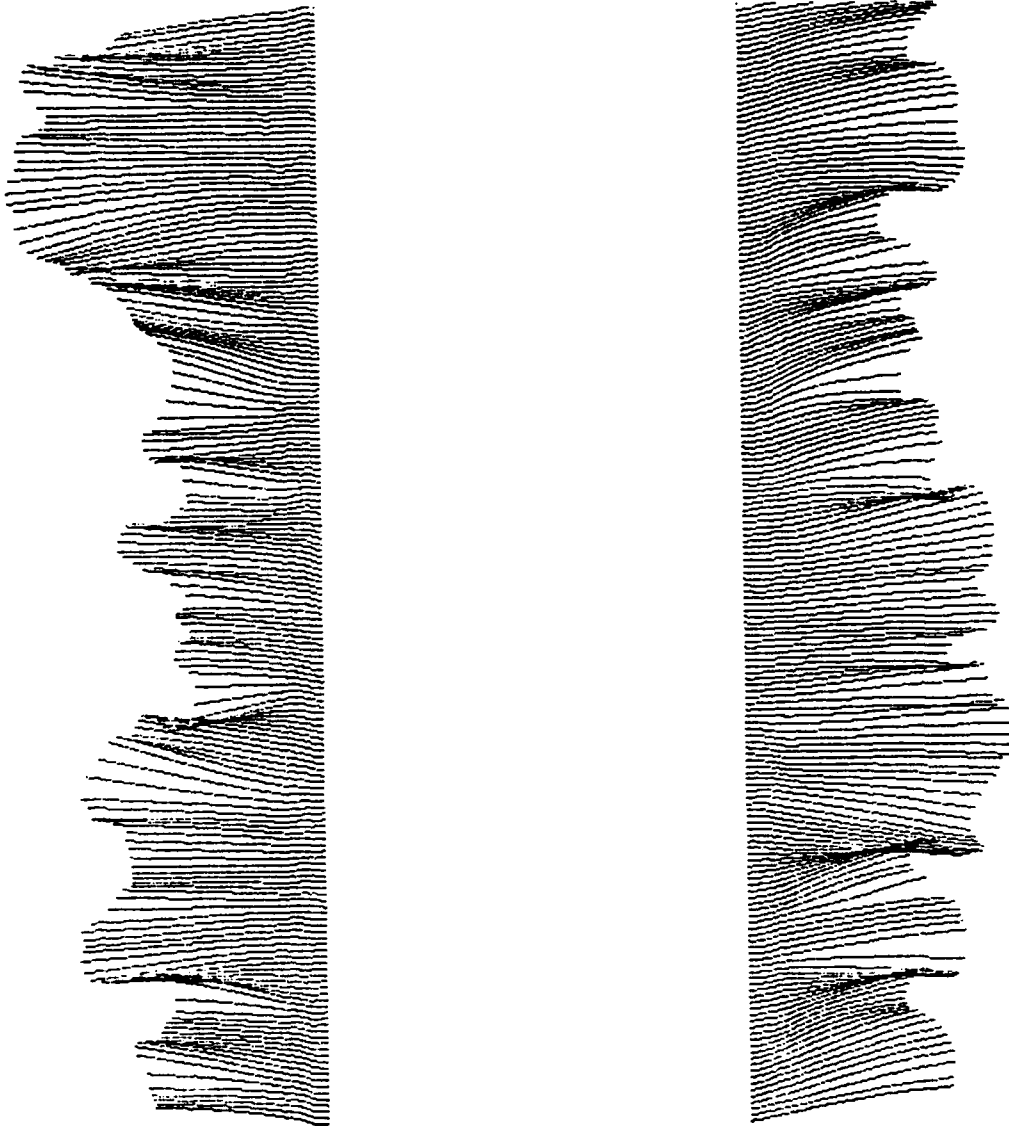
Figure 22   Typical Pathlines
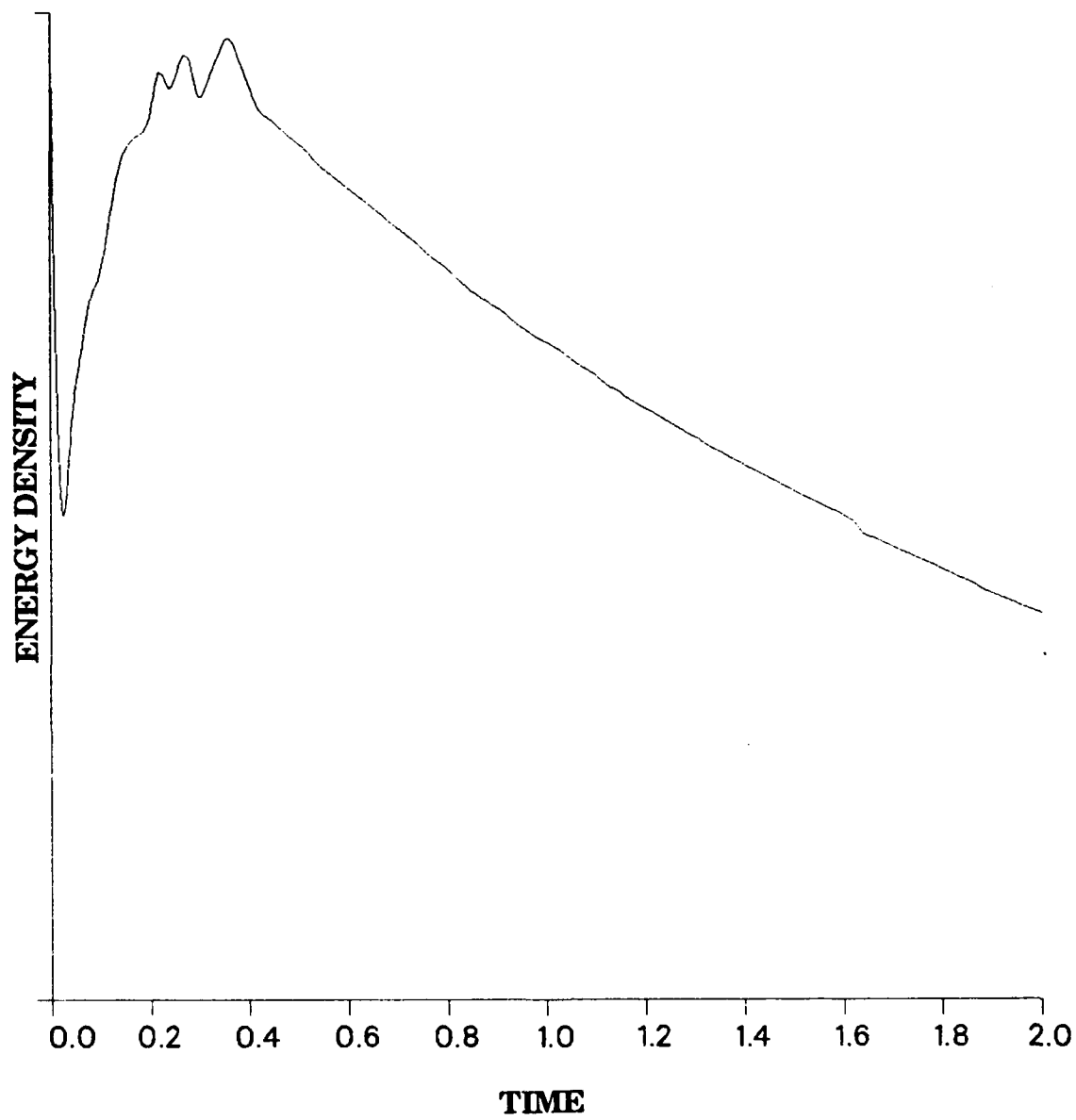
Figure 23   Typical Energy Density Plot
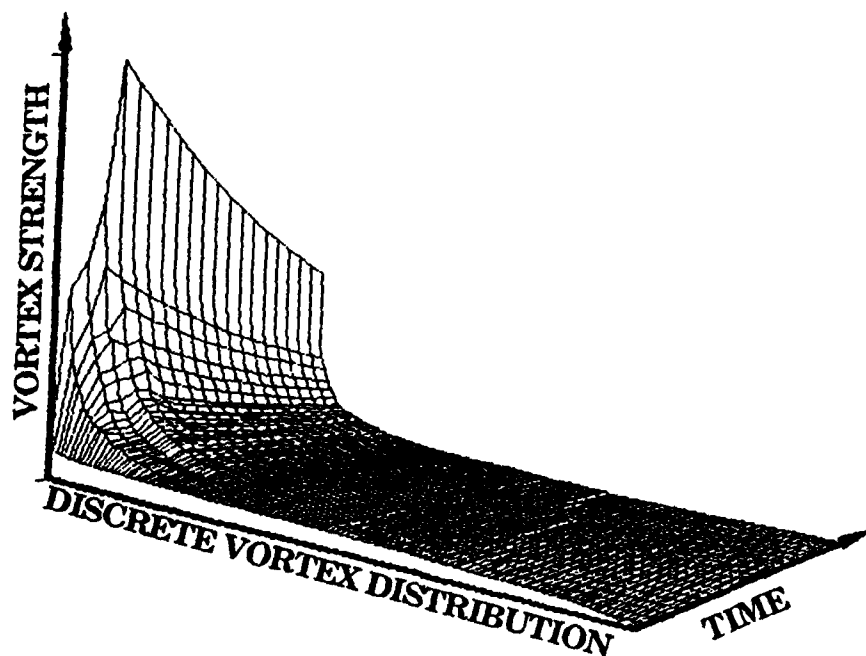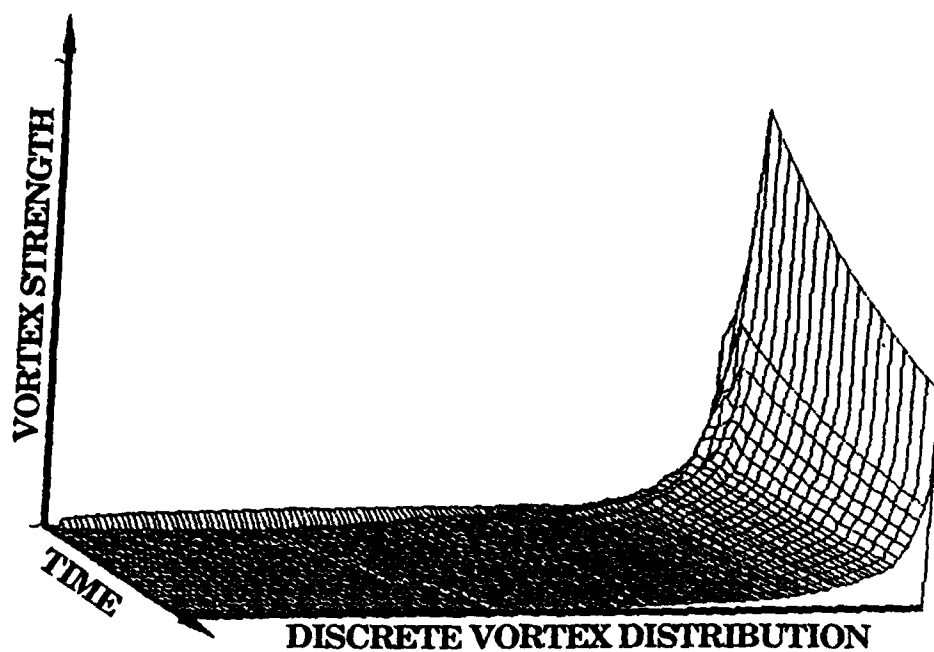
Figure 24   Typical Evolution and Cascading of Whirl Strengths
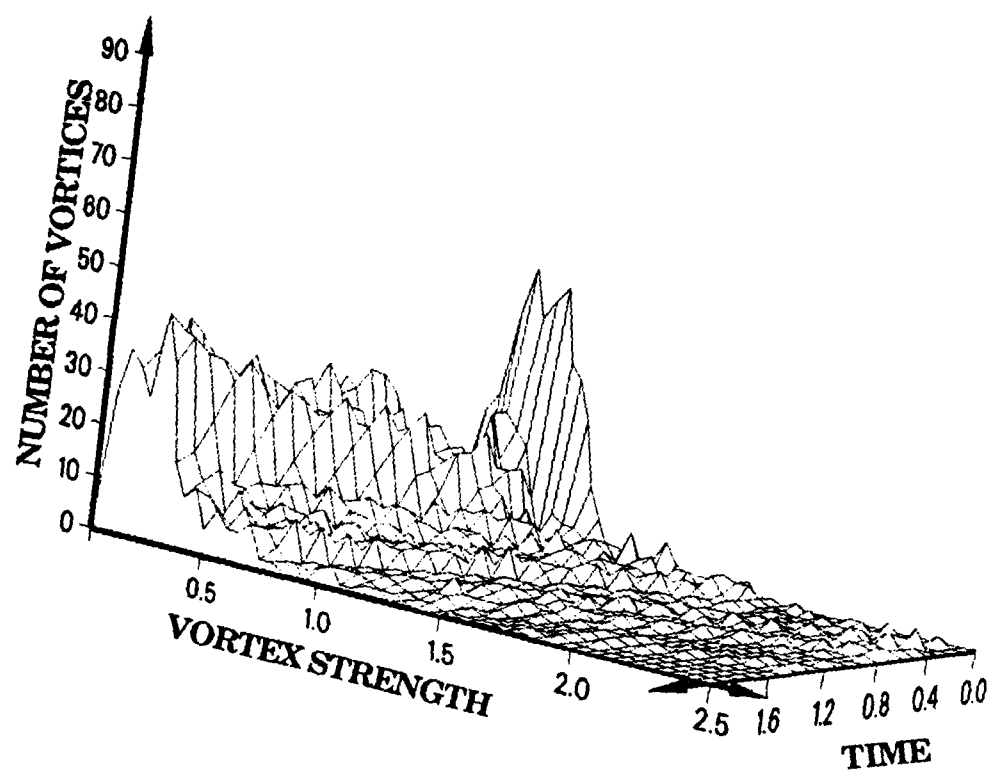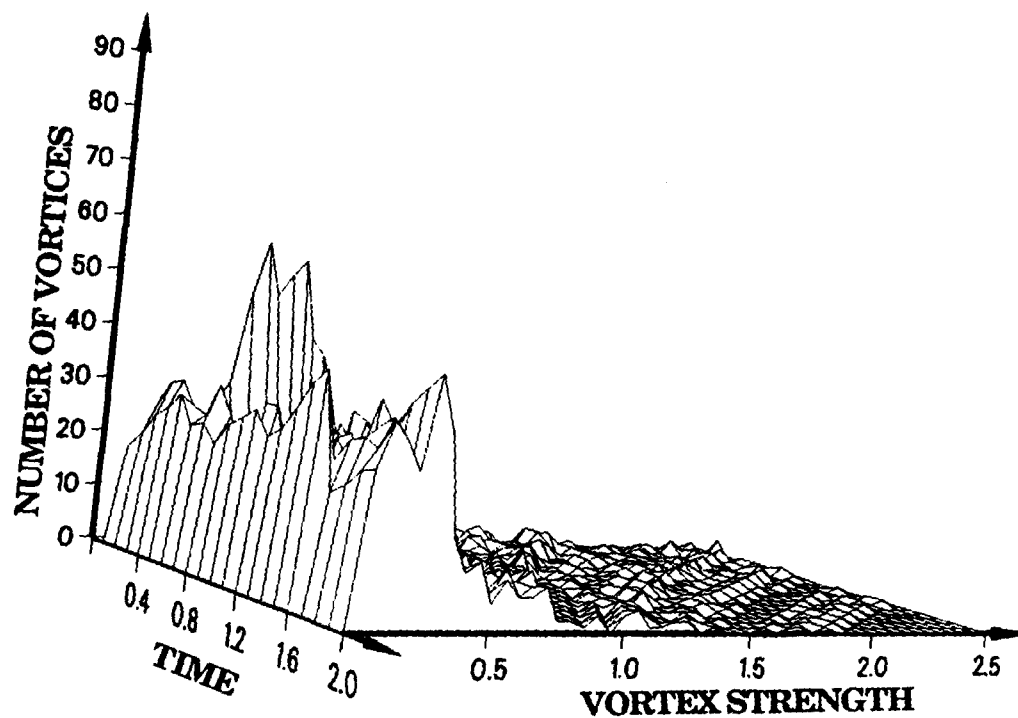
Figure 25   Typical Whirl Strength Distribution

69

Figure 26   Development of Instabilities on a Kelvin Oval

Figure 27   Initial Surface Deformation by a Rising Vortex Pair

Figure 28   The Metamorphosis of the Instabilities into Striations

Figure 29   The Generation of Whirls at the Striation Ends

73

Figure 30   Whirls on the Free Surface
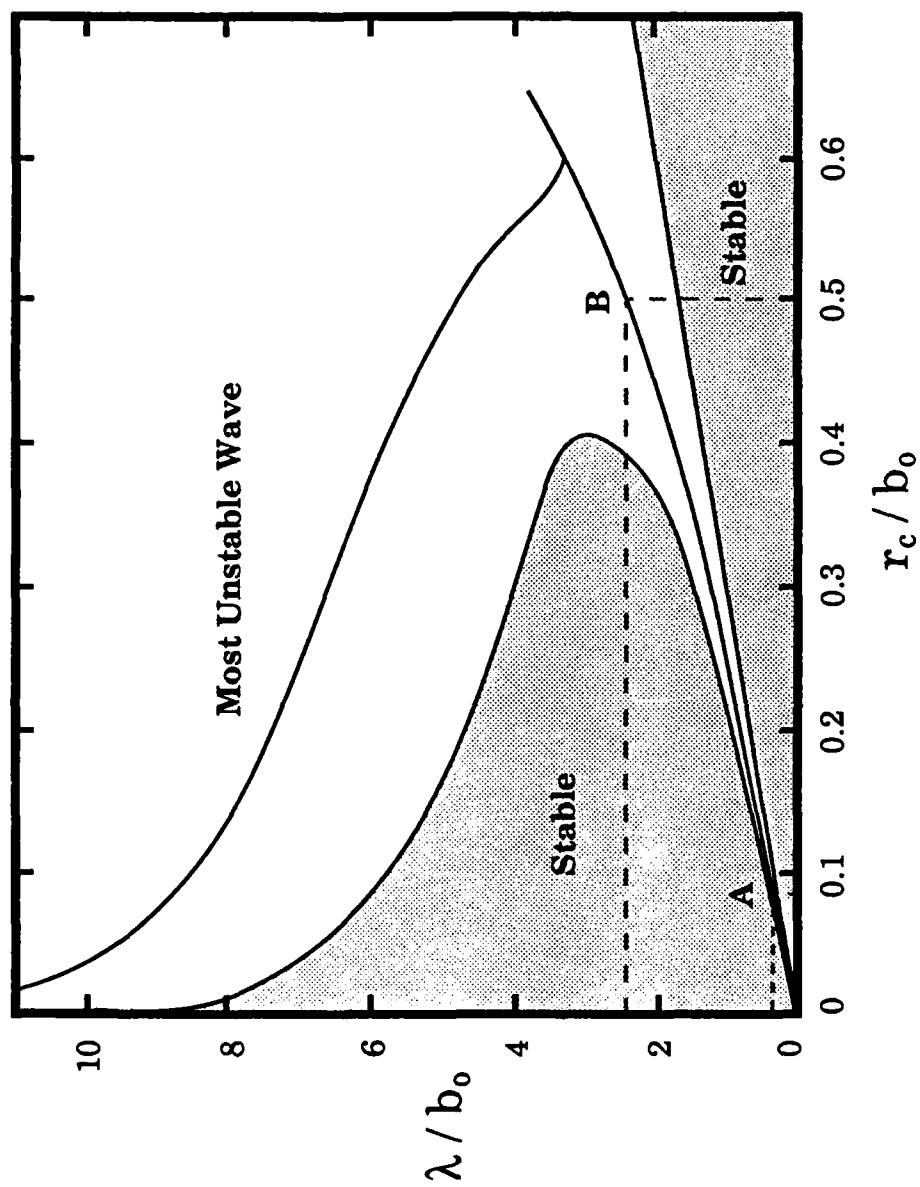
Figure 31   Stability Diagram for a Vortex Pair

75
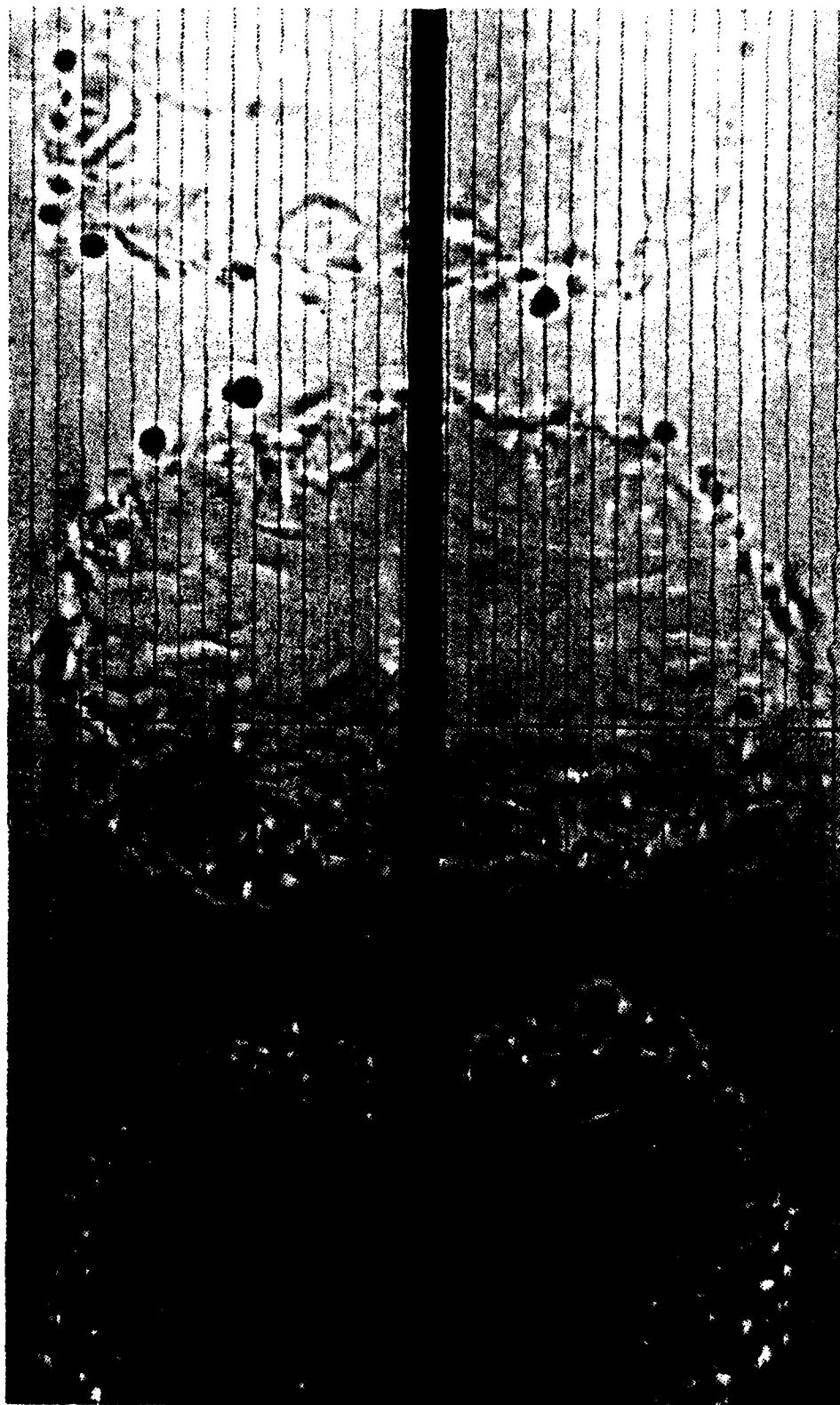
Figure 32   Short and Long Wavelength Instabilities Superimposed
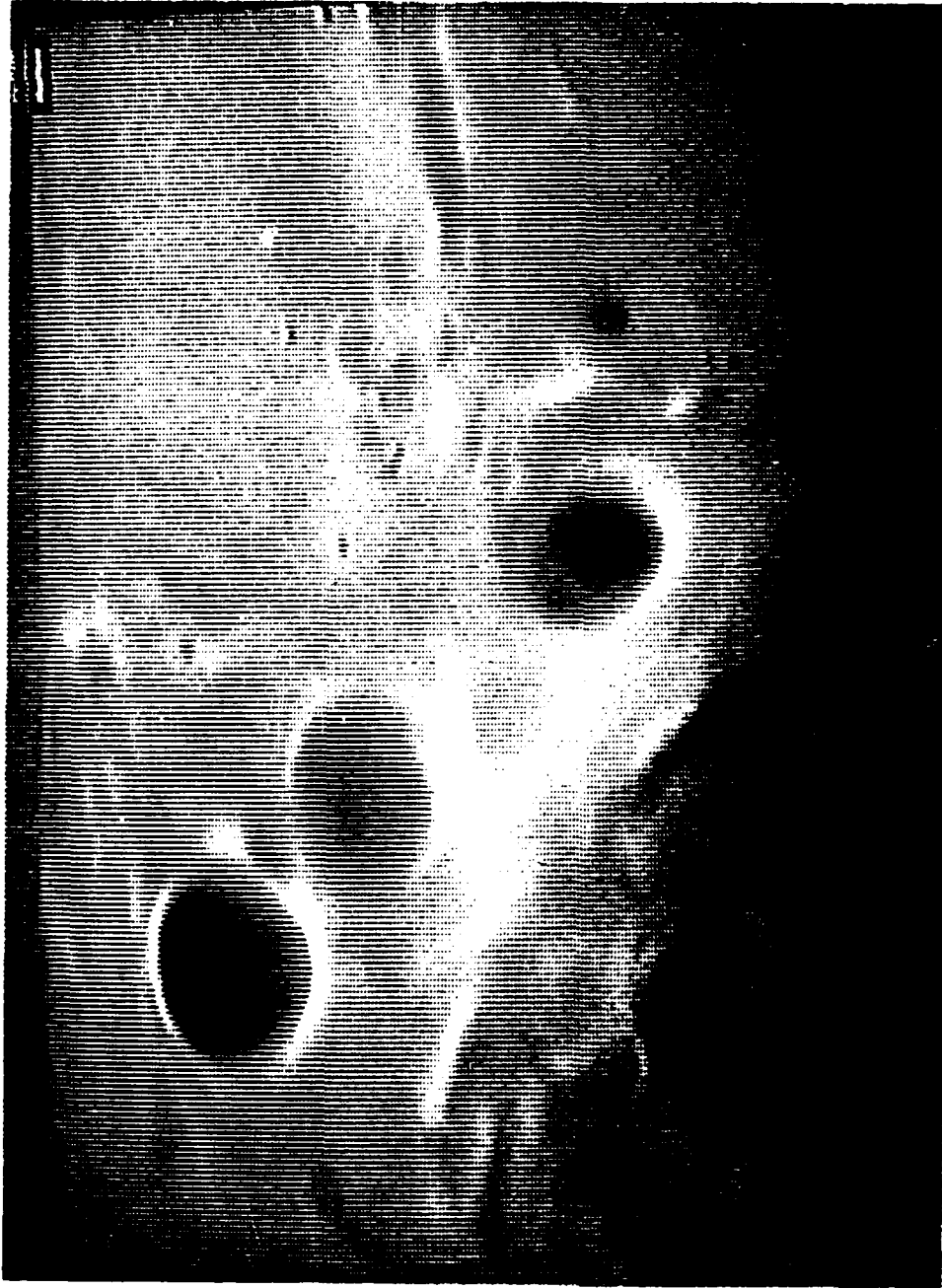
Figure 33   Whirls Created From Rotating Cylinders (Photograph #1)

Figure 34   Whirls Created From Rotating Cylinders (Photograph #2)

78
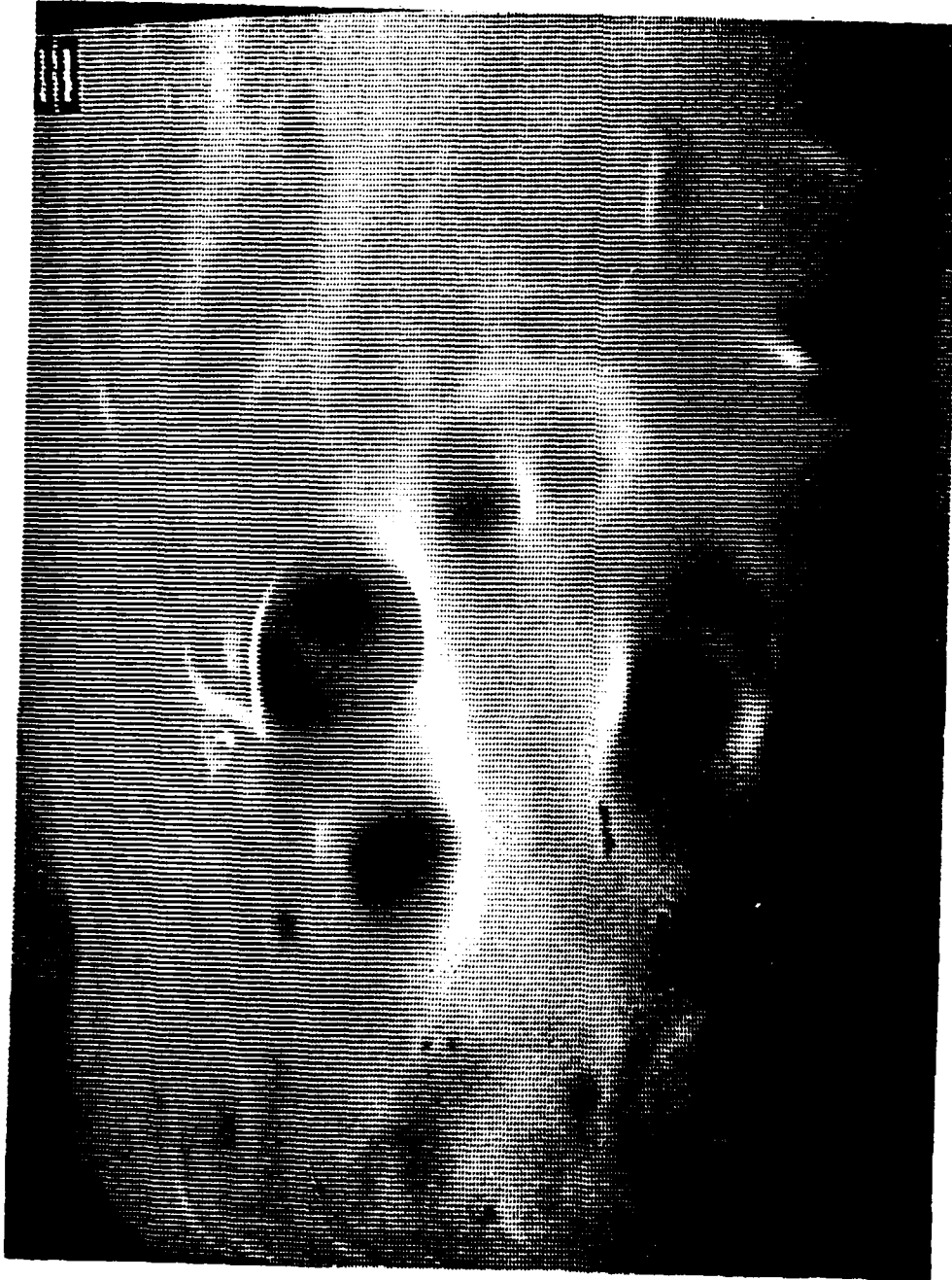
Figure 35   Whirls Created From Rotating Cylinders (Photograph #3)

79
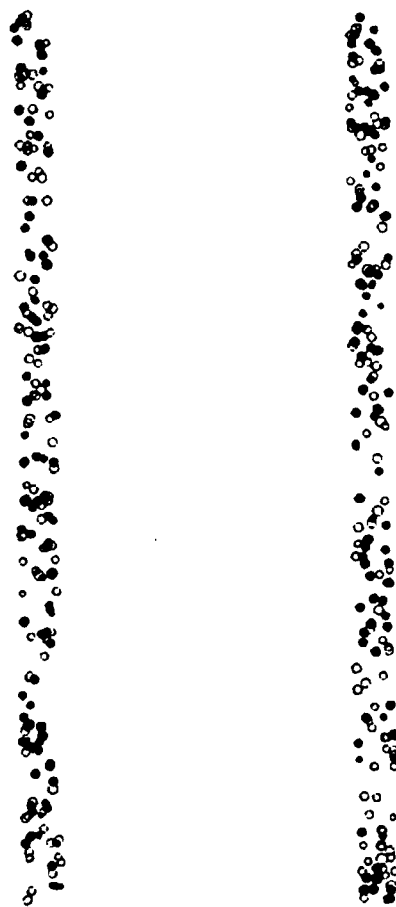
Figure 36   Whirl Position at t = 0.0
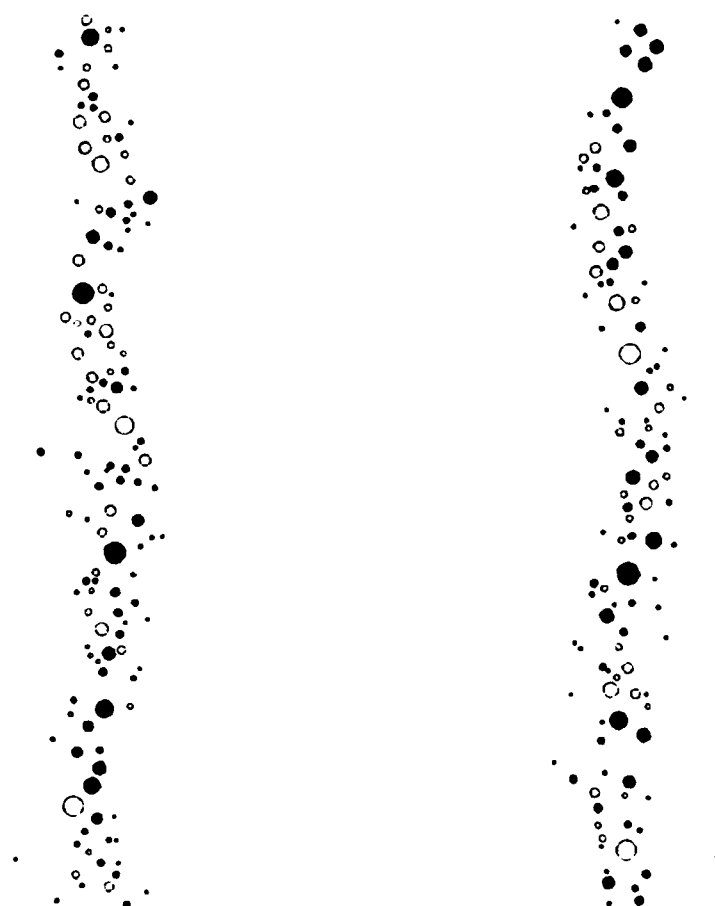
Figure 37   Whirl Position at t = 0.4

81
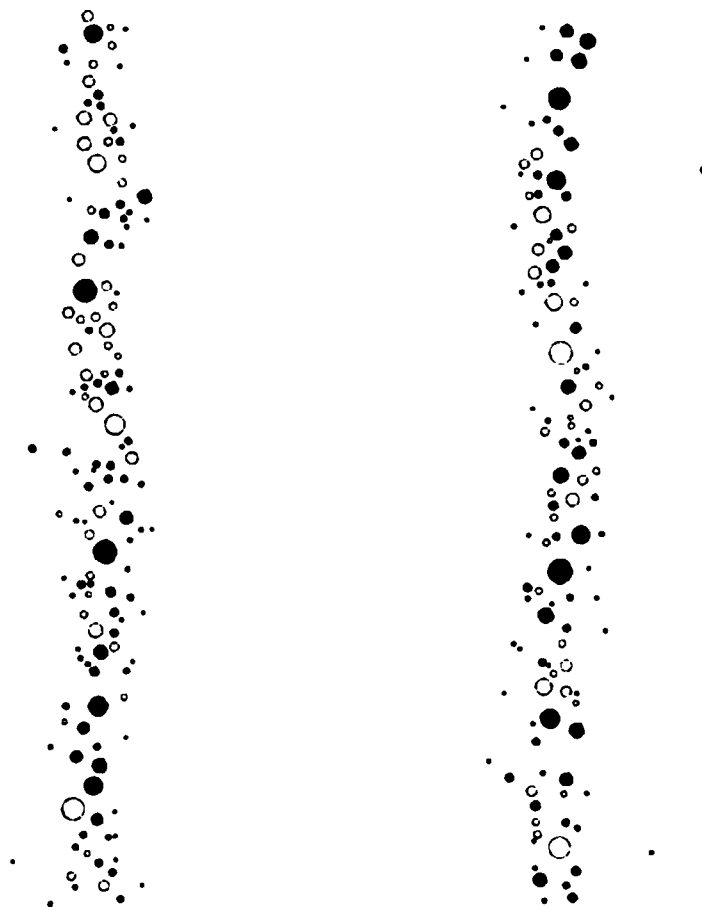
Figure 38   Whirl Position at t = 0.8
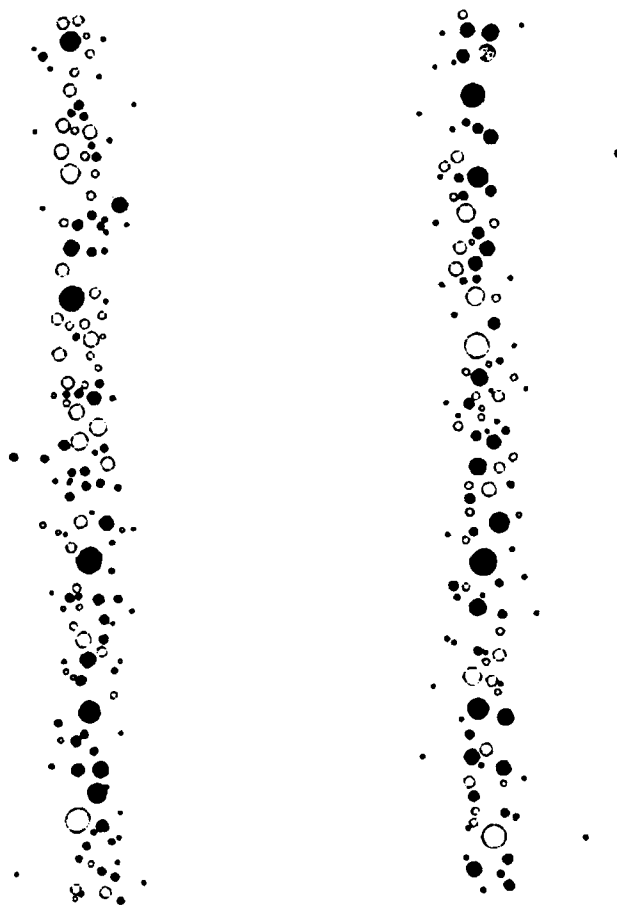
Figure 39   Whirl Position at t = 1.2
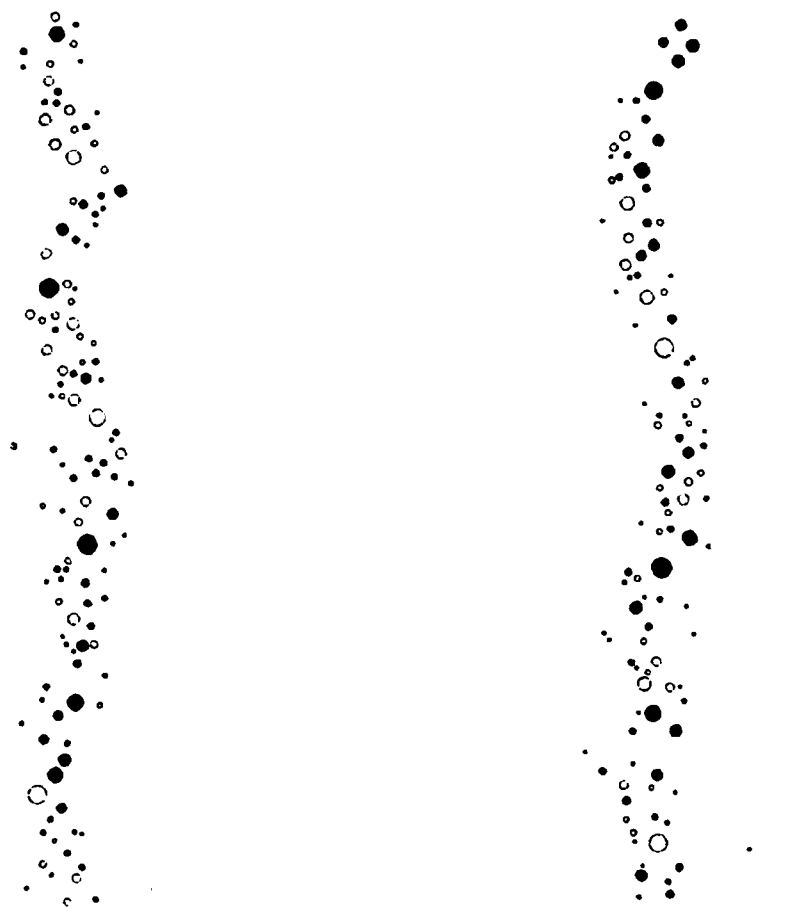
Figure 40   Whirl Position at t = 1.6
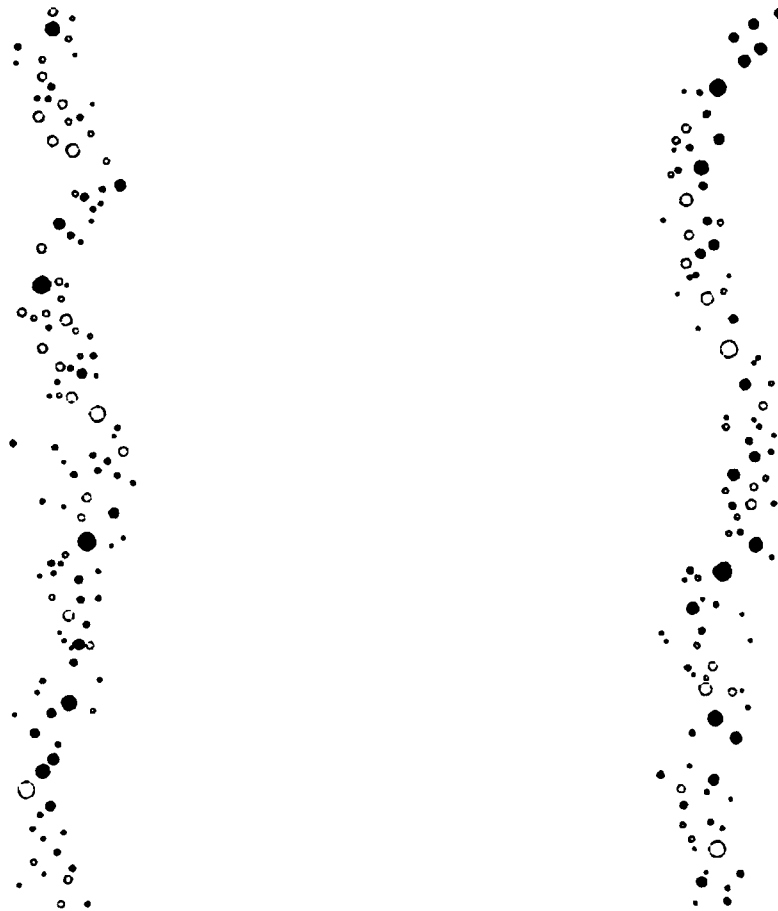
Figure 41   Whirl Position at t = 2.0

85
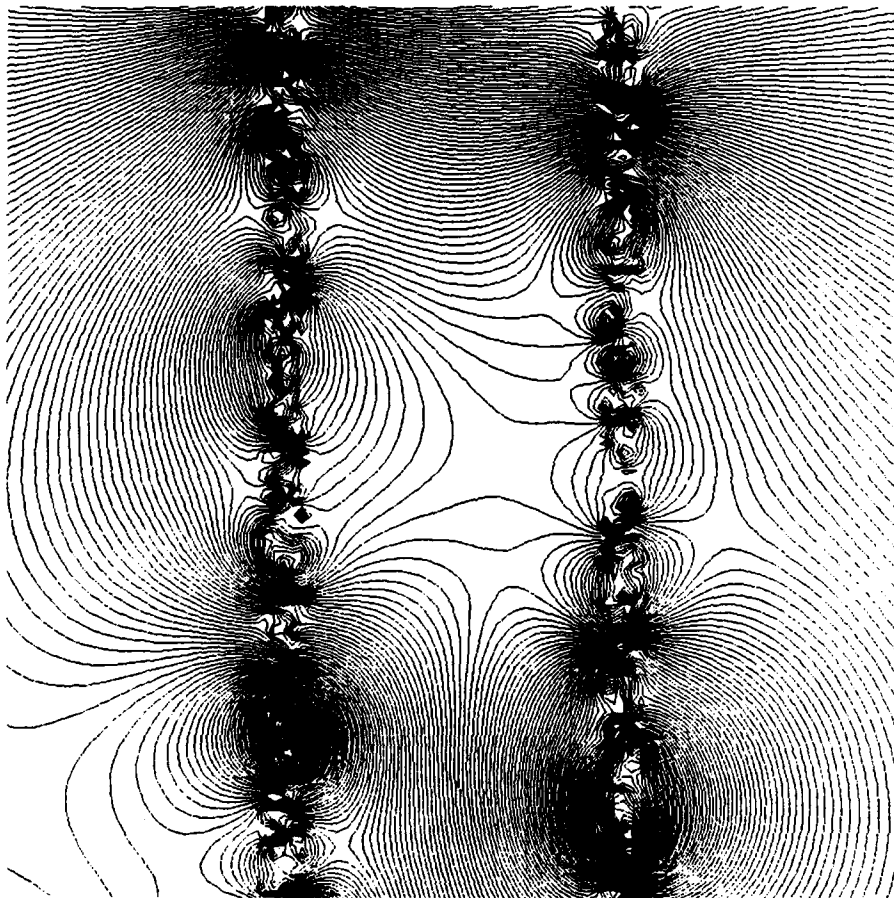
Figure 42   Streamlines at t = 0.0 (Comoving Coordinates)

86
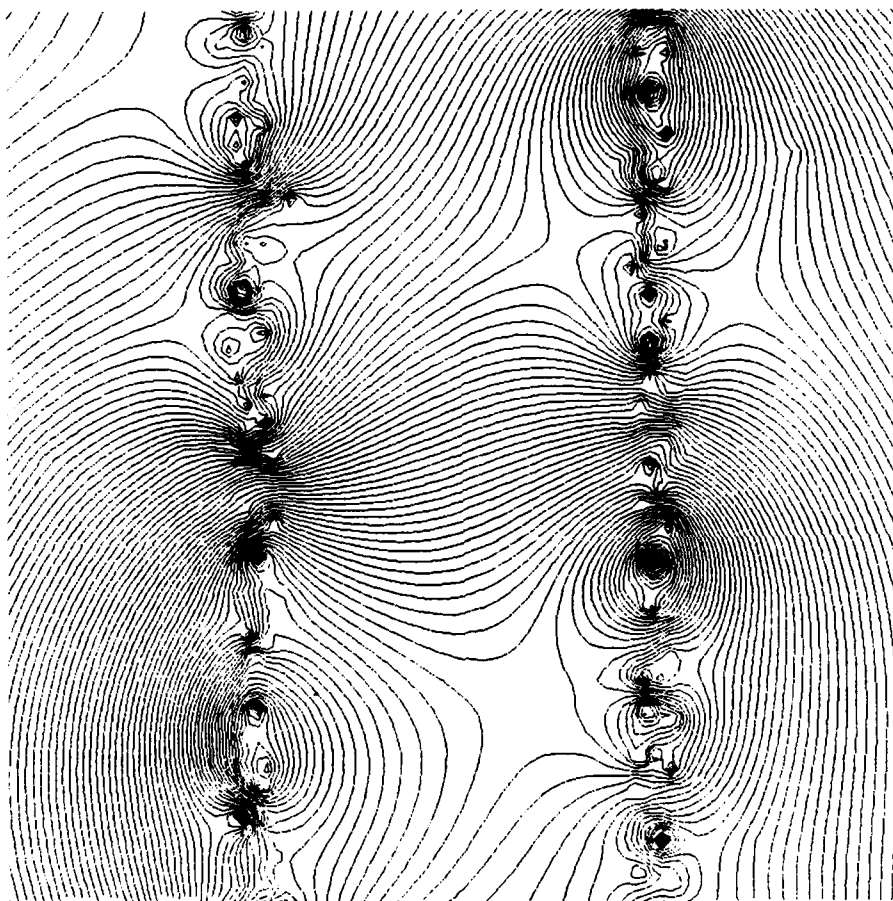
Figure 43   Streamlines at t = 0.4 (Comoving Coordinates)
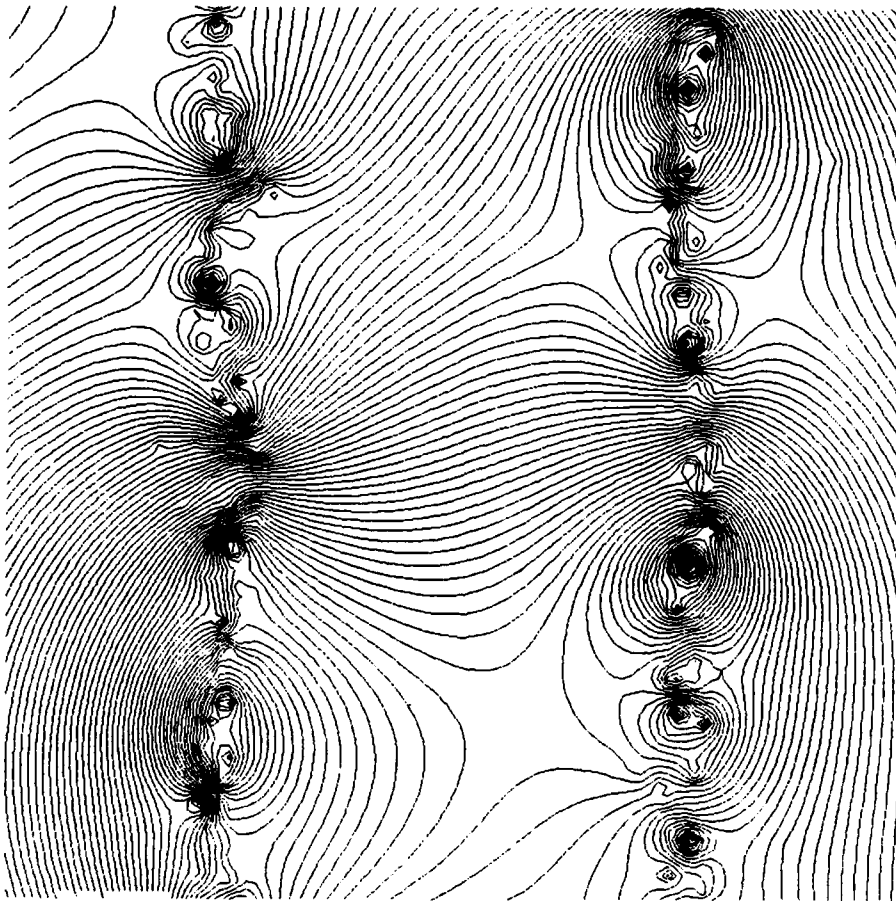
Figure 44 **Streamlines at t = 0.8 (Comoving Coordinates)**
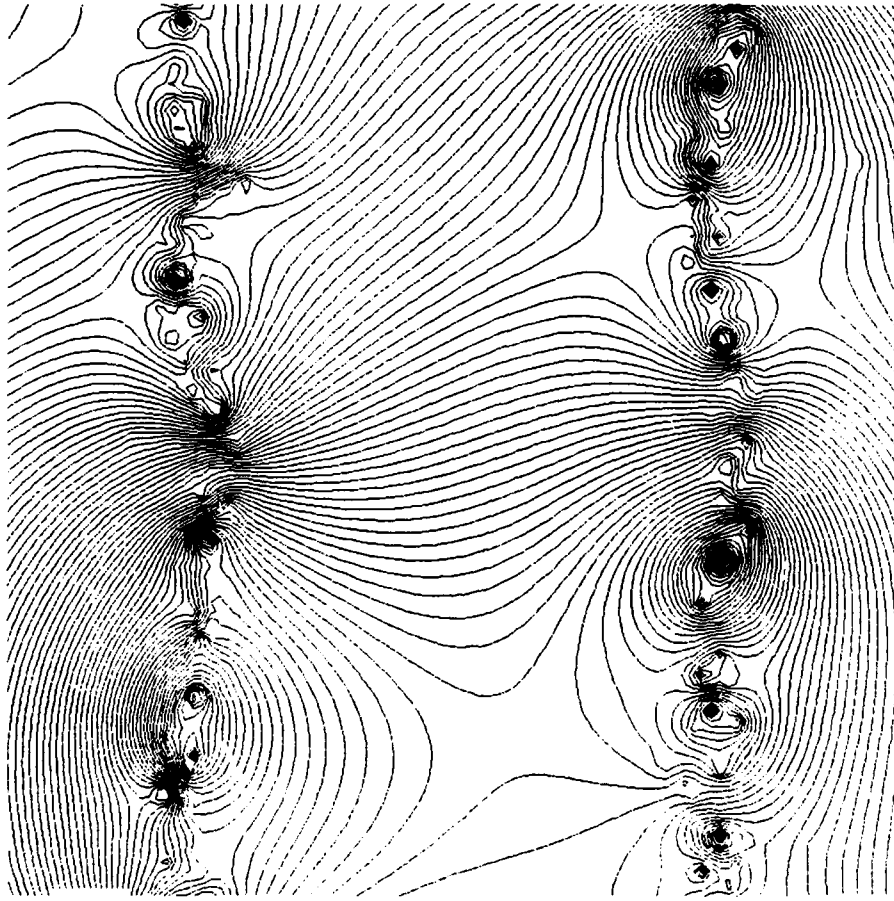
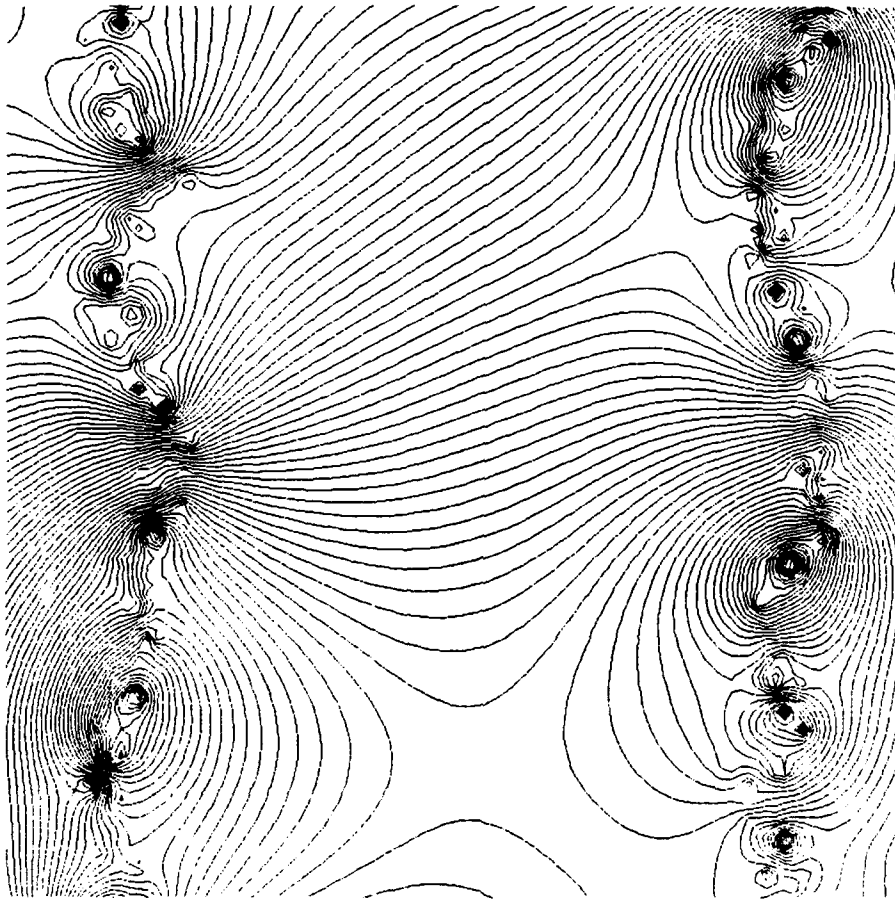**Figure 45   Streamlines at t = 1.2 (Comoving Coordinates)**
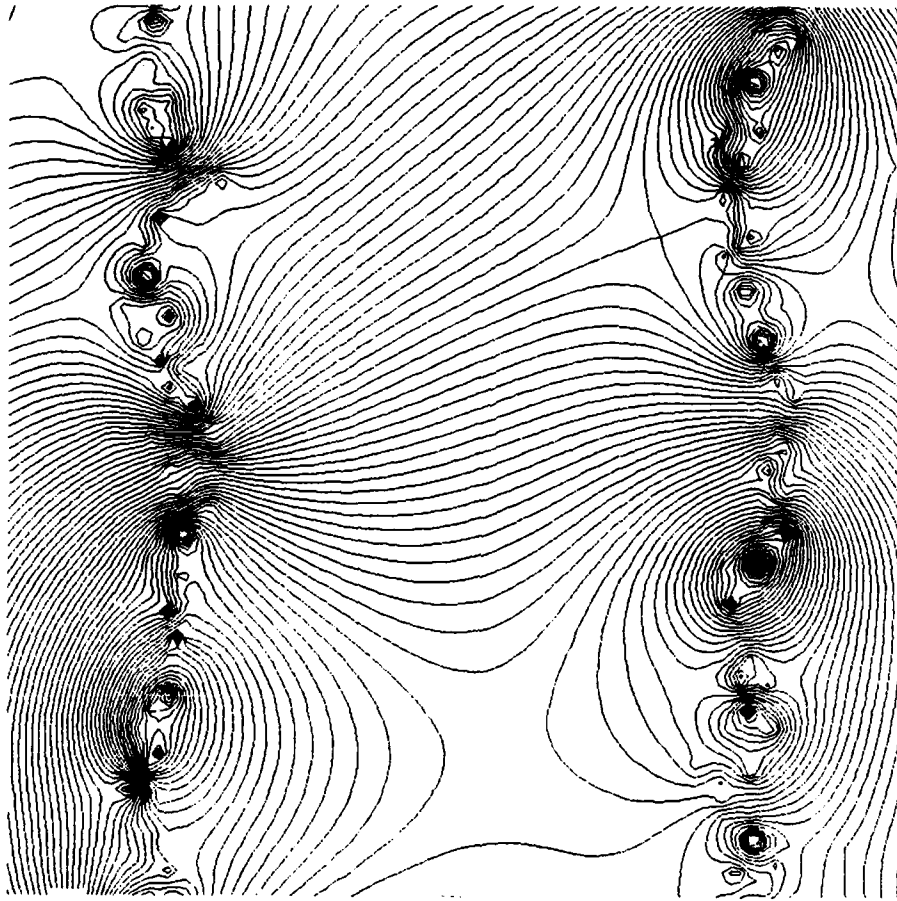
Figure 46   Streamlines at t = 1.6 (Comoving Coordinates)

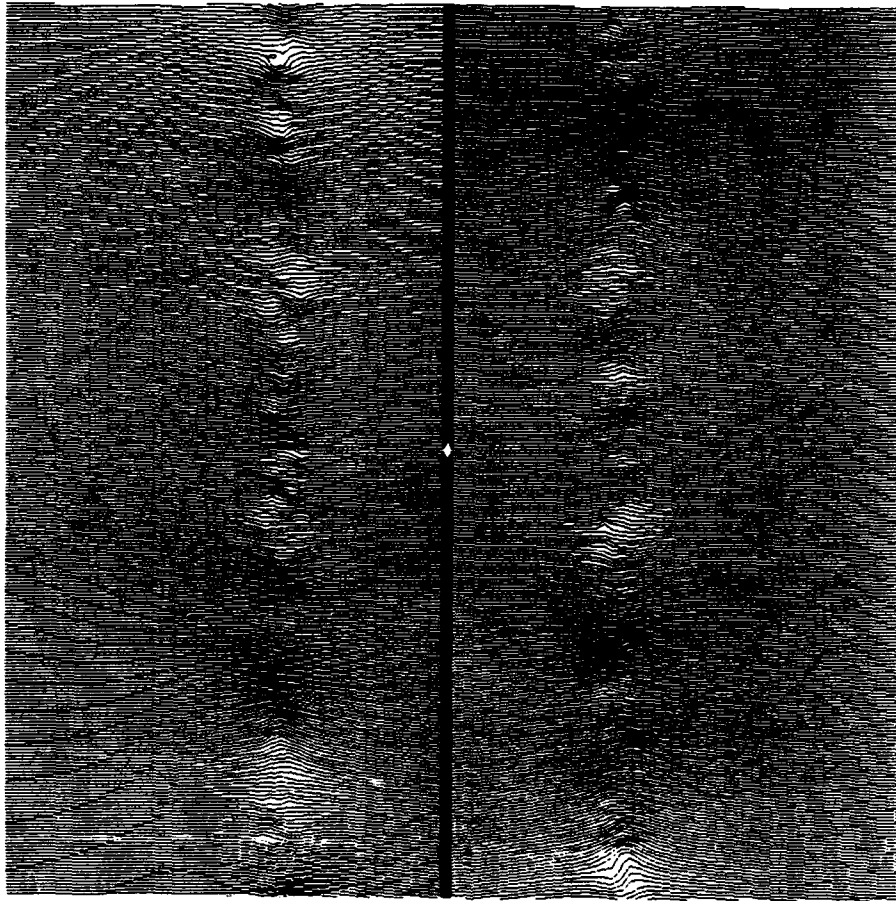**Figure 47   Streamlines at t = 2.0 (Comoving Coordinates)**

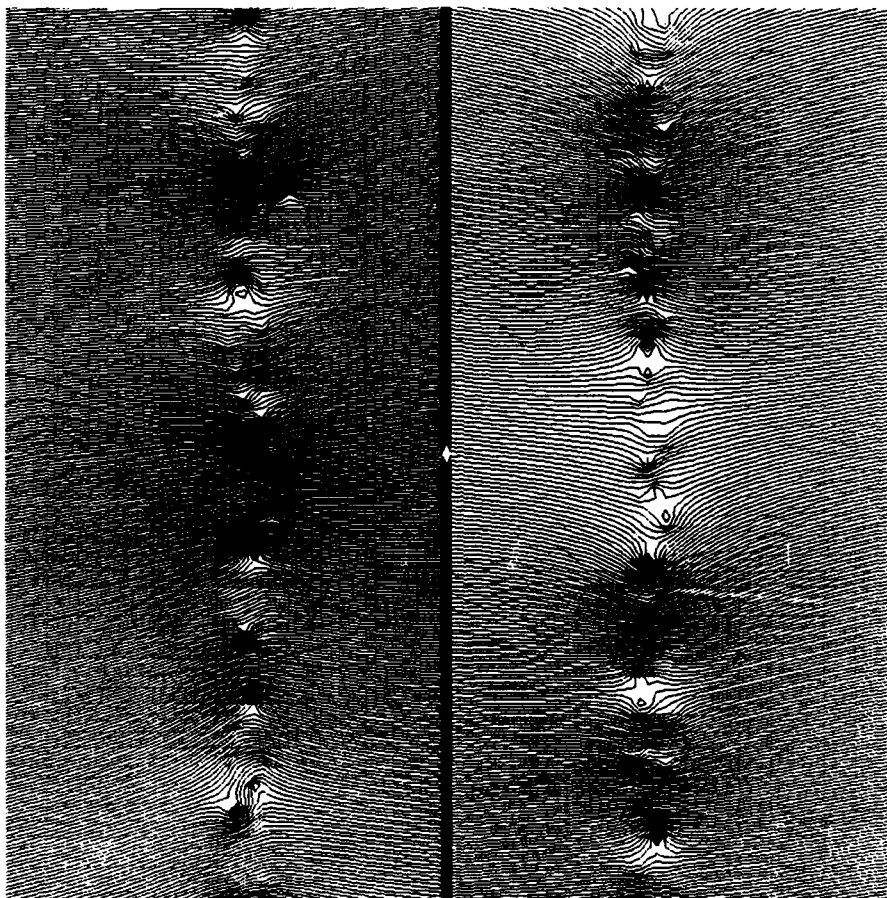91

Figure 48   Streamlines at t = 0.0 (Fixed Coordinates)

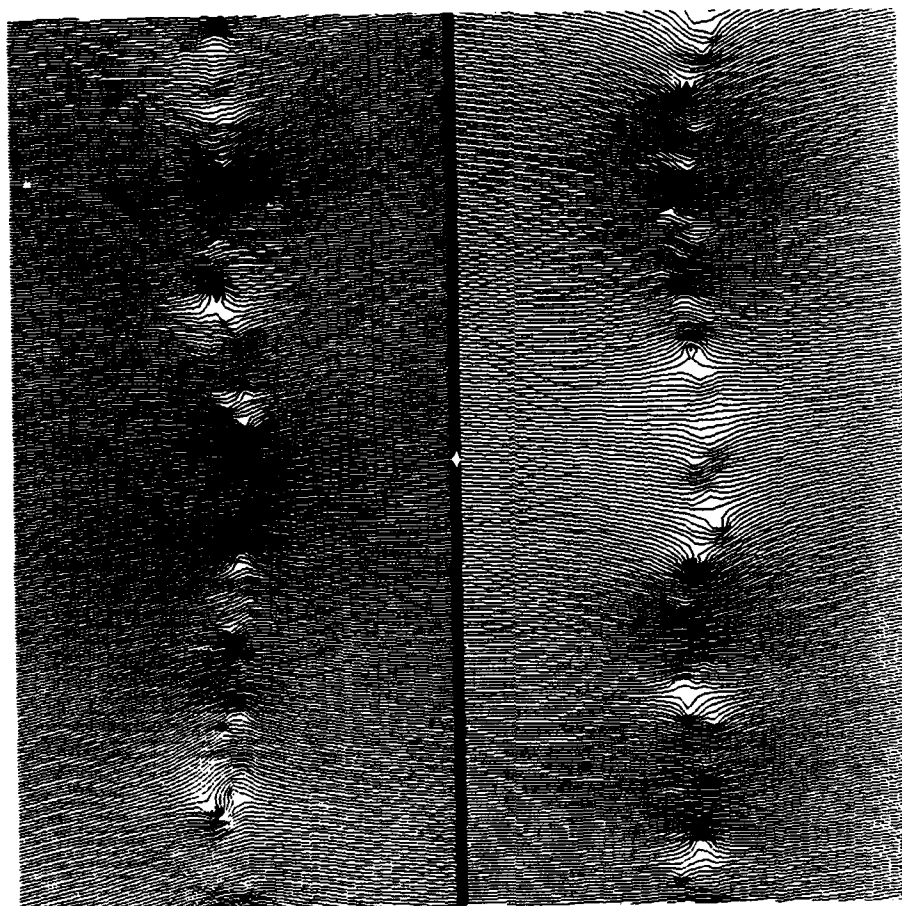**Figure 49   Streamlines at t = 0.4 (Fixed Coordinates)**

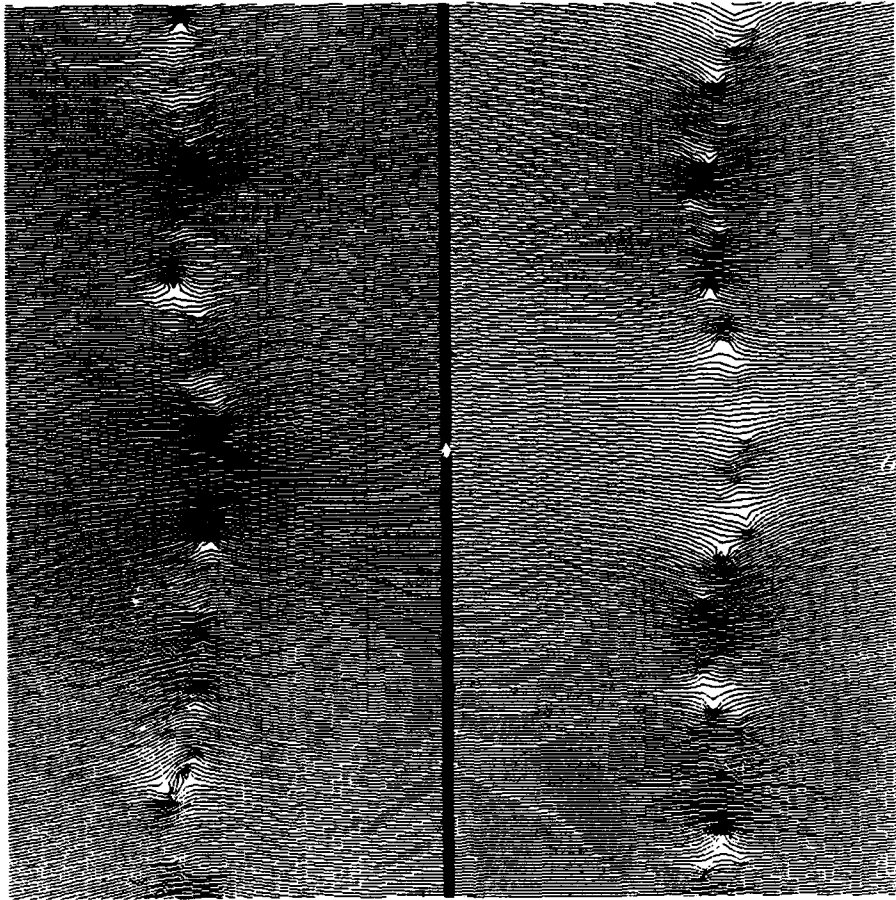**Figure 50**   **Streamlines at t = 0.8 (Fixed Coordinates)**

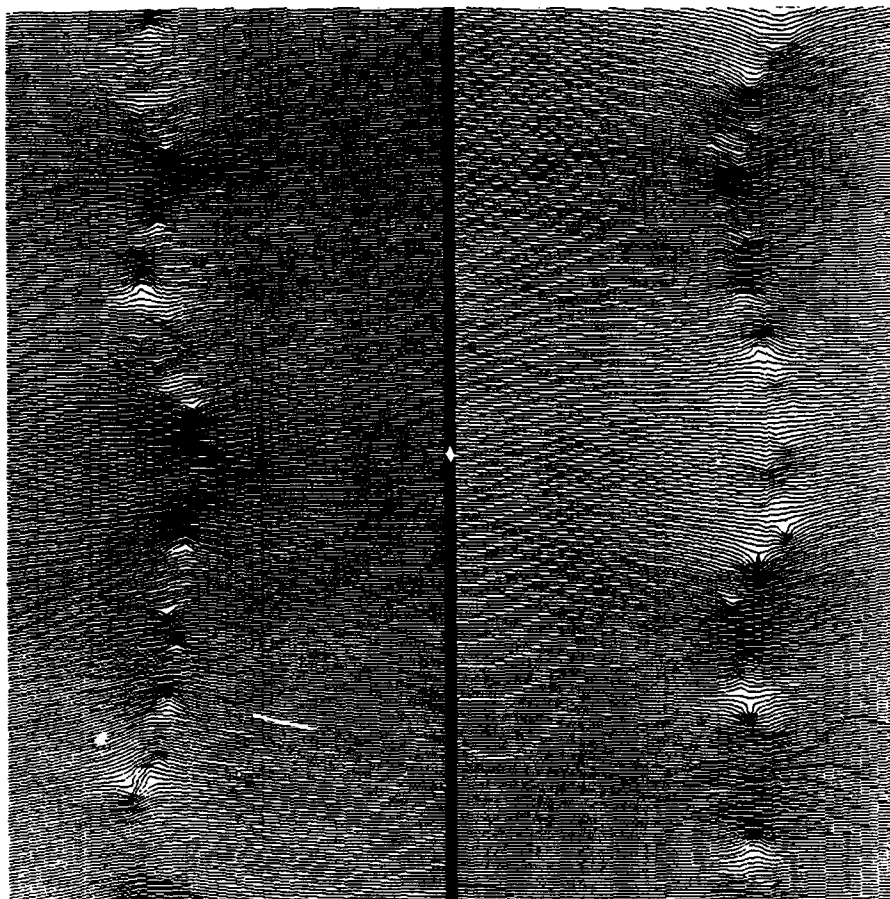**Figure 51   Streamlines at t = 1.2 (Fixed Coordinates)**

Figure 52   Streamlines at t = 1.8 (Fixed Coordinates)
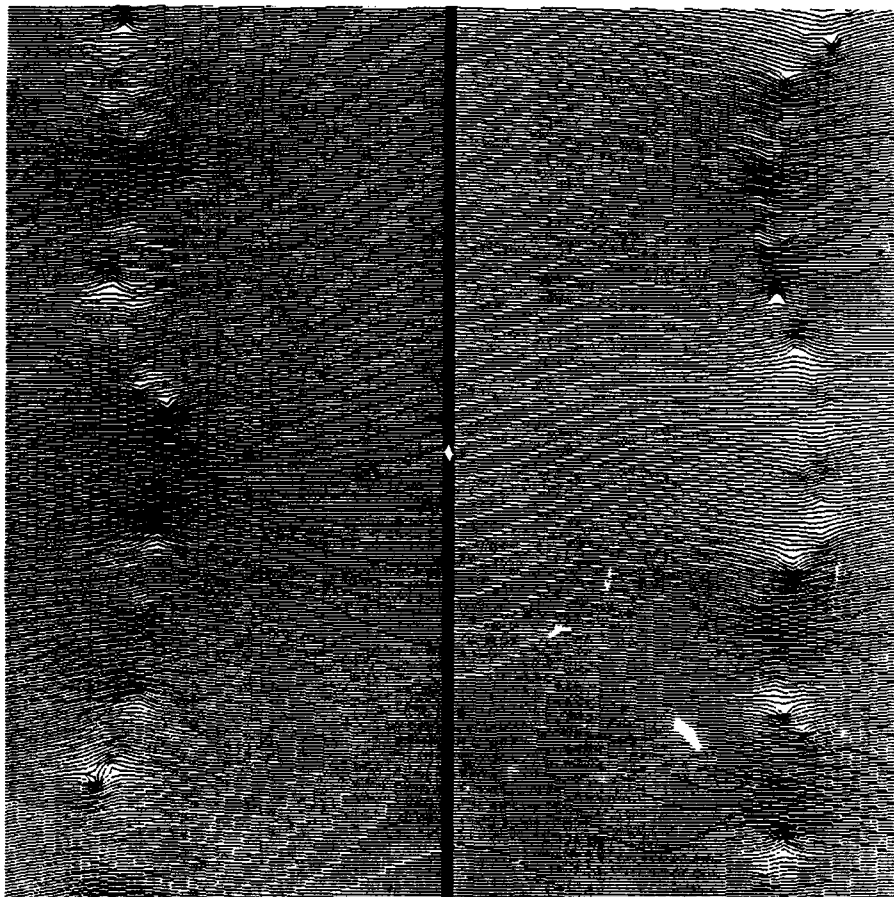
Figure 53   Streamlines at t = 2.0 (Fixed Coordinates)

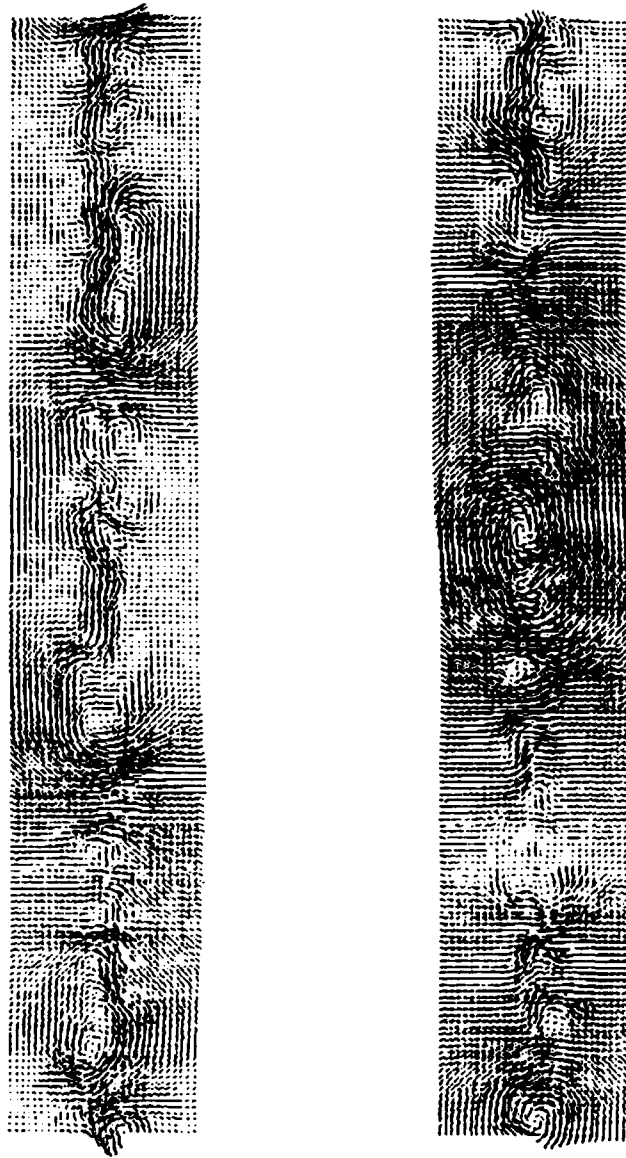**Figure 54   Velocity Vector Field at t = 0.0**
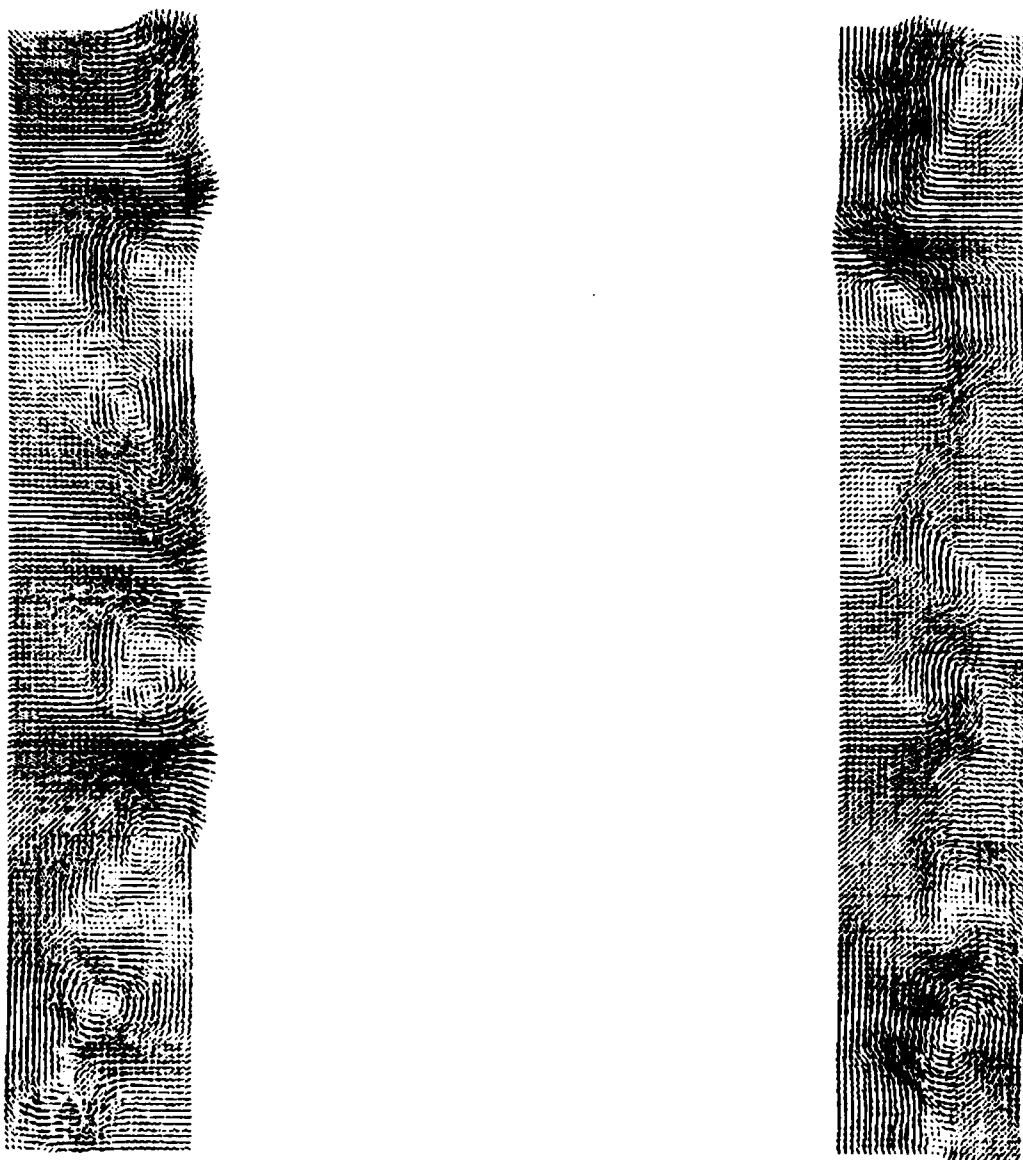
Figure 55   Velocity Vector Field at t = 2.0
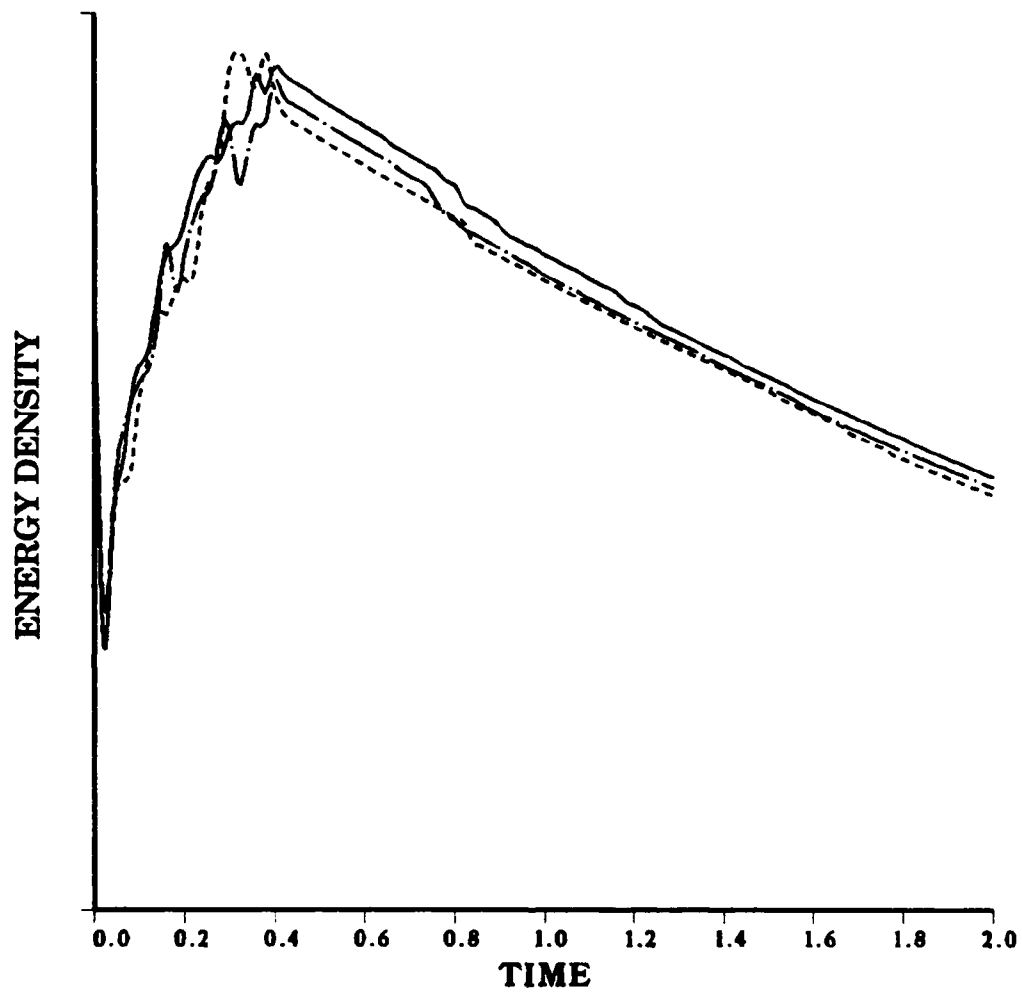
Figure 56   Energy Density for Three Different Random Seedings
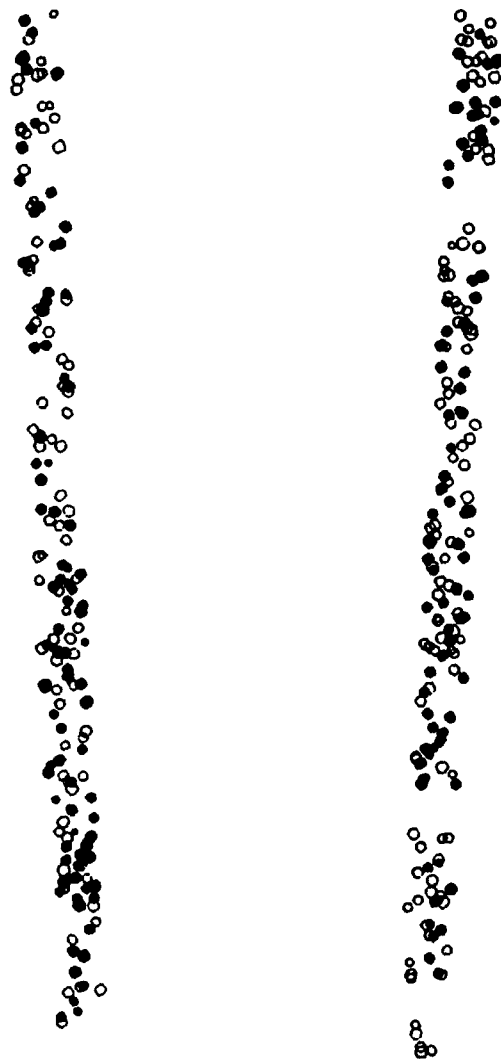
Figure 57   Whirl Position for Divergent Scars at t = 0.0

101
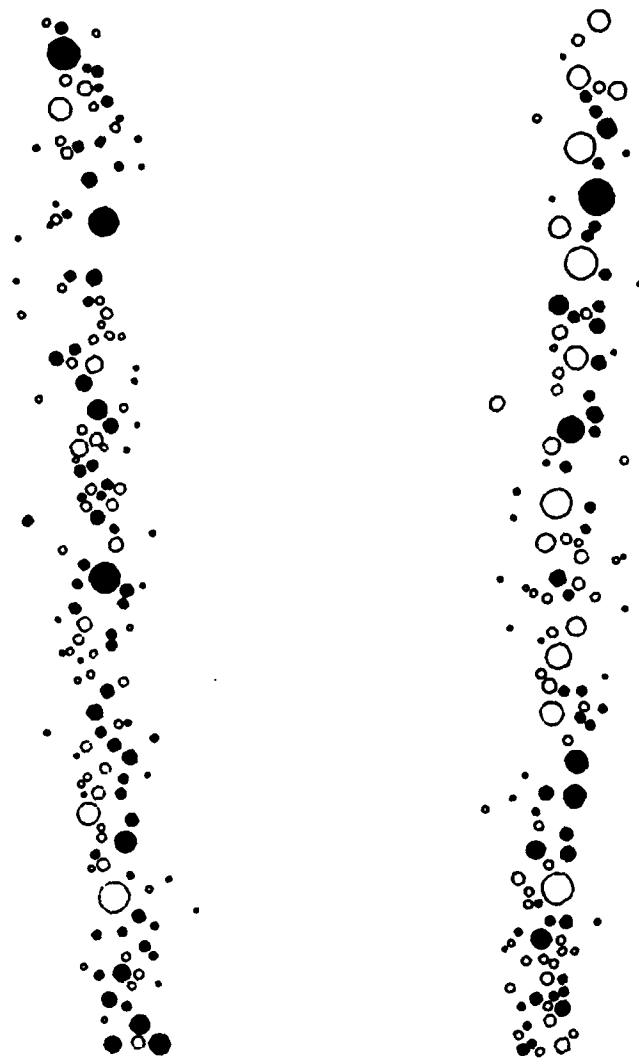
Figure 58   Whirl Position for Divergent Scars at t = 0.4
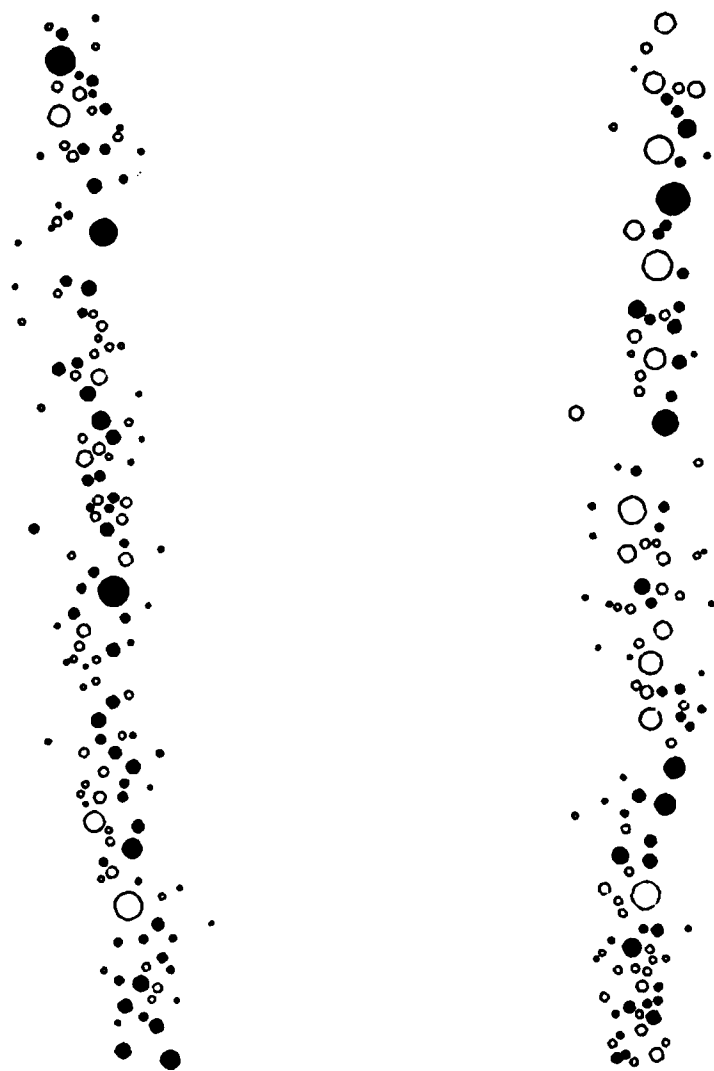
Figure 59   Whirl Position for Divergent Scars at t = 0.8

103
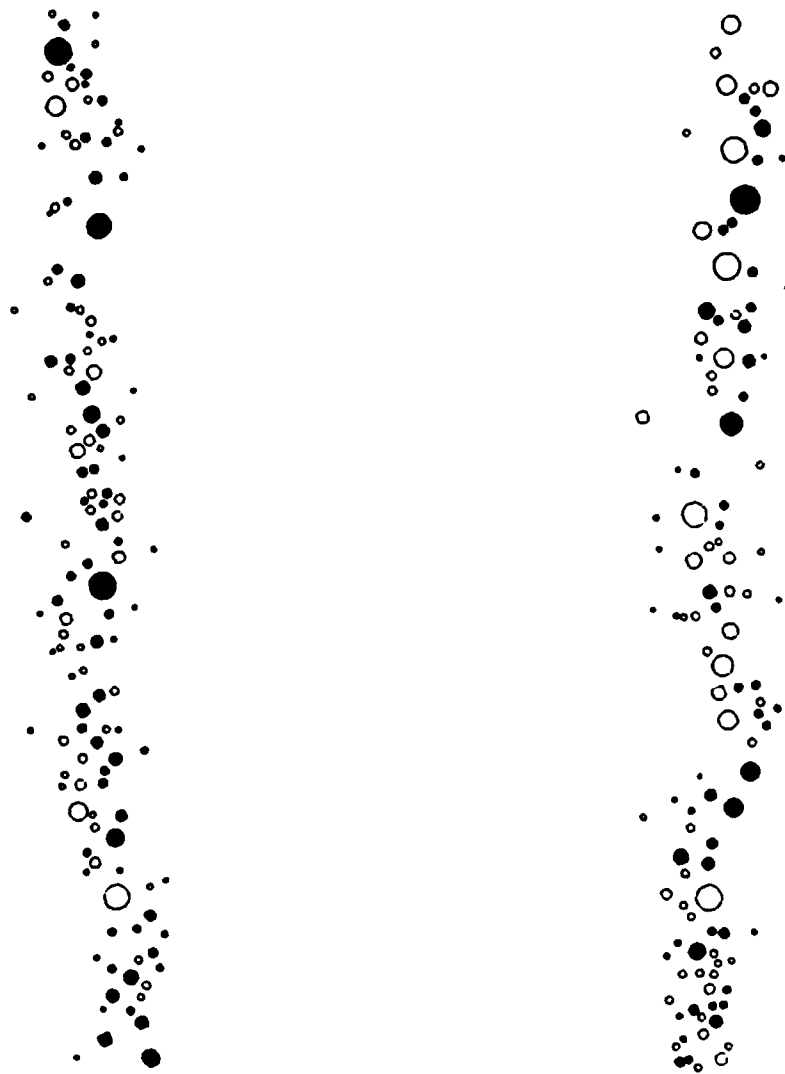
Figure 60   Whirl Position for Divergent Scars at t = 1.2
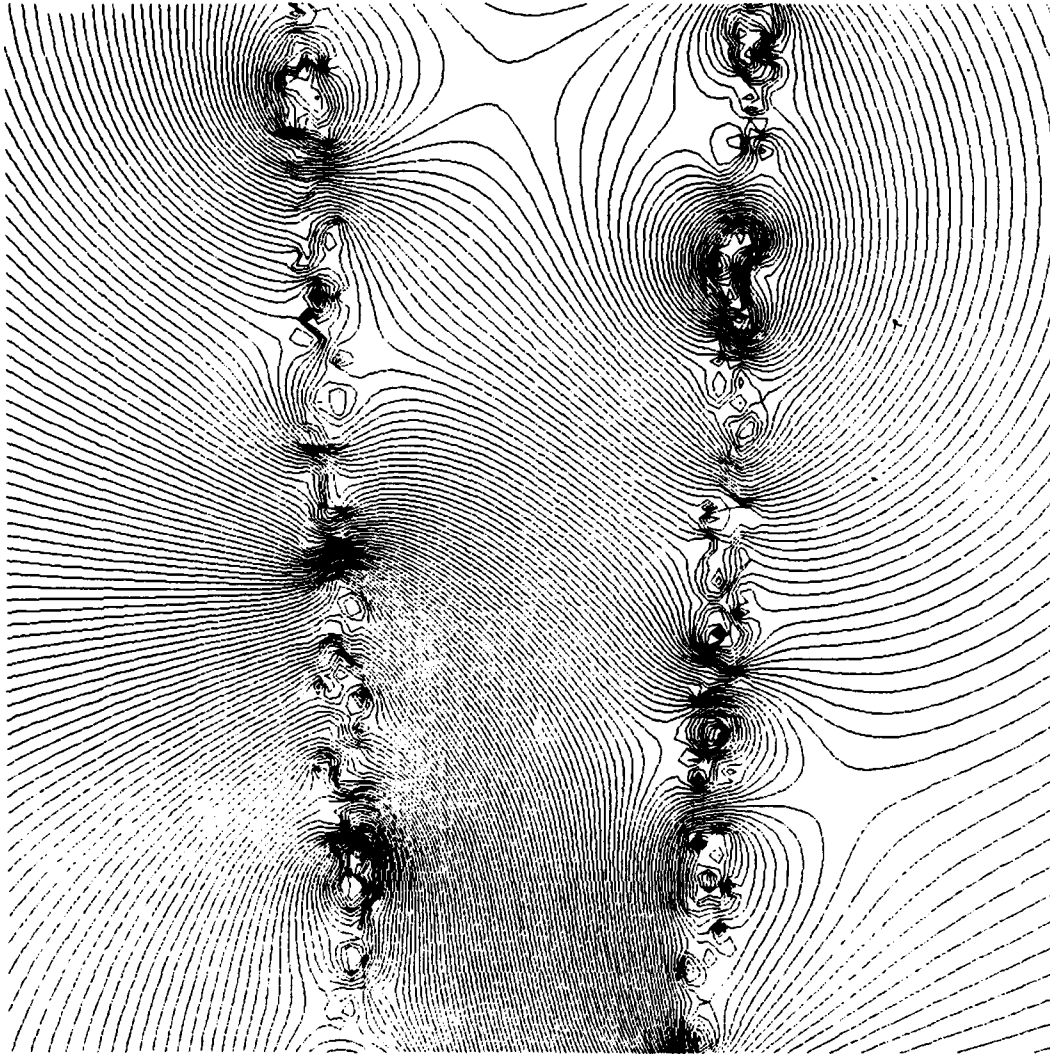
Figure 61   Streamlines For Divergent Scars at t = 0.0 (Comoving Axes)
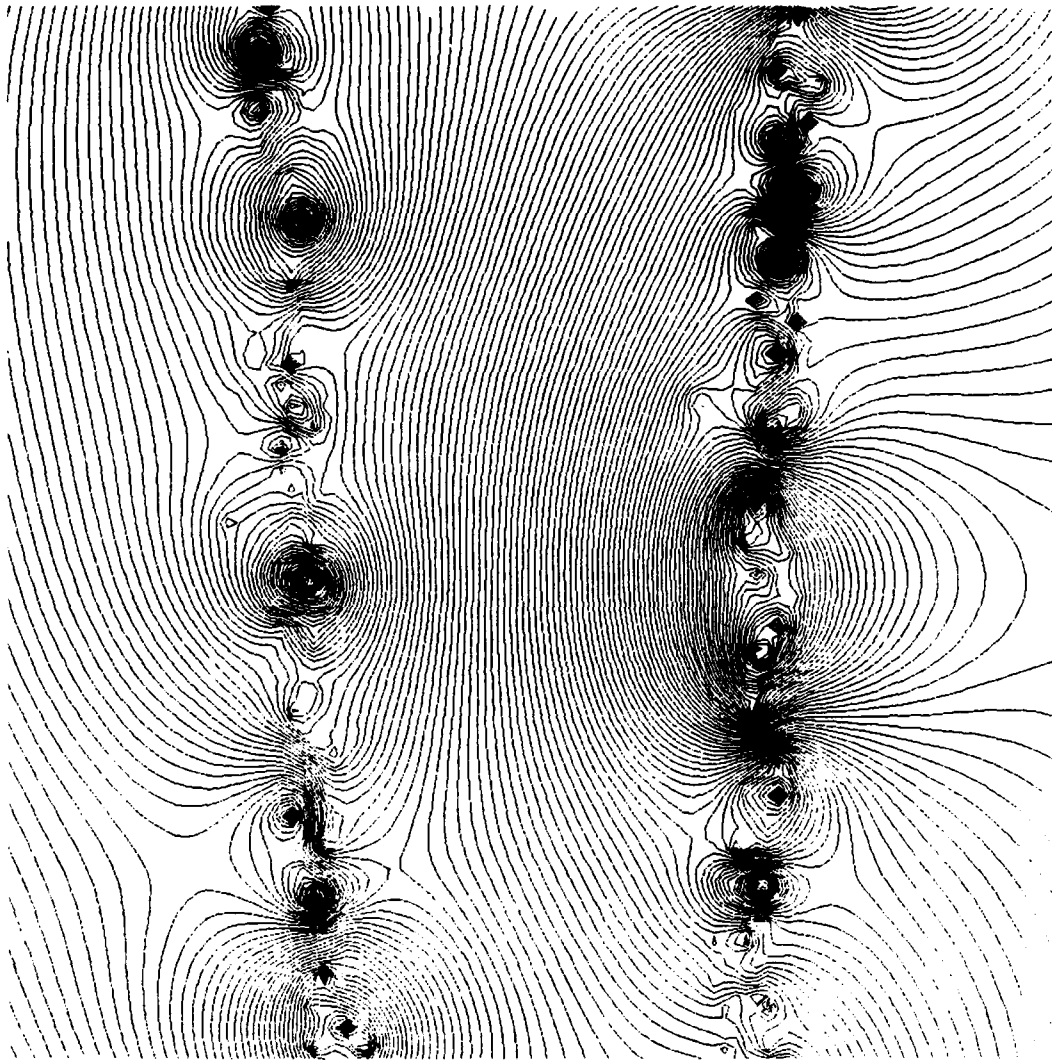
Figure 62   Streamlines For Divergent Scars at t = 0.4 (Comoving Axes)

106
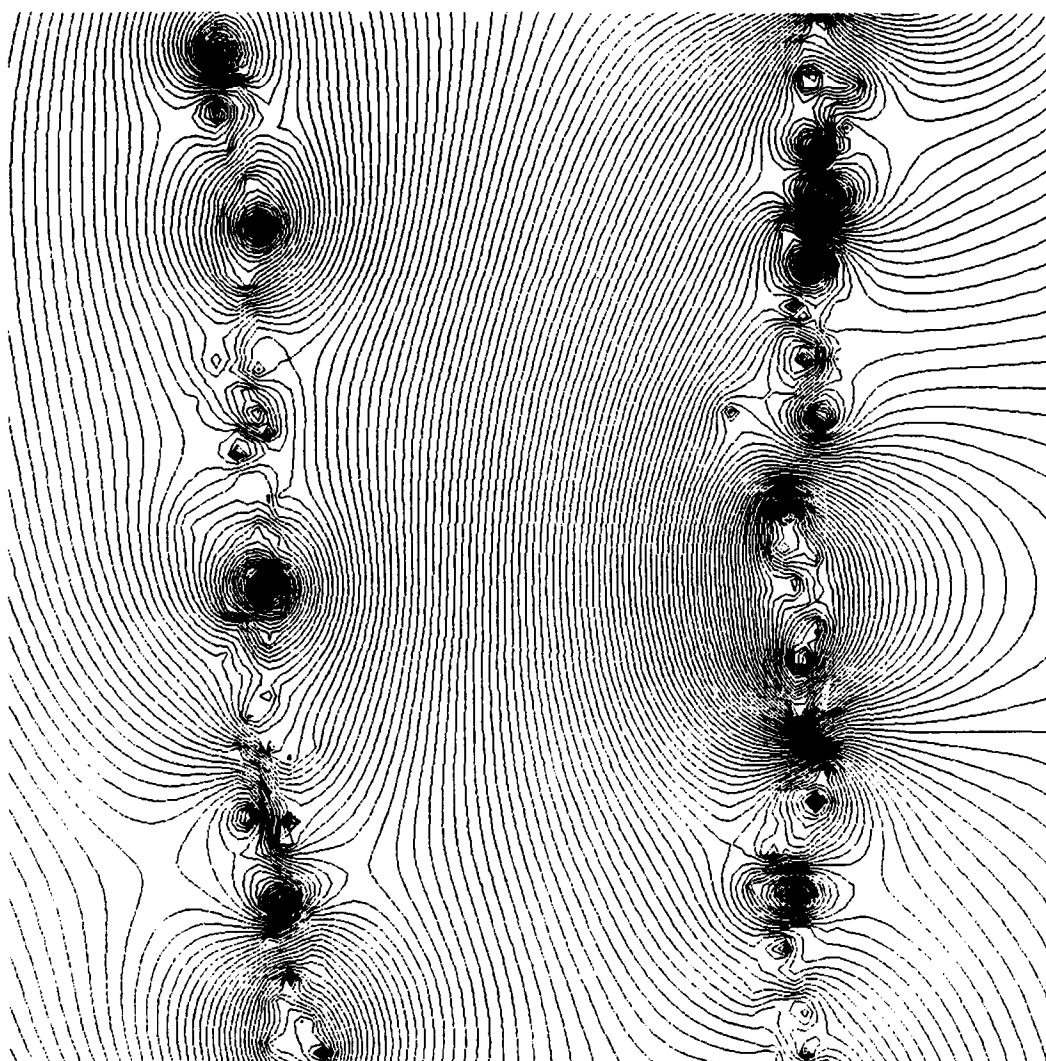
Figure 63   Streamlines For Divergent Scars at t = 0.8 (Comoving Axes)
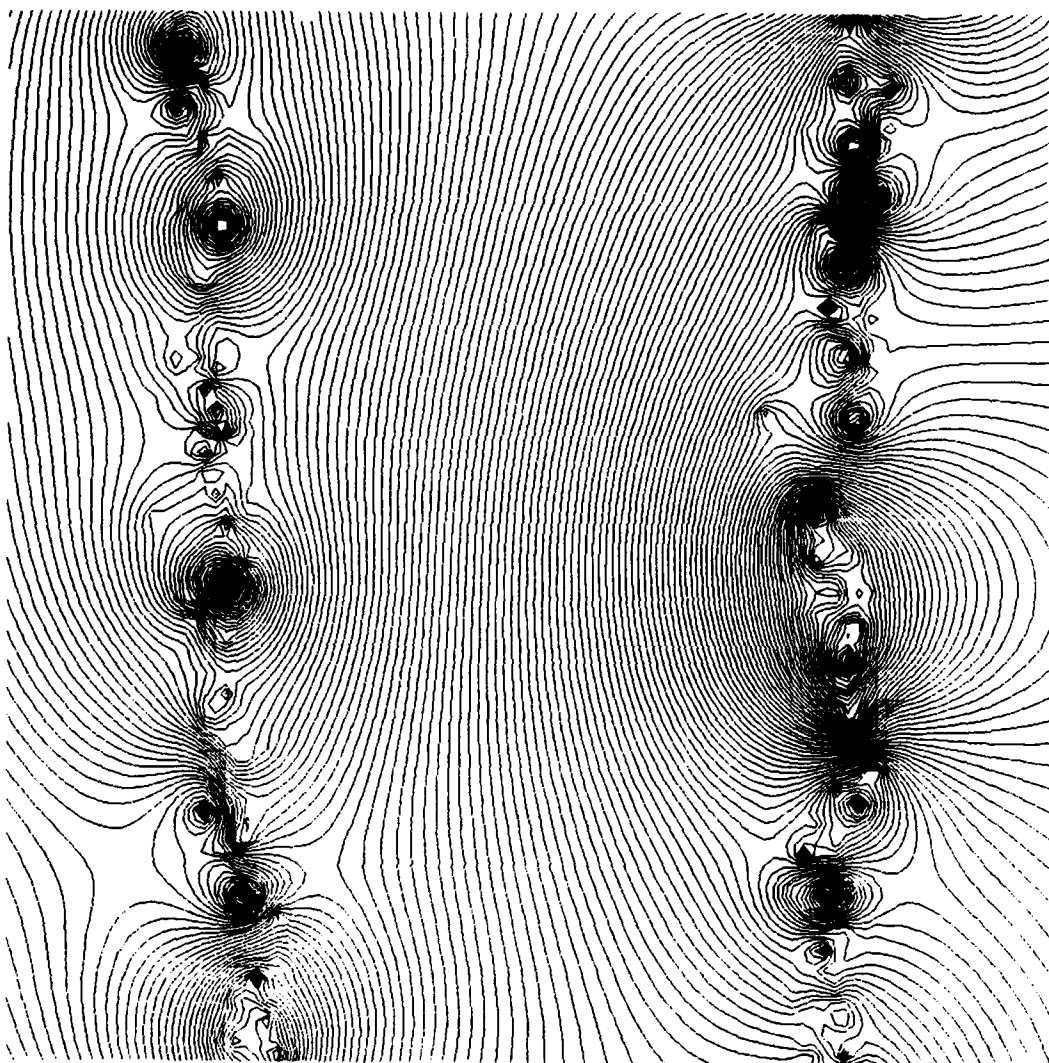
Figure 64   Streamlines For Divergent Scars at t = 1.2 (Comoving Axes)

108
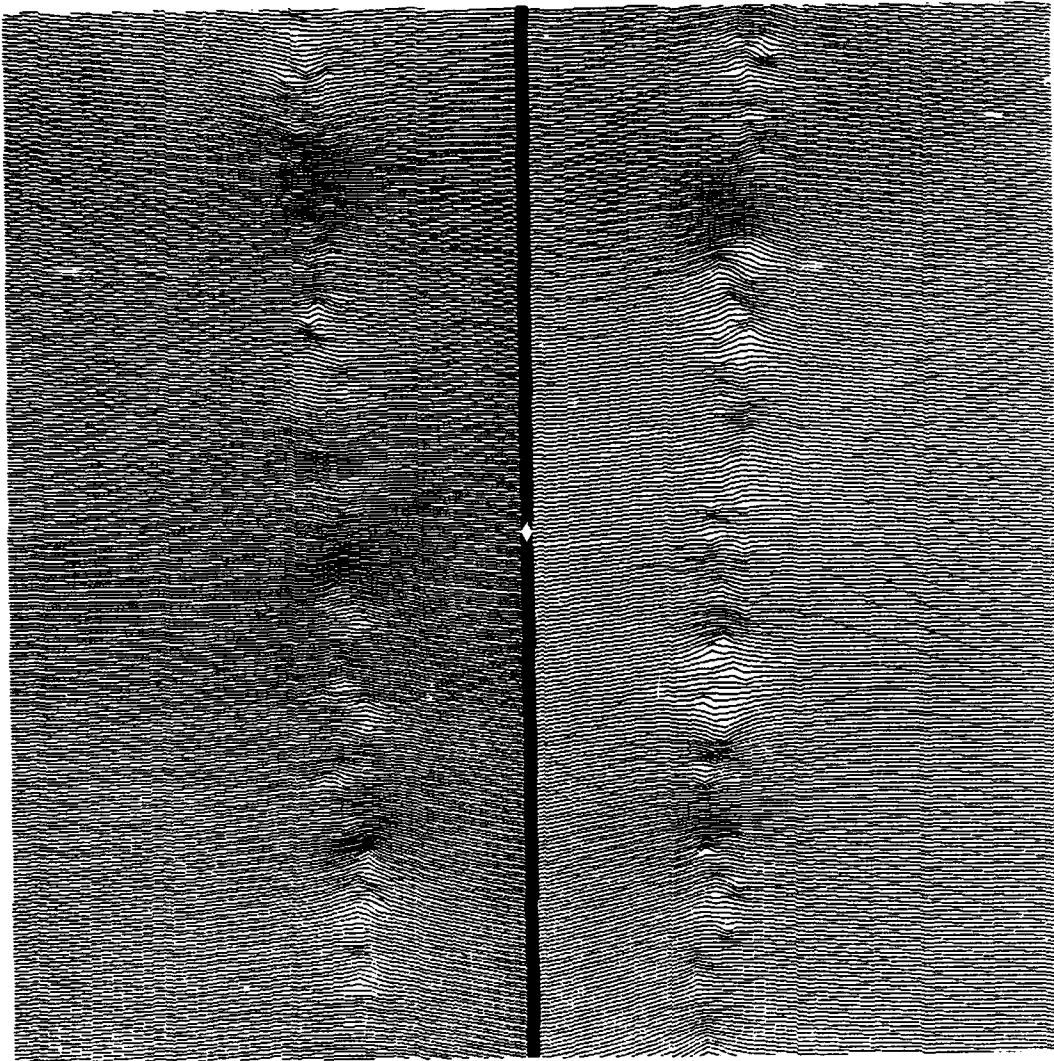
Figure 65   Streamlines For Divergent Scars at t = 0.0 (Fixed Axes)

109
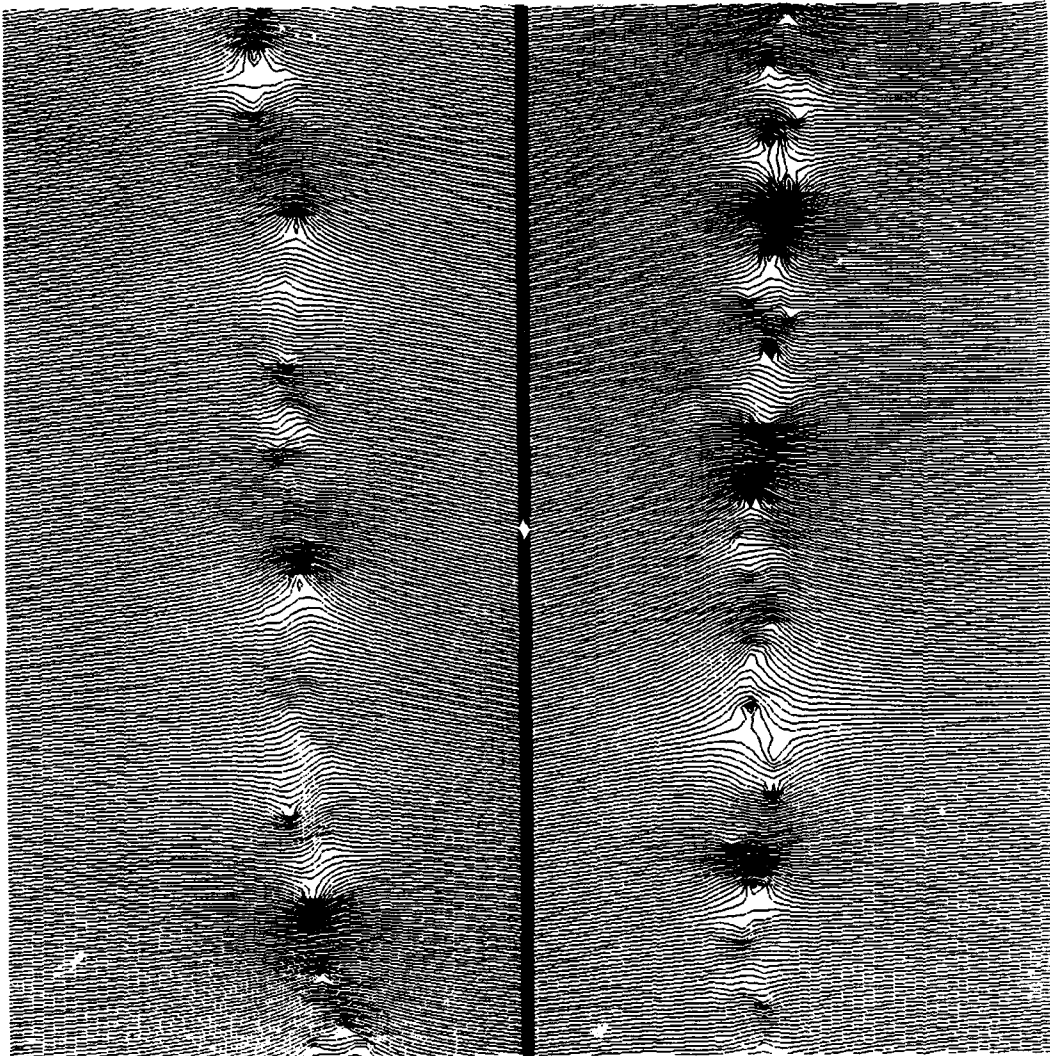
Figure 66   Streamlines For Divergent Scars at t = 0.4 (Fixed Axes)
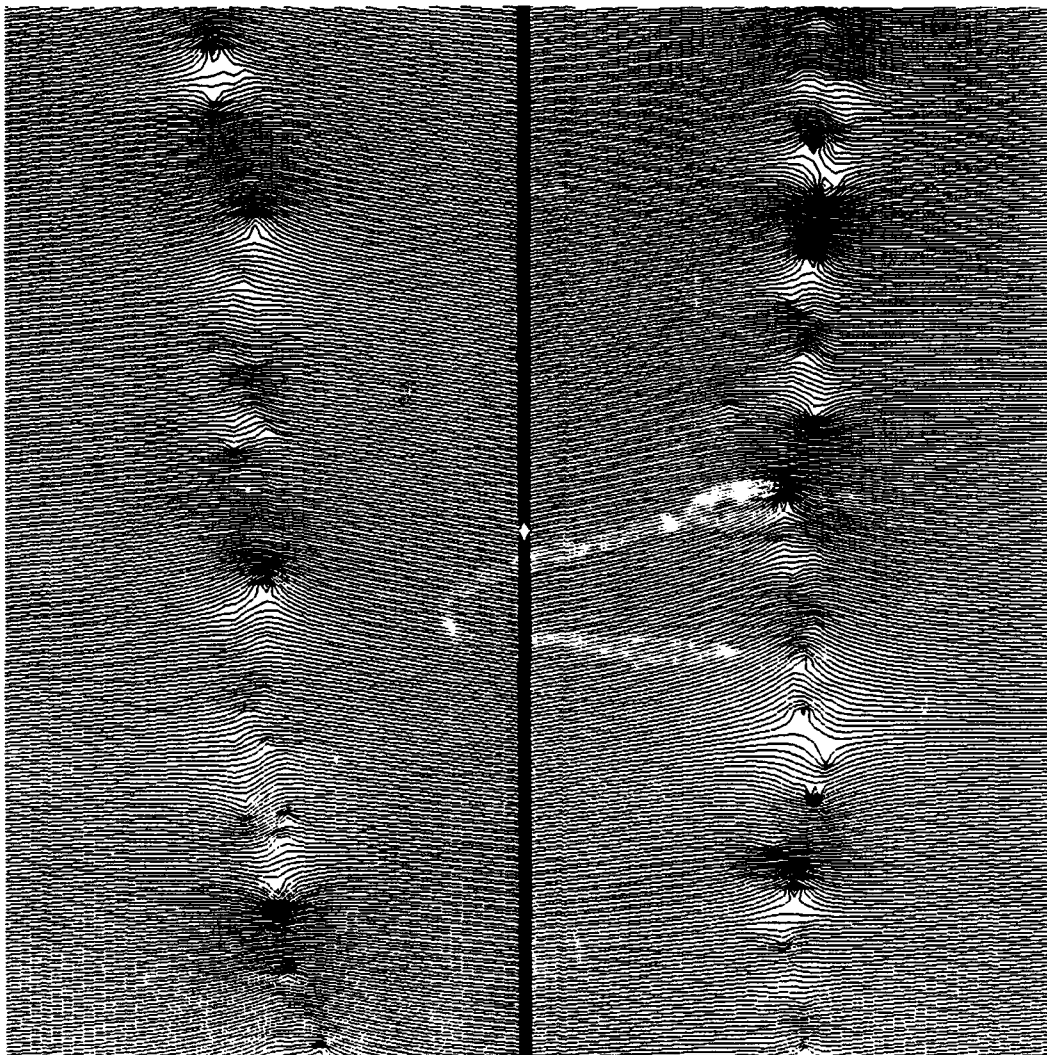
Figure 67   Streamlines For Divergent Scars at t = 0.8 (Fixed Axes)

111
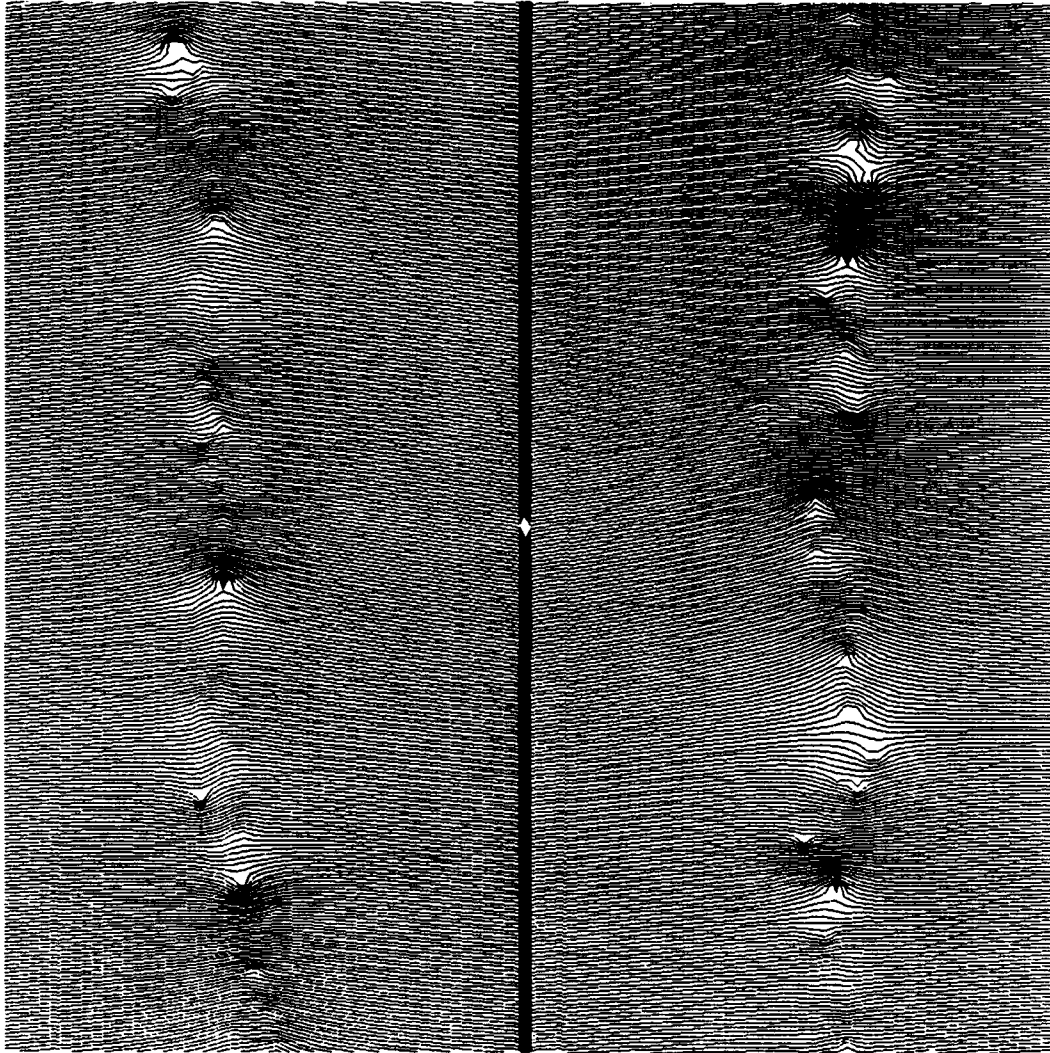
Figure 68   Streamlines For Divergent Scars at t = 1.2 (Fixed Axes)

112
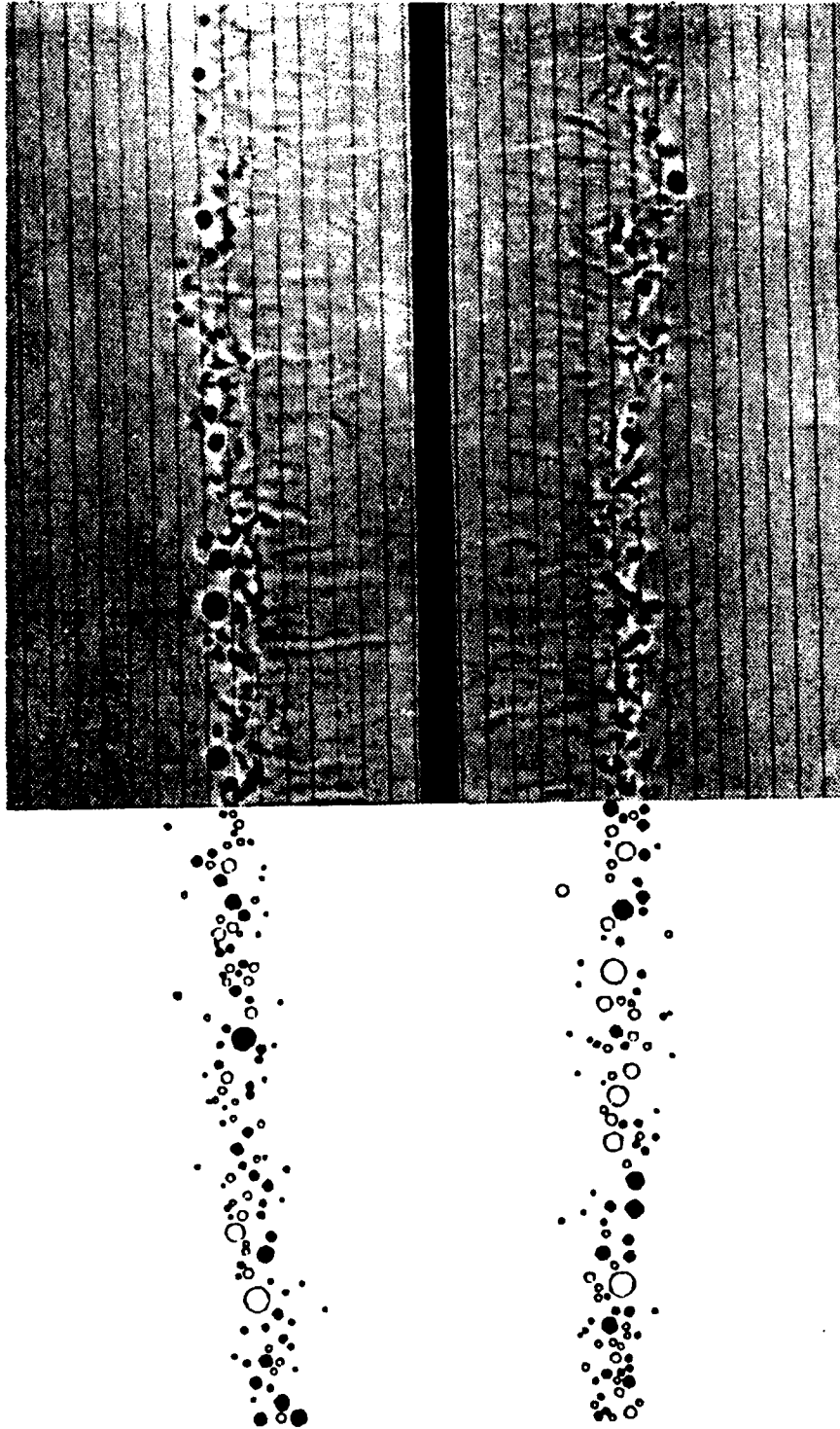
Figure 69   Comparison of Experimental and Numerical Results (#1)
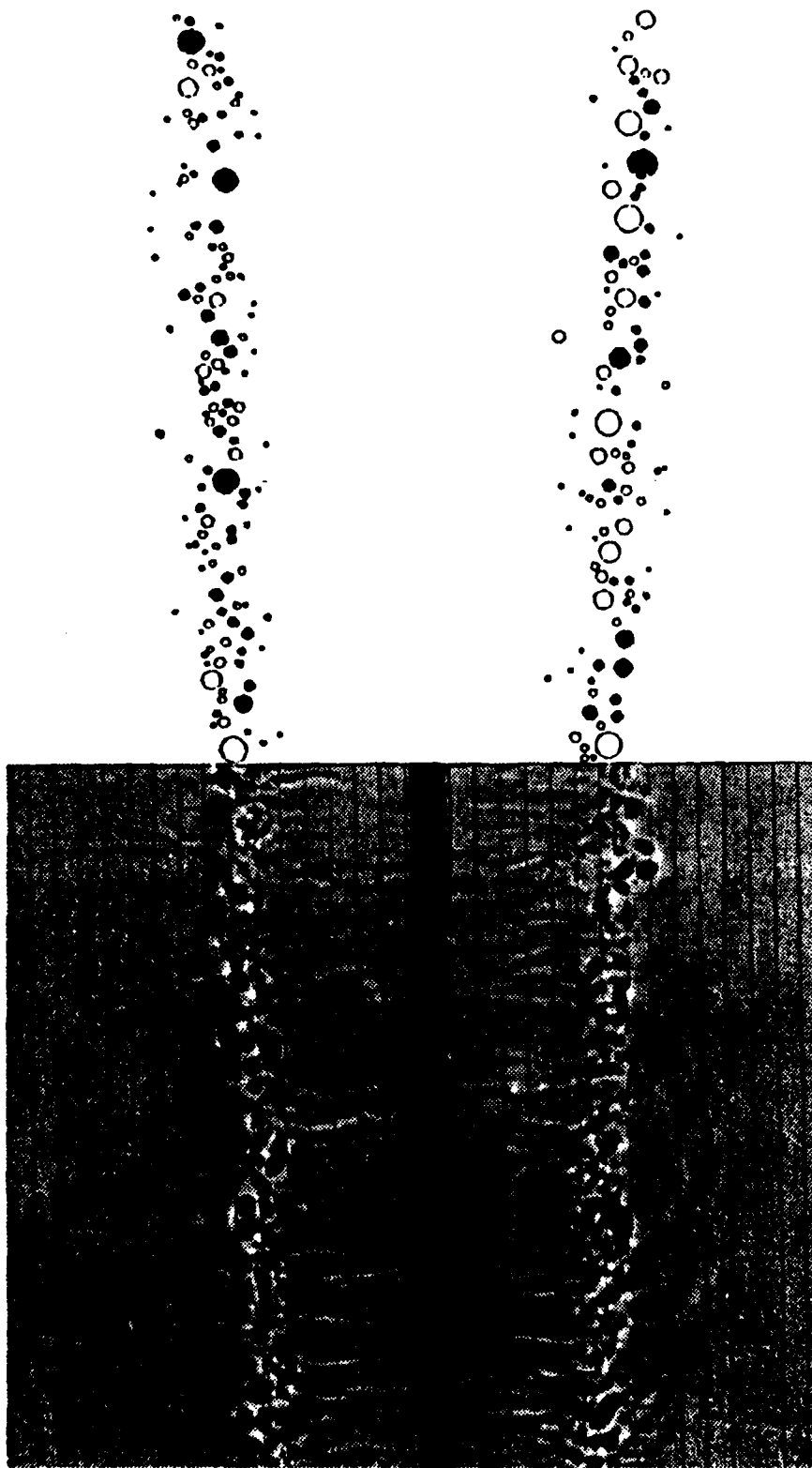
Figure 70   Comparison of Experimental and Numerical Results (#2)

114

APPENDIX B

Rectangular Plate Model With a NACA 0012 Cross Section

$$b_0 = 3.534 \text{ inches} \qquad \alpha = 12° \qquad \frac{V_0}{U} = 0.0285$$

$$\frac{d_0}{b_0} = 2$$

$U = 3.63 \frac{ft}{sec}$		$U = 3.67 \frac{ft}{sec}$		$U = 3.55 \frac{ft}{sec}$	
$\frac{V_0 t}{b_0}$	$\frac{S}{b_0}$	$\frac{V_0 t}{b_0}$	$\frac{S}{b_0}$	$\frac{V_0 t}{b_0}$	$\frac{S}{b_0}$
1.12	0.74*	1.38	0.71*	1.45	0.60*
1.37	0.87*	1.74	1.19*	1.78	1.12*
1.62	1.38*	2.10	1.64	2.05	1.37*
1.90	1.58	2.45	1.77	2.68	1.60
2.18	1.64	2.81	1.83	3.01	1.99
2.53	1.77	3.09	2.03	3.55	2.09
2.88	2.03	3.52	2.22	3.97	2.36
2.95	2.21	3.80	2.41		
3.23	2.39	4.26	2.48		
3.48	2.48	4.62	2.60		
3.97	2.67				
4.00	2.67				

$U = 3.55 \frac{ft}{sec}$		$U = 3.55 \frac{ft}{sec}$	
$\frac{V_0 t}{b_0}$	$\frac{S}{b_0}$	$\frac{V_0 t}{b_0}$	$\frac{S}{b_0}$
0.97	0.72*	1.26	0.77*
1.25	0.94*	1.50	0.94*
1.75	1.36*	1.79	1.25*
2.20	1.50*	2.03	1.31*
2.63	1.79	2.27	1.45*
3.04	1.98	2.54	1.62
3.25	2.12	2.81	1.76
3.61	2.39	3.08	1.86
3.91	2.54	3.29	2.00
4.14	2.65	3.56	2.21

* corresponds to striation mode

Rectangular Plate Model With a NACA 0012 Cross Section

$$b_0 = 3.534 \text{ inches} \qquad \alpha = 12° \qquad \frac{V_0}{U} = 0.0285$$

$$\frac{d_0}{b_0} = 3$$

$U = 3.63 \frac{ft}{sec}$		$U = 3.63 \frac{ft}{sec}$		$U = 3.60 \frac{ft}{sec}$	
$\frac{V_0 t}{b_0}$	$\frac{S}{b_0}$	$\frac{V_0 t}{b_0}$	$\frac{S}{b_0}$	$\frac{V_0 t}{b_0}$	$\frac{S}{b_0}$
2.21	0.91*	2.07	0.52*	2.65	0.79*
2.35	0.84*	2.42	0.78*	3.21	1.41*
2.63	0.91*	2.60	0.88*	3.80	1.76
2.92	1.16*	2.99	1.16*	3.87	1.80
3.20	1.66	3.13	1.60	4.46	2.09
3.41	1.72	3.41	1.75	4.60	2.26
3.69	1.85	3.69	1.85	4.95	2.42
3.97	1.97	4.32	2.10		
4.25	2.15	4.53	2.22		
4.26	2.22	4.81	2.50		
4.74	2.47	5.09	2.72		
5.02	2.59	5.45			
5.37	2.66				

$U = 3.60 \frac{ft}{sec}$		$U = 3.99 \frac{ft}{sec}$	
$\frac{V_0 t}{b_0}$	$\frac{S}{b_0}$	$\frac{V_0 t}{b_0}$	$\frac{S}{b_0}$
3.96	1.35*	3.40	1.49*
3.38	1.62	3.82	1.74
3.55	1.71	4.09	1.80
4.29	2.09	4.83	2.14
4.98	2.26	5.10	2.26
5.12	2.39	5.48	2.42
		5.52	2.48

* corresponds to striation mode

116

Rectangular Plate Model With a NACA 0012 Cross Section

$$b_0 = 3.534 \text{ inches} \qquad \alpha = 12° \qquad \frac{V_0}{U} = 0.0285$$

$$\frac{d_0}{b_0} = 4$$

$U = 3.63 \frac{\text{ft}}{\text{sec}}$		$U = 3.61 \frac{\text{ft}}{\text{sec}}$		$U = 3.55 \frac{\text{ft}}{\text{sec}}$	
$\frac{V_0 t}{b_0}$	$\frac{S}{b_0}$	$\frac{V_0 t}{b_0}$	$\frac{S}{b_0}$	$\frac{V_0 t}{b_0}$	$\frac{S}{b_0}$
3.37	0.69*	3.70	0.75*	3.50	0.85*
3.65	0.72*	4.05	1.17*	4.03	1.07*
3.93	0.84*	4.30	1.47*	4.30	1.49*
4.36	1.44*	4.54	1.65	4.57	1.54
4.71	1.68	4.82	1.71	4.78	1.65
4.92	1.77	5.10	1.83	5.05	1.81
5.23	1.95	5.59	2.07	5.26	2.03
5.41	2.01	5.80	2.13	5.53	2.19
5.97	2.19	6.15	2.31	5.77	2.24
6.39	2.38	6.50	2.56	6.16	2.39
6.74	2.62	6.64	2.62	6.28	2.48
6.92	2.74	6.85	2.74		

$U = 3.55 \frac{\text{ft}}{\text{sec}}$	
$\frac{V_0 t}{b_0}$	$\frac{S}{b_0}$
3.00	0.69*
3.45	0.83*
3.69	0.96*
3.93	1.36*
4.20	1.47*
4.23	1.54
4.50	1.64
4.86	1.75
5.33	1.97
5.46	2.14
5.84	2.24
6.23	2.42

* corresponds to striation mode

117

Rectangular Plate Model With a NACA 0012 Cross Section

$$b_0 = 3.534 \text{ inches} \qquad \alpha = 12° \qquad \frac{V_0}{U} = 0.0285$$

$$\frac{d_0}{b_0} = 5$$

$U = 3.63 \frac{ft}{sec}$		$U = 3.61 \frac{ft}{sec}$		$U = 3.63 \frac{ft}{sec}$	
$V_0 t / b_0$	S / b_0	$V_0 t / b_0$	S / b_0	$V_0 t / b_0$	S / b_0
4.71	0.73*	4.51	0.79*	3.86	0.80*
4.85	0.79*	4.79	0.91*	4.41	1.08*
5.13	1.03*	5.07	0.97*	4.96	1.12*
5.41	1.44*	5.35	1.03*	5.11	1.36*
5.69	1.50*	5.56	1.62	5.39	1.71
6.15	1.79	5.83	1.85	6.19	2.01
6.29	1.79	6.11	1.97	6.70	2.16
6.53	1.91	6.60	2.08		
6.82	1.97	6.88	2.26		
7.10	2.20	7.16	2.32		
7.31	2.26	7.44	2.50		
7.66	2.44	7.65	2.61		
7.87	2.50	7.93	2.67		
		8.21	2.79		

$U = 3.60 \frac{ft}{sec}$		$U = 3.60 \frac{ft}{sec}$	
$V_0 t / b_0$	S / b_0	$V_0 t / b_0$	S / b_0
4.28	0.60*	4.13	0.70*
4.34	0.65*	4.56	0.78*
4.73	0.95*	4.71	1.02*
5.04	1.02*	4.92	1.10*
5.22	1.48*	5.32	1.47*
5.41	1.51	5.52	1.51
5.77	1.79	5.83	1.69
5.86	1.86	5.95	1.81
6.28	1.99	6.38	1.93
6.40	2.09	6.68	1.95
6.83	2.21	6.83	2.26
7.04	2.31	6.89	2.26

*   corresponds to striation mode

118

Rectangular Plate Model With a NACA 0012 Cross Section

$b_0 = 3.534$ inches $\alpha = 12°$ $\dfrac{V_0}{U} = 0.0285$

$$\frac{d_0}{b_0} \;=\; 6$$

$$U = 3.99 \frac{\text{ft}}{\text{sec}}$$

$V_0 t / b_0$	S / b_0
5.08	0.77*
5.29	1.03*
5.99	1.41*
6.33	1.79
6.43	1.92
6.73	2.06
6.97	2.16
7.24	2.25
7.51	2.34
7.81	2.48

* corresponds to striation mode

LIST OF REFERENCES

Baird, M. H. I., 1959, "The Stability of Inverse Bubbles," *Transactions of the Faraday Society*, Vol. 56, pp. 213–219.

Crow, S. C., 1970, "Stability Theory for a Pair of Trailing Vortices," *AIAA Journal*, Vol. 8, No. 12, pp. 2172–2179.

Dahm, W. J. A., Scheil, C. M., and Tryggvason, G., 1988, *Dynamics of Vortex Interaction with a Density Interface*, Report No. MSM-8707646-88-01, The University of Michigan, Ann Arbor, Michigan.

Elnitsky II, J., 1987, *Interaction of a Vortex Pair With a Free Surface*, M.S. and Engineer Degree Thesis, Naval Postgraduate School, Monterey, California.

Furey, R. J., 1989, *A Free-Surface Vorticity Layer Model of the Ships Wake*, Technical Memorandum No. DTRC/SESD-89/05, David Taylor Research Center, Bethesda, Maryland.

Furey, R. J., 1990, *Hydrodynamic Stability and Vorticity in a Ship-Model Wake*, Research and Development Report No. DTRC-90/005, David Taylor Research Center, Bethesda, Maryland.

Garrett, C., 1976, "Generation of Langmuir Circulation by Surface Waves: A Feedback Mechanism," *Journal of Marine Research*, Vol. 34, pp. 117–130.

Garrett, W. D., and Smith, P. M., 1984, *Physical and Chemical Factors Affecting the Thermal IR Imagery of Ship Wakes*, NRL Memorandum Report 5376, Naval Research Laboratory, Washington, D. C.

Gray W. E., Jr., 1985, *Scars and Striations Due to Trailing Vortices*, M.S. and Engineer Degree Thesis, Naval Postgraduate School, Monterey, California.

Henderson, D. O., Jr., 1984, *Surface Disturbances Due to Trailing Vortices*, M.S. and Engineer Degree Thesis, Naval Postgraduate School, Monterey, California.

Johnson, S., K., 1982, *Trailing Vortices in Stratified Fluids*, M.S. Thesis, Naval Postgraduate School, Monterey, California.

Kochin, N. E., Kibel, I. A., and Roze, N. V., 1964, *Theoretical Hydrodynamics*, Interscience Publishers, New York.

Krasny, R., 1987, "Computation of Vortex Sheet Roll-Up in the Trefftz Plane," *Journal of Fluid Mechanics*, Vol. 184, pp. 123–155.

Lamb, H. (Sir), 1945, *Hydrodynamics*, 6th ed., Dover Publications, pp. 221–224.

Langmuir, I., 1938, "Surface Motion of Water Induced by Wind," *Science*, Vol. 87, pp. 119–123.

Leeker, R. E., Jr., 1988, *Free Surface Scars Due to a Vortex Pair*, M.S. and Engineer Degree Thesis, Naval Postgraduate School, Monterey, California.

Lyden J.D., Lygenga D. R., Scuchman, R. A., and Kasischke, E. S., 1985, *Analysis of Narrow Ship Wakes in Georgia Strait SAR Data*, Topic Report Number 155900-20-T, Environmental Institute of Michigan, Ann Arbor, Michigan.

Marcus, D. L., 1988, *The Interaction Between a Pair of Counter-Rotating Vortices and a Free Boundary*, Ph.D. Thesis, University of California, Berkeley, California.

Marcus, D. L., 1990, Personal Communication.

Marcus, D. L., and Berger, S. A., 1989, "The Interaction Between a Counter-Rotating Vortex Pair in Vertical Ascent and a Free Surface," *Physics of Fluids*, A-1, Vol. 12, pp. 1988–2000.

Ohring, S., and Lugt, H. J., 1989, *Two Counter-Rotating Vortices Approaching a Free Surface in a Viscous Fluid*, Research and Development Report No. DTRC-89/013, David Taylor Research Center, Bethesda, Maryland.

Rau, D. H., 1989, *Free Surface Scars and Striations*, M.S. and Engineer Degree Thesis, Naval Postgraduate School, Monterey, California.

Rosenhead, L., 1930, "The Spread of Vorticity in the Wake Behind a Cylinder," *Proceedings of the Royal Society of London*, Series A, Vol. 127, pp. 590–612.

Sarpkaya, T., 1983, "Trailing Vortices in Homogeneous and Density Stratified Media," *Journal of Fluid Mechanics*, Vol. 136, pp. 85–109.

Sarpkaya, T., 1985, "Surface Signatures of Trailing Vortices and Large Scale Instabilities," presented at the Colloquium on Vortex Breakdown, Aachen, Germany, 11–12 February 1985.

Sarpkaya, T., 1986, "Trailing-Vortex Wakes on the Free Surface," *Proceedings of the 16th Symposium on Naval Hydrodynamics*, National Academy Press, Washington, D. C., pp. 38–50.

Sarpkaya, T., 1989, "Computational Methods with Vortices—1988 Freeman Scholar Lecture," *Journal of Fluids Engineering, Transactions of ASME*, Vol. 111, No. 1, pp. 5–52.

Sarpkaya, T., Elnitsky, J., and Leeker, R. E., 1988, "Wake of a Vortex Pair on the Free Surface," *Proceedings of the 17th Symposium on Naval Hydrodynamics*, National Academy Press, Washington, D. C., pp. 47–54.

Sarpkaya, T., and Henderson, D. O., Jr., 1984, *Surface Disturbances Due to Trailing Vortices*, Technical Report No. NPS-69-84-004, Naval Postgraduate School, Monterey, California.

Sarpkaya, T., and Henderson, D. O., Jr., 1985, "Free Surface Scars and Striations Due to Trailing Vortices Generated by a Submerged Lifting Surface," AIAA 85-0445, presented at the 23rd Aerospace Sciences Meeting, Reno, Nevada, 14–17 January 1985.

Sarpkaya, T., and Johnson, S., K., 1982, *Trailing Vortices in Stratified Fluids*, Technical Report No. NPS-69-82-003, Naval Postgraduate School, Monterey, California.

Sarpkaya, T., and Suthon, P. B., 1990, "Scarred and Striated Signature of a Vortex Pair on the Free Surface," *Proceedings of the 18th Symposium on Naval Hydrodynamics*, Ann Arbor, MI., August 20-24, 1990; (To be published by the National Academy Press, Washington, D. C.)

Scott, J. C., 1982, "Flow Beneath a Stagnant Film on Water, The Reynolds Ridge," *Journal of Fluid Mechanics*, Vol. 116, pp. 283–296.

Telste, J. G., 1989, "Potential Flow about Two Counter-Rotating Vortices Approaching a Free Surface," *Journal of Fluid Mechanics*, Vol. 201, pp. 259–278.

Turkmen, C., 1982, *Trailing Vortices in Stratified Fluids and Unstratified Fluids*, M.S. Thesis, Naval Postgraduate School, Monterey, California.

Willmarth, W. W., Tryggvason, G., Hirsa, A., and Yu, D., 1989, "Vortex Pair Generation and Interaction with a Free Surface," *Physics of Fluids*, A-1, Vol. 1, pp. 170–172.

Witting, J. M., and Vaglio-Laurin, R., 1985, *Mechanisms and Models of Narrow-V Wakes*, ORI Inc. Technical Report 2529, Washington, D. C.

INITIAL DISTRIBUTION LIST

No. Copies

1. Defense Technical Information Center   2
   Cameron Station
   Alexandria, VA 22304–6145

2. Library, Code 0142   2
   Naval Postgraduate School
   Monterey, CA 93943-5002

3. Department Chairman, Code 69   1
   Department of Mechanical Engineering
   Naval Postgraduate School
   Monterey, CA 93943-5000

4. Professor T. Sarpkaya, Code ME-SL   10
   Department of Mechanical Engineering
   Naval Postgraduate School
   Monterey, CA 93943-5000

5. LT Peter B.R. Suthon   2
   13134 Dwyer Blvd.
   New Orleans, LA 70129

6. Office of Naval Research   1
   ATTN: Dr. Edwin P. Rood, Code: 1132F
   800 North Quincy Street
   Arlington, VA 22217

7. Naval Sea Systems Command   1
   PMS 350
   Washington, D. C. 20362

8. Defense Advanced Research Projects Agency   1
   ATTN: S. Resnick
   1400 Wilson Blvd.
   Arlington, VA 22209